

DISSERTATION

MIXING IN STABLY STRATIFIED TURBULENT FLOWS: IMPROVED  
PARAMETERIZATIONS OF DIAPYCNAL MIXING IN OCEANIC FLOWS

Submitted by

Amrapalli Garanaik

Department of Civil and Environmental Engineering

In partial fulfillment of the requirements

For the Degree of Doctor of Philosophy

Colorado State University

Fort Collins, Colorado

Summer 2018

Doctoral Committee:

Advisor: Subhas Karan Venayagamoorthy

Bogusz Bienkiewicz

Elizabeth Barnes

Pierre Y. Julien

Copyright by Amrapalli Garanaik 2018

All Rights Reserved

## ABSTRACT

### MIXING IN STABLY STRATIFIED TURBULENT FLOWS: IMPROVED PARAMETERIZATIONS OF DIAPYCNAL MIXING IN OCEANIC FLOWS

Mixing of fluid with different properties across a gravitationally stable density interface, due to background turbulence is an ubiquitous phenomenon in both natural and engineered flows. Fundamental understanding and quantitative prediction of turbulent mixing in stratified flows is a challenging problem, with a broad range of applications including (but not limited to) prediction of climate, ocean thermohaline circulation, global heat and mass budget, pollutant and nutrients transport, etc. Large scale geophysical flows such as in the ocean and atmosphere are usually stably stratified i.e. the density increases in the direction of gravitational force. The stabilizing nature of the density layers has a tendency to inhibit the vertical motion. In such flows, diapycnal mixing, i.e. mixing of fluid across the isopycnal surfaces of constant density, plays a crucial role in the flow dynamics. In numerical models of large scale flows, turbulent mixing is inherently a small scale phenomenon that is difficult to resolve and is therefore generally parameterized using known bulk parameters of the flow. In oceans, the mixing of water masses is typically represented through a turbulent (eddy) diffusivity of mass  $K_\rho$ . A widely used formulation for  $K_\rho$  in oceanic flows is given as  $K_\rho = \Gamma\epsilon/N^2$ , where  $\epsilon$  is the rate of dissipation of turbulent kinetic energy,  $N = \sqrt{(-g/\rho)(\partial\rho/\partial z)}$  is the buoyancy frequency of the background stratification,  $\rho$  is the density,  $\Gamma = R_f/(1 - R_f)$  is a mixing coefficient and  $R_f$  is the mixing efficiency, that is widely (but questionably) assumed to be constant or sometimes parameterized. However, a robust and universal parameterization for the mixing efficiency remains elusive to date despite numerous studies on this topic.

This research focuses on improved parameterizations of diapycnal mixing through an integration of theoretical knowledge with observational and high resolution numerical simulation data. The main objectives are: (1) to provide a better assessment of field microstructure data and

methodology for data analysis in order to develop/test appropriate parameterization of the mixing efficiency, (2) to determine the relevant length and velocity scales for diapycnal mixing, (3) to provide improved parameterization(s) of diapycnal mixing grounded on physical reasoning and scaling analysis, (4) to provide a practical field method to identify the dynamic state of turbulence in stably stratified flows from measurable length scales in the ocean.

First, an analysis of field microstructure data collected from different locations in the ocean was performed to verify existing parameterizations. A key finding is that the mixing efficiency,  $R_f$  does not scale with buoyancy Reynolds number,  $Re_b$ , as been proposed previously by others. Rather,  $R_f$  depends on the strength of background stratification. In a strongly stratified thermocline, a constant value for the mixing efficiency is found to be reasonable while for weakly stratified conditions (e.g. near boundaries) a parameterization is required. A discussion on different methods to estimate the background shear and stratification from field data is provided. Furthermore, the present state-of-the-art microstructure instruments measure the small scale dissipation rate of turbulent kinetic energy  $\epsilon$  from one dimensional components by invoking the small scale isotropy assumption that is strictly valid for high Reynolds number flows. A quantitative assessment of the departure from isotropy in stably stratified flows is performed and a pragmatic method is proposed to estimate the true three dimensional dissipation ( $\epsilon_{3D}$ ) from one dimensional dissipation ( $\epsilon_{1D}$ ) obtained from microstructure profilers in the ocean.

Next, a scaling analysis for strongly stratified flow is presented to show that, the true diapycnal length scale  $L_d$  and diapycnal velocity scale  $w_d$  can be estimated from the measurable Ellison length scale,  $L_E$  and a measurable root mean square vertical velocity,  $w'$ , using a turbulent Froude number defined as  $Fr = \epsilon/Nk$ , where  $k$  is the turbulent kinetic energy. It is shown that the eddy diffusivity  $K_\rho$  can be then directly inferred from  $L_E$  and  $w'$ . For weakly stratified flow regimes,  $Fr > \mathcal{O}(1)$ ,  $K_\rho \sim w'L_E$  and for strongly stratified flow regimes,  $Fr < \mathcal{O}(1)$ ,  $K_\rho \sim w'L_E \times Fr$ . This finding is confirmed with direct numerical simulation (DNS) data for decaying as well as sheared stratified turbulence. This result indicates that  $Fr$  is a relevant non-dimensional parameter to identify strength of stratification in stably stratified turbulent flows. DNS with particle tracking

is performed to separate isopycnal and diapycnal displacements of fluid particles, an analysis that is not possible from an Eulerian approach or from standard field measurements. The Lagrangian analysis show that  $L_E$  is indeed an isopycnal length scale.

Furthermore, having established that  $Fr$  is the signature parameter which can describe the state of stratified turbulence, a parameterization of mixing coefficient,  $\Gamma$  (or  $R_f$ ) as a function of turbulent Froude number  $Fr$  is developed using scaling arguments of energetics of the flow. Proposed parameterization is then verified using DNS data of decaying, sheared and forced stratified turbulence. It is shown that for  $Fr \ll \mathcal{O}(1)$ ,  $\Gamma \sim Fr^0$ , for  $Fr \sim \mathcal{O}(1)$ ,  $\Gamma \sim Fr^{-1}$  and for  $Fr \gg \mathcal{O}(1)$ ,  $\Gamma \sim Fr^{-2}$ .

Finally, a practically useful method to identify the dynamic state of turbulence in stably stratified flows is developed. Two commonly measurable length scales in the ocean are the Thorpe overturning length scale,  $L_T$  and the dimensionally constructed Ozmidov length scale,  $L_O$ . From scaling analysis and DNS data of decaying, sheared and forced stratified turbulence a new relation between  $Fr$  and the ratio of the length scales,  $L_T/L_O$  is derived. The new scaling is, for  $L_T/L_O > \mathcal{O}(1)$ ,  $Fr \sim (L_T/L_O)^{-2}$  and for  $L_T/L_O < \mathcal{O}(1)$ ,  $Fr \sim (L_T/L_O)^{-2/3}$ .

## ACKNOWLEDGEMENTS

Firstly, I would like to express my sincere gratitude to my advisor Dr. Karan Venayagamoorthy for providing me with the opportunity to work with him at Colorado State University. I appreciate all his contributions of time, his patience and constant motivations that have made this dissertation possible. As my mentor he always encouraged and guided me, for which I am deeply grateful. Looking forward, I hope to follow his example as an excellent teacher and researcher. Besides my advisor, I would like to thank my Ph.D committee, Drs. Pierre Julien, Bogusz Bienkiewicz and Elizabeth Barnes, for their insightful comments and suggestions that challenged me to widen my research from various perspectives.

I thank my fellow labmates with special thanks to my fellow Ph.D students, Dr. Jian Zhou and Oladapo Aseperi for their friendship over the years. All the technical and non-technical coffee break discussions allowed me to grow as a researcher and as a person. I also thank my former labmates Dr. Benjamin Mater and Dr. Farid Karimpour for their guidance during my early Ph.D career. Thanks also to my friends in CSU who are my family away from home and have always been there for me through the thick and thin of the graduate school.

I am forever indebted to my parents Mr. Sarat Kumar Garanaik and Mr. Sujata Garanaik and my siblings, Monalisa, Swetalina and Amrutansu for their constant support and encouragement throughout my life to achieve any dream. This dissertation is dedicated to my family for their faith and love.

Also, fundings from the National Science Foundation under Grant No. OCE-1151838 and the office of Naval Research under Grant No. N00014-16-1-3015 are gratefully acknowledged.

## TABLE OF CONTENTS

	ABSTRACT . . . . .	ii
	ACKNOWLEDGEMENTS . . . . .	v
	LIST OF FIGURES . . . . .	ix
Chapter 1	Introduction . . . . .	1
1.1	Background and motivation . . . . .	1
1.2	Objectives . . . . .	4
1.3	Dissertation layout . . . . .	6
Chapter 2	Background and literature review . . . . .	8
2.1	Geophysical flows . . . . .	8
2.1.1	Stratification and internal waves . . . . .	8
2.1.2	Vertical structure of the ocean . . . . .	9
2.2	Governing equations . . . . .	10
2.2.1	Continuity equation . . . . .	11
2.2.2	Momentum or Navier-Stokes Equations . . . . .	11
2.2.3	Scalar transport equation . . . . .	12
2.3	Scales of motion . . . . .	13
2.3.1	Global length and time scale . . . . .	13
2.3.2	Scales of turbulence . . . . .	14
2.3.3	Scales of stratified turbulence . . . . .	16
2.3.4	Scales of turbulent scalar field . . . . .	17
2.4	Numerical methodology . . . . .	18
2.4.1	Direct numerical simulation (DNS) . . . . .	18
2.4.2	Reynolds average Navier Stokes (RANS) equations . . . . .	19
2.4.3	Parameterization of turbulence/Turbulent closure models . . . . .	21
2.5	Energetics of stratified turbulence . . . . .	22
2.5.1	Turbulent Kinetic energy . . . . .	23
2.5.2	Turbulent Potential Energy . . . . .	24
2.6	Diapycnal mixing . . . . .	25
2.6.1	Mixing efficiency . . . . .	26
2.6.2	Parameterization of $R_f$ or $\Gamma$ . . . . .	27
2.7	Turbulence measurement in the ocean . . . . .	29
2.7.1	CTD: . . . . .	31
2.7.2	ADCP: . . . . .	31
2.7.3	VMP: . . . . .	32
2.8	Lagrangian dispersion and mixing . . . . .	33
2.8.1	Lagrangian frame work . . . . .	33
2.8.2	Particle dispersion . . . . .	34
2.9	Summary . . . . .	37

Chapter 3	Analysis of oceanic diapycnal mixing from microstructure measurements . . .	38
3.1	Introduction . . . . .	38
3.2	Theoretical background . . . . .	41
3.3	Data considered . . . . .	43
3.4	Methodology . . . . .	45
3.4.1	Equation of states and T-S plots . . . . .	45
3.4.2	Bin-wise vs patch-wise analysis . . . . .	46
3.4.3	Identification of turbulent patch- Thorpe resorting method . . . . .	48
3.4.4	Background gradients . . . . .	49
3.5	Results . . . . .	52
3.5.1	Traditional approach: Bin-wise analysis with $\Gamma = 0.2$ . . . . .	52
3.5.2	Patch statistics: temperature sorted vs density sorted . . . . .	53
3.5.3	Background stratification . . . . .	57
3.5.4	Background shear . . . . .	57
3.5.5	Ambiguity of $Re_b$ based parameterization of mixing efficiency, $R_f$ . . . . .	59
3.5.6	Mixing efficiency and gradient Richardson number . . . . .	61
3.6	Concluding remarks . . . . .	63
Chapter 4	Assessment of small scale anisotropy in stably stratified turbulent flows using direct numerical simulations . . . . .	64
4.1	Introduction . . . . .	64
4.2	Theoretical background of small scale isotropy . . . . .	66
4.3	Direct numerical simulations . . . . .	68
4.4	Results and discussions . . . . .	69
4.4.1	Flow dynamics . . . . .	69
4.4.2	Anisotropy of rate of dissipation of turbulent kinetic energy ( $\epsilon$ ) . . . . .	71
4.4.3	Anisotropy of rate of dissipation of density variance ( $\epsilon_\rho$ ) . . . . .	72
4.4.4	Inferring true dissipation from oceanic measurements . . . . .	73
4.5	Concluding remarks . . . . .	74
Chapter 5	Some new insights for inferring diapycnal diffusivity in stably stratified turbulence . . . . .	76
5.1	Introduction . . . . .	76
5.2	Numerical method . . . . .	78
5.3	Theoretical development of a new model for diapycnal diffusivity . . . . .	79
5.3.1	Diapycnal diffusivity in the regime of strongly stratified turbulence ( $Fr < 1$ ) . . . . .	80
5.3.2	New model for diapycnal diffusivity . . . . .	84
5.4	Towards field application . . . . .	85
5.5	Concluding remarks . . . . .	87
Chapter 6	A practical recipe for parameterization of mixing in oceanic flows using direct numerical simulations . . . . .	89
6.1	Introduction . . . . .	89
6.2	Theoretical analysis . . . . .	90

6.2.1	Scaling argument for $\Gamma$ as a function of $Fr$ . . . . .	90
6.2.1.1	In the limit of weak stratification $Fr \gg \mathcal{O}(1)$ . . . . .	91
6.2.1.2	In the limit of moderate stratification $Fr \sim \mathcal{O}(1)$ . . . . .	91
6.2.1.3	In the limit of strong stratification $Fr \ll \mathcal{O}(1)$ . . . . .	92
6.2.2	Inferring $Fr$ from Ozmidov and Thorpe length scales . . . . .	92
6.3	Data considered . . . . .	95
6.4	Results . . . . .	96
6.4.1	Mixing coefficient ( $\Gamma$ ) as a function of turbulent Froude number ( $Fr$ ) . . . . .	96
6.4.2	Thorpe length scale, Ellison length scale and Ozmidov length scale . . . . .	98
6.4.3	$Fr$ as a function of $L_E/L_O$ : Inferring the state of turbulence . . . . .	100
6.5	Concluding remarks . . . . .	101
Chapter 7	Lagrangian analysis for diapycnal mixing and dispersion . . . . .	103
7.1	Introduction . . . . .	103
7.2	Isopycnal and diapycnal components of length and velocity scales from Lagrangian perspective . . . . .	104
7.3	Methodology . . . . .	106
7.4	Results . . . . .	107
7.4.1	Validation of Lagrangian statistics with Eulerian statistics . . . . .	107
7.4.2	Lagrangian particle dispersion . . . . .	110
7.4.3	Isopycnal and diapycnal displacement . . . . .	110
7.4.4	Isopycnal and diapycnal velocity . . . . .	112
7.4.5	Diapycnal dispersion . . . . .	113
7.4.6	Diapycnal diffusivity from isopycnal length scale and diapycnal veloc- ity scale . . . . .	113
7.5	Concluding remarks . . . . .	114
Chapter 8	Summary and Conclusions . . . . .	117
8.1	Key findings . . . . .	117
8.2	Suggestions for future works . . . . .	119

## LIST OF FIGURES

1.1	(a) Schematic of global overturning circulation adapted from (Kuhlbrodt <i>et al.</i> , 2007). (b) schematic showing vertical structure of the ocean with nutrients rich deep water (Edgar, 2011). . . . .	3
2.1	Vertical structure of the ocean showing spatial and seasonal variation of mixed layer depth and thermocline. . . . .	10
2.2	The range of temporal and spatial scales involved in processes of the tropical climate. Image courtesy of MetEd, The COMET Program, UCAR. . . . .	13
2.3	Typical energy spectrum for a turbulent flow plotted against wave number ( $\hat{k}$ ) (Thompson <i>et al.</i> , 2015). URANS, LES and DNS are the numerical methods described in section 2.4 . . . . .	15
2.4	Schematic showing energetics of diapycnal mixing . . . . .	23
2.5	Pictures of commonly used instruments in the field of oceanography. (a): CTD Rosette, (b): UCTD (c) ADCP and (d): VMP . . . . .	30
3.1	T-S plot for (a) BBTRE and (b) IWISE with depth in color bar. Density difference from $1000kg/m^3$ are shown in dashed contour lines. . . . .	46
3.2	Example showing identification of a turbulent patch based on density sorted profile. . . . .	48
3.3	A schematic showing mechanism of shear. . . . .	51
3.4	The left panel is showing T-S plot with depth of measurement in color bar for BoB data with an inset plot of average vertical profiles of potential temperature $\theta$ , potential density $\sigma_\theta$ and salinity (S). The middle panel presents the average vertical profile of eddy diffusivity of temperature $K_T$ (3.4) and mass $K_\rho$ (3.8). The right panel average vertical profile of mixing efficiency (3.10). Vertical line corresponds to $R_f = 0.17$ . Here average signifies the average over all measured profiles. For better visualization average vertical profiles are shown with 5m depth average values. . . . .	52
3.5	(a) Average vertical profiles of $\chi$ ( $^0C/s$ ) and $\epsilon$ ( $m^2/s^3$ ) (b)the average background stratification. . . . .	53
3.6	(a) Density sorted Thorpe length scales for all the profiles of IWISE through out the depth (b) Temperature sorted Thorpe length scale for all the profiles of IWISE throughout the depth. (c) Histogram of density sorted $L_T$ with patch statistics for IWISE, (d)Histogram of temperature sorted $L_T$ with patch statistics for IWISE. . . . .	54
3.7	(a) Density sorted Thorpe length scales for all the profiles of BBTRE through out the depth (b) Temperature sorted Thorpe length scale for all the profiles of BBTRE throughout the depth. (c) Histogram of density sorted $L_T$ with patch statistics for BBTRE, (d)Histogram of temperature sorted $L_T$ with patch statistics for BBTRE. . . . .	56
3.8	A comparative study of Thorpe length $L_T$ and patch length $L_P$ for corresponding patches for (a) IWISE data (b) BBTRE data. . . . .	57
3.9	Statistics of background stratification obtained from different methods for BBTRE thermocline data. . . . .	58

3.10	Statistics of background shear obtained from different methods for BBTRE thermo- cline data. . . . .	58
3.11	Left panel:Variation of mixing efficiency with buoyancy Reynolds number ( $Re_b = \epsilon/\nu N^2$ ) in deep ocean region for (a) BBTRE data (b) IWISE data. $N = N_{bulk}$ . The red solid line shows the parameterization of $R_f$ as per Shih <i>et al.</i> (2005). Blue boundary lines suggest 95 CI. Right panel:Distribution of patches over different bins considered to obtain left panel mean data. . . . .	59
3.12	Left panel: Variation of mixing efficiency with buoyancy Reynolds number ( $Re_b = \epsilon/\nu N^2$ ) in thermocline region for (a) BBTRE data (b) IWISE data. $N = N_{bulk}$ . The red solid line shows the parameterization of $R_f$ as per Shih <i>et al.</i> (2005). Blue boundary lines suggest 95% CI. Right panel: Distribution of patches over different bins considered to obtain left panel mean data. . . . .	60
3.13	Variation of mixing efficiency with gradient Richardson number ( $Ri = N^2/S^2$ ) for BBTRE deep ocean data. (a) Patch-across shear (b) Patch-average shear. Solid circle: $N_{2pt}$ , star: $N_{bulk}$ . Vertical line corresponds to $Ri = 0.25$ . . . . .	62
3.14	Variation of mixing efficiency with gradient Richardson number ( $Ri_g = N^2/S^2$ ) for IWISE thermocline data. (a) Patch-across shear (b)Patch-average shear. Solid circle: $N_{2pt}$ , star: $N_{bulk}$ . The dashed vertical line corresponds to $Ri_g = 0.25$ . . . . .	63
4.1	(a) The time evolution of kinetic energy, $E_k$ , (dashed line) and potential energy, $E_p$ , (solid line). (b) The ratio of horizontal kinetic energy to total kinetic energy, $E_{kh}/E_k$ , (dashed line) and the ratio of vertical kinetic energy to total kinetic energy, $E_{vk}/E_k$ , (solid line). (c) The ratio of potential energy to horizontal kinetic energy, $E_p/E_{hk}$ , (dashed line) and the ratio of potential energy to vertical kinetic energy, $E_p/E_{vk}$ (solid line) with turbulent Froude number, $Fr$ . The color indicates different values of initial Richardson number ( $Ri_0$ ). . . . .	69
4.2	Snapshot (2D) of instantaneous density instability at eddy turnover time 5 in the $X$ - $Z$ plain (at $Y = \pi$ ) where, $Z$ is the vertical axis along which linear stratification is imposed. Color from red to blue indicates heavy to lighter fluid respectively. Stratification increases from left panel to right. Black lines indicate isopycnals. . . . .	71
4.3	Contributions of each isotropic dissipation components to the true rate of dissipation of turbulent kinetic energy $\epsilon$ , normalized by $\epsilon$ . . . . .	73
4.4	Contributions of each isotropic density dissipation components to the true rate of dissipation of density variance $\epsilon_\rho$ , normalized by $\epsilon_\rho$ . . . . .	74
4.5	Ratio of $\epsilon(3D)$ to $\epsilon(1D)$ varying with $Re_b(1D)$ . The horizontal line shows that the isotropy assumption is valid. The dashed line shows the empirical relation as provided in 4.8. . . . .	75
5.1	(a) Comparison of nondimensional model eddy diffusivity given by (5.5) with the nondimensional true eddy diffusivity given by (5.2). The dashed line shows the one to one comparison line. (b) Ratio of proposed eddy diffusivity to true eddy diffusivity as a function of the turbulent Froude number $Fr$ . . . . .	80
5.2	The ratio of Ellison length scale $L_E$ to the diapycnal length scale $L_d$ as a function of the turbulent Froude number, $Fr$ . . . . .	81

5.3	The ratio of vertical velocity fluctuation $w'$ to the diapycnal velocity $w_d$ as a function of the turbulent Froude number, $Fr$ . . . . .	82
5.4	a: similar to fig 5.2, b: similar to fig 5.3 for sheared DNS data of Shih <i>et al.</i> (2005). . .	83
5.5	Comparison of predicted diapycnal diffusivity using the refined model given by (5.15) with the true diapycnal diffusivity given by (5.2). The dashed line shows the one-to-one comparison line. . . . .	84
5.6	a:similar to fig 5.1(a), b:similar to fig 5.5 for sheared DNS data of Shih <i>et al.</i> (2005) . .	85
5.7	Turbulent Froude number as a function of overturn Reynolds number. . . . .	87
6.1	Mixing coefficient, $\Gamma$ as a function of turbulent Froude number $Fr$ . The color bar shows values of $Re_b$ . star: decaying DNS; circle: forced DNS of Maffioli <i>et al.</i> (2016). . . . .	97
6.2	Mixing coefficient, $\Gamma$ as a function of turbulent Froude number $Fr$ for sheared DNS of Shih <i>et al.</i> (2005). The color bar shows values of $Re_b$ . . . . .	98
6.3	Relation between Thorpe length scale and Ellison length scale from high resolution DNS data of decaying stably stratified turbulence. . . . .	99
6.4	Relation between Thorpe length scale and Ozmidov length scale from high resolution DNS data of decaying stably stratified turbulence. . . . .	99
6.5	Froude number as a function of $L_E/L_O$ for decaying and forced DNS data. . . . .	100
6.6	Froude number as a function of $L_E/L_O$ for sheared DNS data. . . . .	101
7.1	Validation of Lagrangian statistics and Eulerian statistics for turbulent kinetic energy (TKE, $1/2u_i^2$ ) in (a, c and e) and for density flux ( $\langle \rho'w' \rangle$ ) in (b, d and f). with varying stratification . . . . .	108
7.2	The mean square of the horizontal displacement (a) $\langle \Delta x^2 \rangle$ , (b) $\langle \Delta y^2 \rangle$ and (c) vertical displacement $\langle \Delta z^2 \rangle$ showing ballistic and diffusive region for various $Ri_0$ values. . . . .	109
7.3	Sample particle tracks. . . . .	109
7.4	Mean square of total displacement (solid line), mean square of isopycnal displacement (dashed line) and mean square of diapycnal displacement (dotted line) for different initial Richardson numbers. . . . .	111
7.5	Root mean square of total velocity (solid line), root mean square of isopycnal velocity (dashed line) and root mean square of diapycnal velocity (dotted line) for different initial Richardson numbers. . . . .	112
7.6	Dispersion coefficients for different initial Richardson number. . . . .	113
7.7	Relation between root mean square isopycnal displacement with Ellison length scale for different initial Richardson numbers $Ri_0$ as shown in the legend. . . . .	114
7.8	The ratio or rms diapycnal velocity to rms isopycnal velocity with turbulent Froude number with $Re_b$ in the color bar. . . . .	115
7.9	Left panel: Relation between true diapycnal diffusivity and diapycnal dispersion. Right panel: Relation between true diapycnal diffusivity with modeled diapycnal diffusivity. The Color bar is showing turbulent Froude number. . . . .	115

# Chapter 1

## Introduction

### 1.1 Background and motivation

Turbulence is the most common state of fluid motion occurring in both engineering and nature. The highly intermittent and irregular nature of turbulence makes the study of turbulent flow more challenging. In fact, turbulence is said to be "one of the most unsolved problems to date in classical mathematical physics" (Clay Millennium Prize problem). One should note that turbulence is a property of fluid-flows, not that of fluids. One of the prominent features of turbulence is "mixing" of fluid particles with different properties through the mechanism of "stirring" which disperses the fluid particles and the mechanism of "diffusion" which homogenizes the fluid properties (Thorpe, 2005). The complexity of turbulent flow increases further in geophysical flows such as in ocean, atmosphere and lakes due to the presence of stable stratification. A flow is said to be stably stratified when the density of the fluid increases in the direction of gravitational force (due to decrease of temperature or increase of concentration of salt or moisture etc.). Stable stratification acts as a restoring force and inhibits turbulent motions in the direction of stratification due to the buoyancy force. Hence, the fate of turbulent mixing of momentum and scalar (density, temperature, salinity etc.) as well as, particle dispersion in geophysical flows are governed by both turbulent energy and stratification. Fundamental understanding of turbulent mixing and dispersion in the presence of density stratification is crucial to many applications such as pollutant dispersion models in both air and water bodies, ocean global circulation models, global climate models, global mass/energy budget etc. (Fernando, 1991; Gregg, 1987). The overarching goal of this research is to gain better understanding of turbulent mixing in stratified fluids.

In an un-stratified fluid (such as in river), when disturbed, a fluid particle can move indefinitely in the vertical direction depending on the amount of energy available. But, in a stratified fluid, work has to be done against buoyancy forces to move fluid across isopycnal (constant density) surfaces.

Mixing that involves transfer of fluid across the isopycnal surface (diapycnal direction) is known as diapycnal mixing which is an irreversible process involving density change. The density acts as an active scalar and alters the flow dynamics in a stratified fluid. In the ocean, breaking of internal waves and/or any shear instabilities create turbulence leading to mixing. Mixing happens at the expense of turbulent kinetic energy and results in increasing the background potential energy. In spite of vast amount of research on mixing, one of the biggest challenges in physical oceanography is to quantify how much mixing happens and how to parameterize diapycnal mixing (Gregg *et al.*, 2018; Ivey *et al.*, 2008). Accurate prediction of diapycnal mixing has broad implications. Some important applications include:

- Wind driven ocean currents are generally confined to the upper few 100 meters of the ocean. Ocean currents also flow thousands of meters below the surface. These deep currents are generally driven by global density gradients created by temperature (thermo) and salinity (haline) differences. These deep ocean currents are known as the global thermohaline overturning circulation or Meridional overturning circulation (MOC) (see figure 1.1a), which plays an important role in climate and climate variability by storing and transporting heat, fresh water, and carbon around the globe (Marshall & Speer, 2012). Small scale diapycnal mixing drives the MOC (Boos *et al.*, 2003). Generally the warm, lighter water moves from equator to Nordic and Labrador sea as surface flow and sinks by releasing heat to the atmosphere. The cold, heavier water moves as deep water away from the polar region and upwells towards the equator. Some upwellings are due to wind and confined to shallow depths of upper ocean but deep water upwelling is possible only due to diapycnal mixing. Without deep mixing, the ocean would turn, within a few thousand years, in to a stagnant pool of cold salty water (Munk & Wunsch, 1998).
- Vertical mixing is the only mechanism to transport heat and nutrients across isopycnal surfaces and plays an important role in ocean productivity. Generally nutrient rich water is available below thermocline and sunlight (Euphotic zone) is available above the thermocline as shown in figure 1.1b. Due to strong stratification, the thermocline does not allow wind

driven upwelling. In this sense, small scale vertical mixing is the only way for upwelling of nutrients for the ecosystem to survive (Friederich & Codispoti, 1981).

- The diurnal and seasonal variability of the ocean mixed layer depth (upper tens of meters of the ocean) controls the temperature and heat content of the mixed layer which is a primary factor in air-sea exchange of mass and momentum. The depth of mixed layer is not only a product of wind driven mixing but also is a result of shear driven diapycnal mixing from below the mixed layer (Brannigan, 2013).

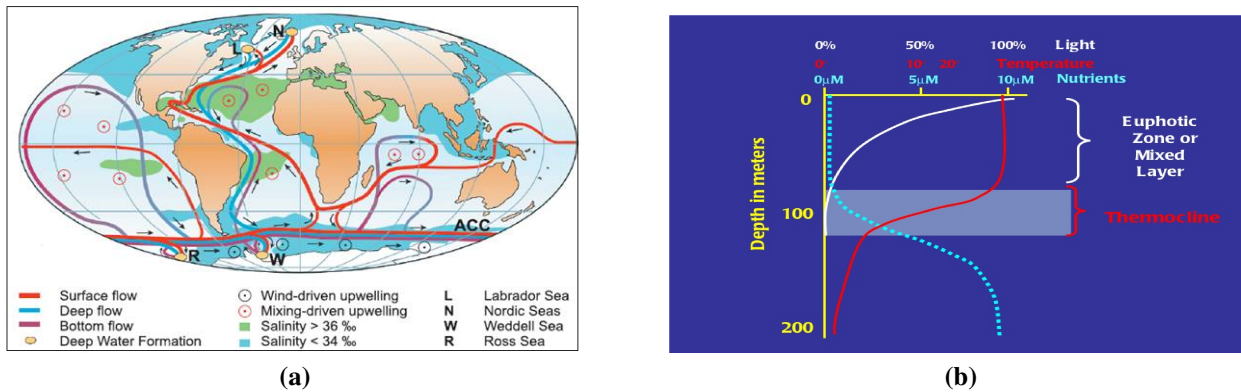


**Figure 1.1:** (a) Schematic of global overturning circulation adapted from (Kuhlbrodt *et al.*, 2007). (b) schematic showing vertical structure of the ocean with nutrients rich deep water (Edgar, 2011).

In geophysical flows such irreversible mixing processes are inherently small scale motions (having magnitudes order of millimeters over small time scales) compared to the large energy inducing scales. Due to the large range of spatial scales involved in turbulent flows, it is challenging to study small processes be it using numerical simulations or observations. Whilst with advancement of technology and instruments such as CTD (Conductivity-Temperature-Depth) profilers, VMP (vertical microstructure profilers) and ADCP (Acoustic Doppler Current Profiler), oceanographers are able to directly measure small scale turbulence quantities such as the rate of dissipation of turbulent kinetic energy  $\epsilon$  (using VMP) or indirectly infer  $\epsilon$  (from CTD), still such measurements are contaminated by noise, use simplifying assumptions (such as isotropy) and lack fine scale resolutions. The effects of physical processes which are too small or too complex or poorly

understood are generally parameterized in the large scale models (such as climate models) that are very sensitive to slightest change in the small scale parameterizations (Richards *et al.*, 2009). Hence it is desirable (for practical reasons) to link small scale mixing events with bulk flow characteristics which are easier to measure. Existing parameterizations do not account for small scale mixing with acceptable accuracy. Furthermore, field measurements do not separate the effect of different forcing mechanisms (e.g., the influence of internal waves) on measured variables. Given such difficulties, direct numerical simulations (DNS) provide an avenue to investigate fundamental understanding of reversible and irreversible mixing, separately considering individual effects of large scale forcing on small scale mixing and hence provide a bridge to close the gap in our current understanding of the physics of small scale mixing. Despite the considerable amount of work that has been done to improve small scale parameterizations the problem is far from being resolved. The best way to improve parameterizations is to understand the physical processes better through observations and high resolution simulations.

To summarize, the specific issues that motivated the undertaking of this dissertation study are

- *Need for better assessment of field data measurements.*
- *Need for better understanding of mixing in stably stratified flows.*
- *Need for improved parameterization of turbulent diapycnal mixing based on physical insights.*
- *Need for providing a recipe to infer mixing in the ocean based on practical methods.*
- *Need for providing appropriate length scales and velocity scales governing diapycnal diffusivity.*

## **1.2 Objectives**

The subject of this dissertation is to investigate the fundamental physics (i.e. small-scale phenomenology) that governs stratified geophysical flows with an emphasis on making practical progress towards improved parameterization of diapycnal mixing. The overarching goal of

this work is to gain a better understanding of stably stratified turbulence by using theory, observational data and numerical models to study and understand the processes in ocean dynamics. The objectives of this research are as follows:

**1. To provide better assessment of microstructure data to determine mixing efficiency.**

Considering the hydrographic and turbulent measurements that are made coincidentally from a field campaign, there are probably a number of (varying) ways to make inferences on oceanic mixing, each subjected to its own specific set of assumptions. The first contribution of this dissertation is an analysis of field data, highlighting different methods to estimate mixing efficiency as discussed in chapter 3. Small scale mixing is generally parameterized with known or measurable quantities. Present state-of-the-art instruments do not measure turbulent quantities with 100% accuracy. For example, the microstructure instrument assumes small scale isotropy (Kolmogorov, 1941) to estimate rates of dissipation of turbulent kinetic energy ( $\epsilon$ ). A discussion on the effect of such an assumption and methodology for possible corrections are presented in chapter 4.

**2. To provide better parameterization of mixing efficiency using reasoning and scaling analysis.**

In spite of a lot of attempts made to parameterize small scale mixing, universal parameterization of mixing efficiency is still elusive. This is because of our lack of understanding of the physics of small scale mixing and ambiguity of different parameters used to parameterize mixing. Through scaling analysis we have shown that mixing efficiency indeed scales with the turbulent Froude number across the full spectrum of stratification. This is discussed in chapter 6.

**3. To determine fundamental length scale and velocity scales that govern small scale diapycnal mixing.**

In chapter 5, true diapycnal length scale and velocity scales are discussed that can be obtained from measurable mixing length scale and characteristic turbulent velocity scale. The separation of isopycnal and diapycnal velocity and length scales are discussed

in chapter 7 from a Lagrangian perspective. A new parameterization for the diapycnal diffusivity is proposed in chapter 5.

4. **To provide an assessment of strength of stratified turbulence in the ocean from measurable length scales.** A diagnostic approach to identify the dynamic state of turbulence in the stratified ocean is presented in chapter 6. This finding will provide oceanographers with a method to determine strength of stratification in the ocean and accordingly use any parameterization of mixing efficiency if, required.

### 1.3 Dissertation layout

This thesis is divided into seven further chapters. The first chapter provides the motivation and objectives of this research. The contents in the chapters 3, 4, 5, 6 and 7 have been written as journal manuscripts (that have either been submitted or will be submitted shortly hereafter) such that they may be read as stand-alone works. As such, some of the concepts presented as introduction and background in these chapters might be repetitive of some of the concepts presented in the literature review. The layout of the remainder of this dissertation is as follows.

- Chapter 2 contains a literature review with a brief discussion of governing equations and background for this study.
- Chapter 3 addresses objective one and provides an assessment of microstructure data analysis to study diapycnal mixing.
- Chapter 4 addresses the fundamental assumption of microstructure instruments and provides a method for correction of measured data.
- Chapter 5 presents a novel method to infer diapycnal diffusivity through scaling analysis, without any parameterization of mixing efficiency.
- Chapter 6 directly addresses objective 3 using direct numerical simulation data where it has been shown that the turbulent Froude number and mixing efficiency can be obtained from measurable length scales in the ocean.

- Chapter 7 addresses the problem of diapycnal diffusivity from a Lagrangian framework which provides a direct approach to separate reversible and irreversible mixing.
- Finally, chapter 8 presents a brief summary of the key findings and the significant contributions of the dissertation with a note for possible future works.

# Chapter 2

## Background and literature review

### 2.1 Geophysical flows

Geophysical flows are the naturally occurring large scale fluid flows on Earth and other planets. The flow dynamics are dominated by the influence of stratification, turbulence and rotation of planetary system. As our interest of study is about small scale dynamics, the rotational effect of earth is ignored. The Earth's atmosphere and the ocean form a coupled system, exchanging heat, momentum and water at the air-sea interface. On the long term, the convergence/divergence of oceanic heat transport provides source/sink of heat for the atmosphere and in this way, the ocean plays significant role in regulating Earth's climate.

In this chapter, a brief discussion of the stratified ocean and its vertical structure is first provided. The governing equations and the numerical methods are then discussed followed by the energetics of small scale diapycnal mixing and its parameterization. A glance at current practice of ocean turbulence measurements is presented to get an overview of available (measurable) parameters for parameterization of mixing.

#### 2.1.1 Stratification and internal waves

Most geophysical flows are affected by density stratification. For example in the ocean, the mean density increases with depth forming a stable stratification. The density of the sea water is related to temperature and salinity through the equation of state (Gill, 1982). The density differences in the stratified flow introduce buoyancy forces. If a small particle of water of density  $\rho$  is displaced vertically from its equilibrium position by a distance  $\eta$ , in a uniform density gradient  $\partial\rho/\partial z$  (where  $z$  is the vertical direction), then the density difference between the particle and its surrounding becomes  $-\eta\partial\rho/\partial z$  and the particle moves upward with an acceleration  $(g\eta)\partial\rho/\partial z$ . If the stratification is unstable,  $\partial\rho/\partial z > 0$ , the net acceleration is positive and the particle moves

away from its initial position. On the other hand, if the fluid is stably stratified as in the ocean,  $\partial\rho/\partial z < 0$ , the particle moves upward, being heavier than surrounding, moves downward, overshoots its equilibrium position and again being lighter than the surrounding moves upward due to buoyancy force. Thus creating a simple harmonic motion described as

$$\frac{\partial^2\eta}{\partial t^2} = g\frac{\partial\rho}{\partial z}\eta. \quad (2.1)$$

The frequency of this oscillation is given as  $N^2 = -(g/\rho_0)\partial\rho/\partial z$ , known as buoyancy frequency. The oscillatory motion created by any disturbance of fluid particles in a stably stratified flow leads to generation of internal waves in the flow. Internal waves move the isopycnals (surfaces of constant density) up and down. When an internal wave breaks (due to shear instability or convective instability), turbulence is generated. Identifying irreversible fluxes due to turbulence from the reversible fluxes due to internal wave is challenging but necessary for the study of turbulent mixing in the ocean.

### 2.1.2 Vertical structure of the ocean

The vertical structure of the ocean is primarily divided into three parts (figure 2.1). The upper part, adjacent to atmospheric boundary layer is known as ocean mixed layer. In the mixed layer, hydrographic properties such as temperature, density, salinity are constant with depth. The water is almost homogeneous with very weak to no stratification. The mixing in upper mixed layer is driven by wind currents, convection, Langmuir circulation and many other processes which are difficult to model. The depth of mixed layer varies spatially and also temporarily. For example the summer time equatorial mixed layer depth couple tens of meter but winter time arctic mixed layer depth goes to thousands of meters.

Just below the mixed layer, strongly stratified regime is present where temperature, density and salinity show a sharp gradient. Most of the internal waves are generated in the thermocline. The thermocline creates a barrier between upper ocean and deep ocean mixing.

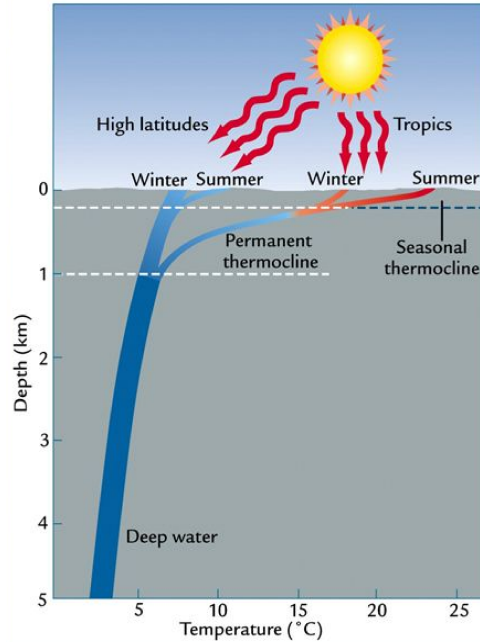


**Figure 2.1:** Vertical structure of the ocean showing spatial and seasonal variation of mixed layer depth and thermocline.

The third part is the deep ocean which extends from below the thermocline to the bottom of the ocean. Deep ocean is weakly stratified. Wide range of research are done to simulate mixed layer depth by parameterizing the vertical fluxes using a slab model or bulk model or one dimensional turbulence model. These models do not provide the true depth since the parameterization of mixing is not accurate in such one dimensional water column models (Belcher *et al.*, 2012).

## 2.2 Governing equations

The equations governing fluid flow motions of geophysical flows are derived from the basic concepts of conservation of mass, conservation momentum and conservation of energy within the continuum hypothesis framework. The three dimensional governing equations for an incompressible, stratified fluid flow with the Boussinesq approximation are discussed in the following sub-sections.

## 2.2.1 Continuity equation

The mass of a given fluid element is defined as density integrated over the volume of fluid element. Total mass of fluid of a given system is conserved i.e. the material rate of change of mass or total derivative of mass following a fluid parcel is zero. Thus the continuity equation (using the Einstein summation convention<sup>1</sup>) from Lagrangian perspective is given as:

$$\frac{D\rho}{Dt} + \rho \frac{\partial u_i}{\partial x_i} = 0, \quad (2.2)$$

where  $D/Dt = \partial/\partial t + u_i(\partial/\partial x_i)$  is the material derivative or total derivative. It involves the sum of local and convective derivatives of an intrinsic property which in this case is the density of the fluid  $\rho$  and  $u_i$  is velocity field. Using the Eulerian reference frame and the well-known concept of a control volume, the Continuity equation can be written as:

$$\frac{\partial \rho}{\partial t} + \frac{\partial(\rho u_i)}{\partial x_i} = 0. \quad (2.3)$$

Evoking the incompressibility assumption (which implies that changes in density due to changes in pressure is negligible), the continuity equation simplifies to

$$\frac{\partial u_i}{\partial x_i} = 0. \quad (2.4)$$

Equation (2.4) implies that the velocity field is divergence free or solenoidal.

## 2.2.2 Momentum or Navier-Stokes Equations

The Conservation of momentum principle given by Newton's second law of motion states that the rate of change of momentum of a system is given by the summation of all the forces acting on the system. Neglecting the effects of the Earth rotation (i.e Rossby number,  $R_o \gg 1$ , note for at larger scales, the Coriolis terms must be included in the momentum equation to account for the

---

<sup>1</sup> $i,j=1, 2, 3$ .  $u_1, u_2$  and  $u_3$  being velocities in  $x_1, x_2$  and  $x_3$  directions respectively.

apparent forces.), the momentum equation or the so called Navier Stokes equations are given as

$$\frac{Du_i}{Dt} = \frac{\partial u_i}{\partial t} + \frac{\partial}{\partial x_i}(u_i u_j) = -\frac{1}{\rho} \frac{\partial p}{\partial x_i} + \nu \frac{\partial^2 u_i}{\partial x_j^2} - g \delta_{i3}, \quad (2.5)$$

where  $\nu$  is molecular kinematic viscosity which is constant,  $\delta_{i3}$  is Kronecker delta<sup>2</sup>,  $p$  is the pressure and  $g$  is acceleration due to gravity. Both the density and pressure can be decomposed into a background and fluctuating components as:  $\rho = \rho_0 + \rho'$  and  $p = p_0 + p'$ , where  $p_0$  is hydrostatic pressure ( $\partial p_0 = -\rho_0 g \partial z$ ). Substituting these decomposition into equation (2.5) and noting that  $\rho'/\rho_0 \ll 1$  in most geophysical flows, yields

$$\frac{Du_i}{Dt} = -\frac{\partial p'}{\rho_0 \partial x_i} + \nu \frac{\partial^2 u_i}{\partial x_j^2} - g \frac{\rho'}{\rho_0} \delta_{i3}. \quad (2.6)$$

Equation (2.6) implies that density variations are negligible except in the gravity term, an approximation that is referred to as the Boussinesq approximation. Note in equation (2.6),  $g\rho'/\rho_0$  is the reduced gravity or buoyancy term.

### 2.2.3 Scalar transport equation

In stratified flows, the density acts as an active scalar as highlighted by the buoyancy term in equation (2.6). Hence, the scalar transport equation for the density is dynamically coupled to the momentum equation and must be solved concurrently. The density transport equation is given as

$$\frac{D\rho}{Dt} = \frac{D\rho'}{Dt} = \frac{\partial \rho'}{\partial t} + \frac{\partial}{\partial x_j}(\rho' u_j) = \kappa \frac{\partial^2 \rho'}{\partial x_j^2}, \quad (2.7)$$

where  $\kappa$  is the molecular diffusivity.

---

<sup>2</sup> $\delta_{ij} = 1$  (if  $i = j$ ) and  $\delta_{ij} = 0$  (if  $i \neq j$ ) for  $i, j = 1, 2$  and  $3$

## 2.3 Scales of motion

### 2.3.1 Global length and time scale

Weather processes and climate variability are analyzed with vast range of spatial and temporal scales. In order from large to small, these scales are global scale, synoptic scale, meso scale and microscale based on idea put forward by Orlanski (1975). The events with spatial and temporal scales for each of these scales are shown in figure 2.2. The length scales and time scales for the big events like climate are much larger than the length scales and time scales of turbulence. Largest eddies ( $\mathcal{L}$ ) happen in the range of micro scales. Another scale orders of magnitude smaller than micro scale is known as fine scale (few of orders of magnitude higher than molecular scale), where oceanic turbulence measurements are done. The small scale effects are generally parameterized in the large scale models. Accuracy of large scale models directly depends on the how efficiently these small scale effects are parameterized.

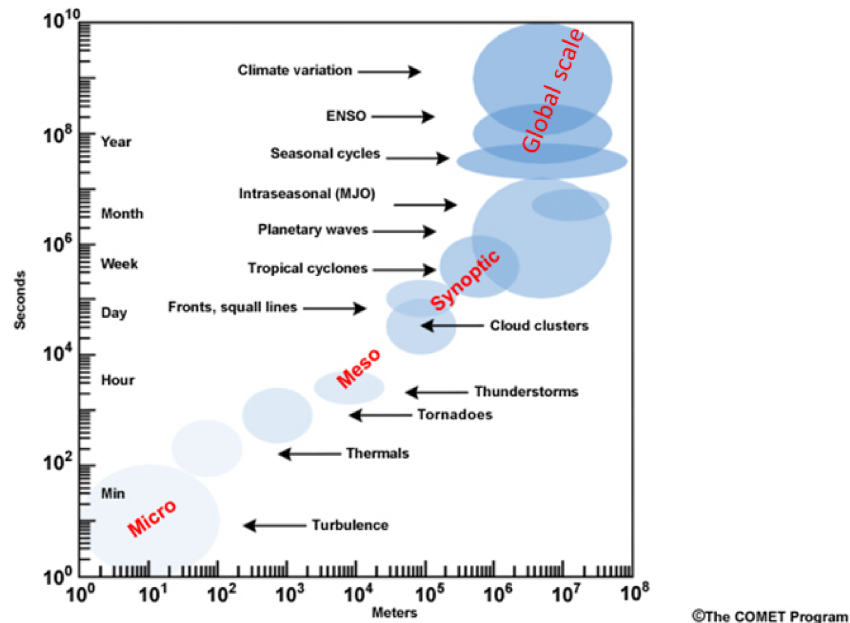


**Figure 2.2:** The range of temporal and spatial scales involved in processes of the tropical climate. Image courtesy of MetEd, The COMET Program, UCAR.

### 2.3.2 Scales of turbulence

Turbulent motions occur over wide range of length and time scales. The size of largest eddy, say,  $\mathcal{L}$  is generally constrained through the physical boundary of the entire system. The region occupied by large eddy also contain smaller eddies. Turbulent kinetic energy is supplied to the turbulent field at the largest eddies. The largest eddy in the flow account for most of the transport of momentum and energy. The energy is generally cascaded to smaller eddies until viscosity dissipates the kinetic energy to heat or internal energy at the smallest scales. The size of smallest eddy, say  $\eta$  is generally determined by viscosity. Richardson (1922) summarized the energy cascade as follows:

Big whorls have little whorls,  
Which feed on their velocity;  
And little whorls have lessor whorls,  
And so on to viscosity  
(in the molecular sense).

Turbulence is generally quantified through a Reynolds number,  $Re = \mathcal{U}\mathcal{L}/\nu$ , where  $\mathcal{L}$  is characteristic length scale and  $\mathcal{U}$  is characteristic velocity scale and  $\nu$  is kinematic viscosity. A complete universal theory of turbulence is still an open problem despite of the vast amount of research on this topic. The fundamental understanding in this field is mostly based on statistical approach with the assumption of homogeneous, stationary and isotropic turbulence which are obviously gross oversimplifications. The modern turbulence theory is based on Kolmogorov's hypotheses (Kolmogorov, 1941) which essentially highlights the existence of three regimes at very high Reynolds number equilibrium flows (i.e. statistically stationary). These are namely: the energy containing range, inertial subrange where the inertial transfer of energy is said to occur and the dissipation range where energy is dissipated (figure 2.3). The dissipation range and inertial subrange together are known as the universal equilibrium range where small scale turbulence are statistically isotropic (statistically invariant under translation). In the universal range, Kolmogorov hypothesized that the statistics are universally determined by only two parameters, the rate of dis-

sipation of turbulent kinetic energy,  $\epsilon$  and viscosity,  $\nu$ . Kolmogorov did not take into consideration the large energy containing scale nor the mechanism of energy cascade. He further postulated that the energy transfer from large eddies to smallest eddies in the inertial subrange depends only on  $\epsilon$  independent of  $\nu$  and that the dissipation of energy in dissipative subrange only depends on  $\nu$ . Distribution of turbulent kinetic energy among eddies of different sizes are generally described in wave number space. Length scale of any eddy  $l$  is related to wave number  $\hat{k}$  as  $\hat{k} = 2\pi/l$ . The energy spectrum scales with  $\epsilon$  and  $\hat{k}$ . For homogeneous turbulence, the energy spectrum in the inertial subrange can be easily derived based on dimensional reasoning as

$$E(\hat{k}) = C\epsilon^{2/3}\hat{k}^{-5/3}, \quad (2.8)$$

where  $C \approx 1.5$  is considered to be a universal constant (Sreenivasan, 1995). This is the famous  $-5/3$  Kolmogorov law and is considered as a signature feature for assessing whether a flow is turbulent or not.

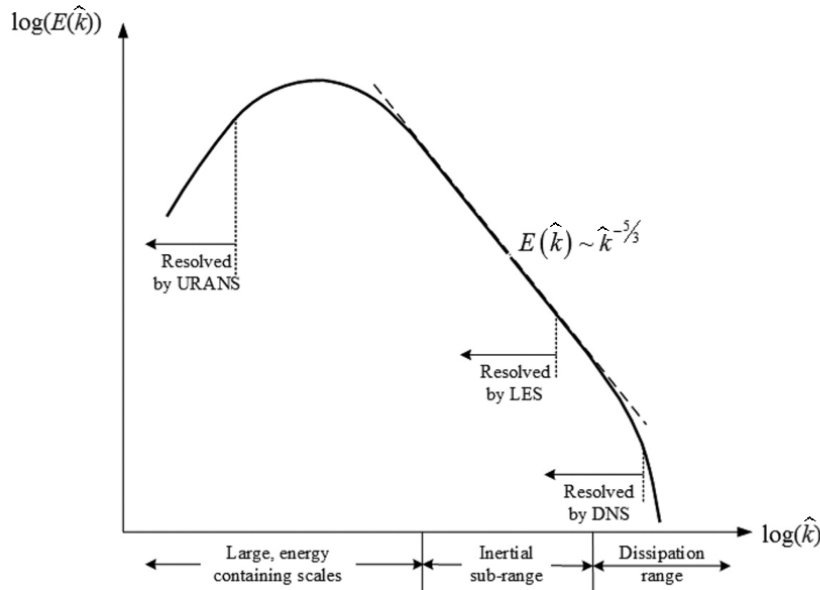


**Figure 2.3:** Typical energy spectrum for a turbulent flow plotted against wave number ( $\hat{k}$ ) (Thompson *et al.*, 2015). URANS, LES and DNS are the numerical methods described in section 2.4

The characteristic small scales (length ( $\eta$ ), velocity ( $u_\eta$ ) and time ( $\tau_\eta$ )) known as Kolmogorov scales (Pope 2000) are defined as

$$\eta \equiv (\nu^3/\epsilon)^{1/4}, \quad (2.9)$$

$$u_\eta \equiv (\nu\epsilon)^{1/4}, \quad (2.10)$$

$$\tau_\eta \equiv (\nu/\epsilon)^{1/2}. \quad (2.11)$$

The turbulent kinetic energy ( $k$ ) at large scales are generated by mean shear and hence the characteristics velocity scale at large scale is comparable to square root of turbulent kinetic energy. Turbulent kinetic energy is dissipated at a rate  $\epsilon$  from which a time scale can be obtained as the ratio of turbulent kinetic energy to rate of dissipation of turbulent kinetic energy. Hence the characteristic scales (velocity scale ( $u_k$ ), length scale ( $L_{k\epsilon}$ ) and time scale ( $T_L$ )) for the largest eddy (Durbin & Petterson-Reif, 2011) are defined as

$$u_k \equiv k^{1/2}, \quad (2.12)$$

$$L_{k\epsilon} \equiv k^{3/2}/\epsilon, \quad (2.13)$$

$$T_L \equiv k/\epsilon. \quad (2.14)$$

A corresponding turbulent Reynolds number can be defined as  $Re_T = k^2/(\nu\epsilon)$ . It should be noted that the precise mechanism(s) by which energy transfer occurs from large scale to small scale is still unknown. Also, it should be noted that Kolmogorov scales are derived by considering small scale isotropy without any consideration for the effect of any mean shear, stratification or rotation that may exist at smaller scales. Excellent reviews on fundamental turbulence theory can be found in Pope (2000) and Durbin & Petterson-Reif (2011).

### 2.3.3 Scales of stratified turbulence

An important length scales in stably stratified geophysical flows is the buoyancy scale defined as

$$L_b = (\langle w'^2 \rangle)^{1/2} / N, \quad (2.15)$$

where  $w'$  is vertical velocity fluctuation.  $L_b$  is indicative of maximum possible vertical displacement for given  $N$  at which all the vertical kinetic energy of an eddy is converted to potential energy by working against buoyancy force. From dimensional reasoning, analogous to the Corrsin length scale, Ozmidov (1965) proposed a length scale for stratified flows at which buoyancy effects are strongly felt by turbulent flows given by

$$L_O = \left( \frac{\epsilon}{N^3} \right)^{1/2}. \quad (2.16)$$

$L_O$  is also known as the largest isotropic vertical scale of motion that can exist in a stratified flow.

### 2.3.4 Scales of turbulent scalar field

Another length scale that is often used as a measure of overturns is the Ellison length scale (Ellison, 1957) defined as

$$L_E = \frac{\langle \rho'^2 \rangle^{1/2}}{\partial \langle \rho \rangle / \partial z}, \quad (2.17)$$

where  $\partial \langle \rho \rangle / \partial z$  is the background mean gradient of density and  $\langle \rho' \rangle$  is the root mean square density fluctuation. In the ocean and lakes, overturn lengths can be calculated from measured density profiles through a sorting method originally proposed by Thorpe (1977). This kinematic scale is known as the Thorpe length scale. If an overturn exists, a measured instantaneous density profile must not be in equilibrium. Thorpe therefore resorted the instantaneous density profile in an ascending order with depth and calculated the vertical displacement  $\delta_T$  associated with each measured value to a gravitationally stable resorted profile. For a given overturning region, the Thorpe scale is calculated as root mean square displacement for that region as follows:

$$L_T = \langle \delta_T^2 \rangle^{1/2}. \quad (2.18)$$

For a linearly stratified fluid, the Thorpe length scale and Ellison length scale are considered to be same (Smyth *et al.*, 2001). However, Cimattoribus *et al.* (2014) using measurements of temperature variance from moored thermistor chains, found that the Thorpe scale is likely to be time dependent and hence a strong correlation between  $L_T$  and  $L_E$  was found to hold for sufficiently high time resolution in deep ocean turbulence.

## 2.4 Numerical methodology

Analytical solutions of the three dimensional Navier-Stokes equations are impossible due to the nonlinear nature of the equations. Hence, numerical methods are used to solve the governing equations for fluid flows. The three main numerical simulations methods for turbulent flows are Direct Numerical Simulations (DNS), Large Eddy Simulations (LES) and Reynolds Average Navier Stokes (RANS) simulations. DNS resolves all spatial and temporal scales of motion and solves the whole flow field without need for any small scale parameterizations (figure 2.3). LES uses spatial averages and solves the flow field for the largest eddies and uses a turbulence model for small scales. RANS (or URANS: Unsteady-RANS ) uses time average (or ensemble average) to solve for mean flow field (mean velocity, mean pressure) and uses turbulence closure schemes (figure 2.3). LES system is not discussed in this dissertation. DNS is most accurate and also considered to be expensive in terms of computational cost and memory of the system. The cost increases with increasing of Reynolds number of the flow as the scale separation of large length scale and small length scale increases. RANS is less accurate and least expensive numerical method. DNS resolves 100% turbulence and RANS uses 100% turbulence modeling. Large scale climate models and ocean circulation models rely on RANS or LES type simulations. The accuracy of RANS simulations can be increased with better and improved small scale parameterizations for turbulence closure models. The comparison of these numerical methods in terms of cost and accuracy is shown in fig 2.3.

### 2.4.1 Direct numerical simulation (DNS)

Direct Numerical Simulation (DNS) solves Navier stokes equations (equations 2.4, 2.6, 2.7) to obtain instantaneous flow fields by resolving all the scales of motion from energy containing largest eddy length scale  $l$  to smallest kolmogorov length scale  $\eta$  at which energy dissipation occurs in molecular level (figure 2.3). This is conceptually the simplest numerical approach and more accurate compared to other methods. The ratio of largest to smallest length scale is given as  $l/\eta \approx Re^{3/4}$  where  $Re$  is the Reynolds number of the flow. For 3-Dimensional flow  $l/\eta \approx Re^{9/4}$ . Hence with increase of Reynolds number of flow, computational cost in terms of CPU memory and time increases drastically in order to resolve both large and small scales making DNS not feasible for high Reynolds number flows. In order to make DNS feasible for higher Reynolds number flows different approaches such as Pseudo-spectral method, low wave number forcing, hyper viscosity etc. have been implemented. In this research only the pseudo-spectral method is discussed.

#### Pseudo-spectral method

Pseudo spectral methods (Orszag & Patterson, 1972) are preferred DNS scheme for homogeneous isotropic decaying turbulence because of their high accuracy. In this method the solution domain is a cube of side  $L$  and velocity field  $\mathbf{u}(\mathbf{x}, t)$  is represented by finite Fourier series as  $\mathbf{u}(\mathbf{x}, t) = \sum e^{i\kappa \cdot \mathbf{x}} \hat{\mathbf{u}}(\mathbf{x}, t)$  in  $N^3$  wave number space where  $\kappa$  is wave number and  $N$  is size of simulation which determines maximum attainable turbulent Reynolds number for the simulation by  $N \sim 1.6Re^{3/4}$  (Pope, 2000). In spectral method with Fast Fourier transform, the non-linear terms of Navier Stokes equations are solved in physical space and linear terms in wave space to reduce the computational cost from  $N^6$  operations to  $N^3 \log N$  operations. Considering all aspects of pseudo-spectral method Rogallo (1981) developed a DNS code for homogeneous isotropic decaying turbulence and Riley, Melcalfe & Weissman (Riley *et al.*, 1981) then extended Rogallo's DNS code for stably stratified homogeneous decaying turbulence. This code is used for the present study.

## 2.4.2 Reynolds average Navier Stokes (RANS) equations

Reynolds Averaged Navier-Stokes (RANS) equations are best suited for engineering application due to less computational cost. In this method the instantaneous quantities are decomposed into mean and turbulent part by Reynolds decomposition (Reynolds, 1895). Reynolds decomposed instantaneous velocity, pressure and density fields are

$$u_i = \langle U_i \rangle + u'_i, \quad p = \langle p \rangle + p', \quad \rho = \langle \rho \rangle + \rho', \quad (2.19)$$

where  $\langle \rangle$  is ensemble or temporal average and  $'$  indicate fluctuating quantity. Applying Reynolds decomposition to governing equations (2.4), (2.6) and (2.7) Reynolds-averaged Navier-Stokes equations are derived as

$$\frac{\partial \langle U_i \rangle}{\partial x_i} = 0, \quad (2.20)$$

$$\frac{D \langle U_i \rangle}{Dt} = -\frac{1}{\rho_0} \frac{\partial \langle p \rangle}{\partial x_i} - \frac{\langle \rho \rangle}{\rho_0} g \delta_{i3} + \frac{\partial}{\partial x_j} \left[ \nu \frac{\partial \langle U_i \rangle}{\partial x_j} - \langle u'_i u'_j \rangle \right], \quad (2.21)$$

$$\frac{D \langle \rho \rangle}{Dt} = \frac{\partial}{\partial x_j} \left[ \kappa \frac{\partial \langle \rho \rangle}{\partial x_j} - \langle u'_j \rho' \rangle \right]. \quad (2.22)$$

These equations are analogues to instantaneous governing equation except for the additional turbulent fluctuation terms  $-\langle u'_i u'_j \rangle$  and  $-\langle u'_j \rho' \rangle$  in equations (2.21) and (2.22) known as Reynolds stress tensor or momentum flux, and turbulent density flux respectively. These two terms include extra nine unknown variables in three-dimensional RANS equations; six from the Reynolds stress tensor and three for the turbulent scalar fluxes, creating an in-determinant system of equations commonly known as the closure problem. Turbulent viscosity hypothesis and gradient diffusion hypothesis (Pope, 2000) are generally used to solve the closure problem which reduce the number of unknown variables. According to gradient diffusion hypothesis, the turbulent transport of scalar flux  $\langle u'_j \rho' \rangle$  is down the mean scalar gradient and is given as

$$-\langle u'_j \rho' \rangle = \kappa_t \frac{\partial \langle \rho \rangle}{\partial x_j}, \quad (2.23)$$

where  $\kappa_t$  is eddy diffusivity that generally varies between molecular diffusivity of the scalar to few orders of magnitude higher than molecular diffusivity. According to turbulent viscosity hypothesis which is analogous to stress-rate of strain relationship of Newtonian fluid, deviatoric Reynolds stress is given as

$$-\langle u'_i u'_j \rangle + \frac{2}{3} k \delta_{ij} = \nu_t \left( \frac{\partial \langle U_i \rangle}{\partial x_j} + \frac{\partial \langle U_j \rangle}{\partial x_i} \right) = 2\nu_t \langle S_{ij} \rangle, \quad (2.24)$$

where  $\nu_t$  is eddy viscosity,  $k = 1/2 u_i'^2$  is turbulent kinetic energy. Now the closure problem can be solved by determining eddy viscosity and eddy diffusivity via turbulence modeling. Eddy viscosity and eddy diffusivity are related by turbulent Prandtl (Schmidt) number

$$Pr_t = \frac{\nu_t}{\kappa_t}. \quad (2.25)$$

In turbulence modeling generally  $\nu_t$  and  $Pr_t$  are modeled and then  $\kappa_t$  is calculated. Accuracy of RANS simulations depend on how efficiently these variables are predicted.

### 2.4.3 Parameterization of turbulence/Turbulent closure models

Vast amount of research have been done on turbulence modeling for unstratified flows. Different turbulent models to model  $\nu_t$  range from zero equation model or algebraic model to one equation models to two equation models (Pope, 2000). A widely used two equation model is standard  $k - \epsilon$  closure model (Jones & Launder, 1972) which solves the transport equation of turbulent kinetic energy per unit mass  $k$  (equation 2.28) and rate of dissipation of turbulent kinetic energy  $\epsilon = k/t$  (equation 2.30 ) for prediction of  $\nu_t$  as  $\nu_t = (1 - R_f) C_\mu \frac{k^2}{\epsilon}$ , where  $R_f = -B/P$  is flux Richardson number which is ratio of buoyancy flux (B) and production of turbulent kinetic energy (P) (Detail is discussed in §2.5.1).  $C_\mu$  is turbulent viscosity parameter which is calibrated from experimental and DNS data to be 0.09 (Kim *et al.*, 1987). This closure method fails to account for effect of stratification. For stratified flow eddy viscosity and eddy diffusivity which define mixing and diffusion, need to be parameterized properly to give right level of both momentum and

scalar mixing. For stably stratified flows turbulent Prandtl number is not constant and accounts for stratification in terms of gradient Richardson number  $Ri_g$  and usually parameterized for homogeneous shear flow (Schumann & Gerz, 1995; Venayagamoorthy & Stretch, 2010) or to account inhomogeneity of flow (Karimpour & Venayagamoorthy, 2014).

For one dimensional shear flows, the vertical momentum ( $\langle u'w' \rangle$ ) and scalar fluxes ( $\langle \rho'w' \rangle$ ) are modeled with vertical eddy diffusivity of momentum  $K_m$  and eddy diffusivity of scalar (density),  $K_\rho$  with respective mean background gradients as

$$K_m = -\frac{\langle u'w' \rangle}{\partial \langle u \rangle / \partial z}, \quad (2.26)$$

$$K_\rho = -\frac{\langle \rho'w' \rangle}{\partial \langle \rho \rangle / \partial z}. \quad (2.27)$$

Mixing in the ocean is typically predicted by parameterizing true eddy diffusivity for stratified turbulence using observational data and numerical simulations.

## 2.5 Energetics of stratified turbulence

Energetics of turbulence is generally expressed through turbulent kinetic energy (TKE) and modeled through the TKE budget equation (2.28). Stratification acts as a stabilizing force in a turbulent flow making it less energetic. For a stratified turbulent flow, any fluid disturbance resulting from turbulent kinetic energy creates buoyant restoring force. There is an energy conversion from turbulent kinetic energy to potential energy resulting farther from its point of origination. This controls the energy budget of stratified flows, specially in ocean and atmosphere where turbulence is often initiated and driven by the breakdown of internal waves (Winters *et al.*, 1995). The mixing or the change of density of a fluid particle is related to increase in background potential energy. Following Lorenz's concept of available potential energy Winters *et al.* (1995) provided a conceptual framework describing energetics of density stratified Boussinesq fluid flow which is summarized in the schematic shown in figure 2.4. In a stably stratified flow, The available potential energy (APE) is the energy released if the fluids were adiabatically rearranged to the state of

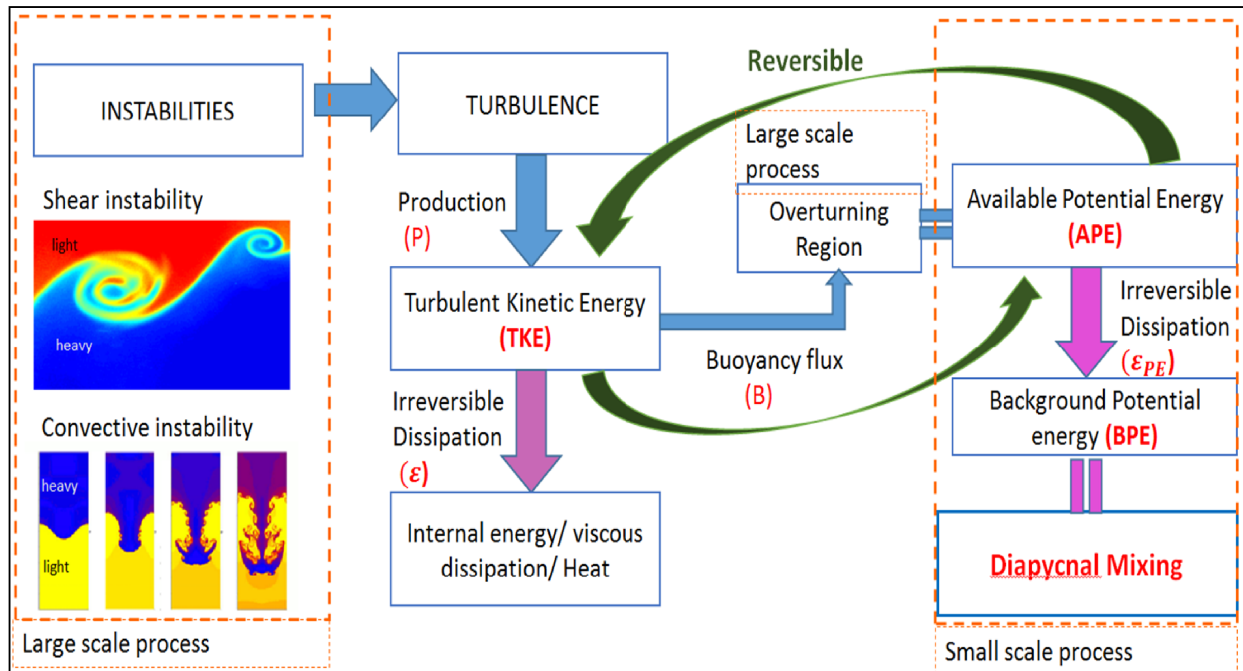


**Figure 2.4:** Schematic showing energetics of diapycnal mixing

minimum potential energy. In oceanic flows, the turbulence is generated due to shear instability or convective instability creating an overturn which increases the available potential energy at the expense of turbulent kinetic energy. Some portion of turbulent kinetic energy gets dissipated to internal energy,  $\epsilon$  and the rest of kinetic energy is used to create an overturn thereby raising its potential energy. When the overturn collapses, some of the potential energy gets converted back to turbulent kinetic energy and in this way there is a portion of energy which relates turbulent kinetic energy to available potential energy in a reversible manner through buoyancy flux. A part of available potential energy is used for mixing of fluid which alters the background potential energy which is an irreversible process. The energy that is irreversibly converted to background potential energy is a measure of diapycnal mixing. The equations for the energetics of diapycnal mixing are described below.

### 2.5.1 Turbulent Kinetic energy

The turbulent kinetic energy (TKE) is given as the sum of the isotropic Reynolds stress terms as  $k = \frac{1}{2}(u_i^2)$ . The evolution equation of  $k$  is obtained from momentum equations of fluctuating

velocity field by taking their dot product with  $1/2u_i$  and is given as follow:

$$\begin{aligned} \frac{Dk}{Dt} = \frac{\partial k}{\partial t} + \langle U_j \rangle \frac{\partial k}{\partial x_j} = & -\langle u'_i u'_j \rangle \frac{\partial \langle U_i \rangle}{\partial x_j} - \nu \langle \frac{\partial u'_i}{\partial x_j} \frac{\partial u'_i}{\partial x_j} \rangle - \frac{g}{\rho_0} \langle \rho' u'_j \rangle \delta_{i3} \\ & + \nu \frac{\partial^2 k}{\partial x_j^2} + \frac{\partial \langle k u'_j \rangle}{\partial x_j} - \frac{1}{\rho_0} \frac{\partial \langle u'_i p' \rangle}{\partial x_j}. \end{aligned} \quad (2.28)$$

The first three terms on the right hand side of equation (2.28) are the production  $P$  of TKE, the rate of dissipation of turbulent kinetic energy  $\epsilon$  and the buoyancy flux  $B$  respectively, The last three terms are the molecular viscous transport of TKE, turbulent transport of TKE and the pressure diffusion of TKE, respectively. These terms are in general small compared to the first three terms in flows where inhomogeneities arising from for example wall effects are negligible. For a statistically homogeneous turbulent flows the turbulent kinetic energy equation can be written as

$$\frac{\partial k}{\partial t} = P + B - \epsilon. \quad (2.29)$$

In a decaying turbulent flow (i.e. in the absence of mean shear) there is no production, hence,  $\partial k / \partial t = B - \epsilon$ . The buoyancy flux term indicates the reversible conversion of turbulent kinetic into turbulent potential energy (TPE) or vice versa. In stably stratified flows the negative buoyancy flux indicates that TKE is lost to TPE. It should be noted that some of the TPE is reversible in the sense that it can reconvert to TKE in a wave dominated environment. Some of the TPE that is fed via the buoyancy flux will be converted to the background potential energy due to diapycnal mixing.

## 2.5.2 Turbulent Potential Energy

The mean turbulent potential energy per unit mass in a stably stratified flow is given as

$$E_p = - \left\langle \frac{g}{\rho_0} \int \rho' dz \right\rangle = - \frac{g}{\rho_0} \left( \frac{\partial \langle \rho \rangle}{\partial z} \right)^{-1} \frac{1}{2} \langle \rho'^2 \rangle = N^2 \left( \frac{\partial \langle \rho \rangle}{\partial z} \right)^{-2} \frac{1}{2} \langle \rho'^2 \rangle, \quad (2.30)$$

where  $N$  is the buoyancy frequency with which a fluid parcel oscillates about its equilibrium position in the background stratification and is defined as  $N^2 = (-g/\rho_o)(\partial\langle\rho\rangle/\partial z)$ . Equation (2.30) is derived by considering the average density fluctuation  $\rho'$  to be a function of vertical displacement  $z'$  from the stable position along a background density gradient  $\langle\rho\rangle/\partial z$ . The density variance equation can be derived as

$$\frac{\partial\langle\frac{1}{2}\rho'^2\rangle}{\partial t} + \langle U_i \rangle \frac{\partial\langle\frac{1}{2}\rho'^2\rangle}{\partial x_j} = -\langle u'_j \rho' \rangle \frac{\partial\rho}{\partial x_j} + \kappa_\rho \frac{\partial^2\langle\frac{1}{2}\rho'^2\rangle}{\partial x_j^2} - \frac{\partial\langle u_j(1/2)\rho'^2 \rangle}{\partial x_j} - \kappa_\rho \left\langle \frac{\partial\rho'}{\partial x_j} \frac{\partial\rho'}{\partial x_j} \right\rangle. \quad (2.31)$$

The first term on the right hand side of equation (2.31) is the production of scalar variance and the last term is the dissipation of density variance  $\epsilon_\rho$ . The second and third terms are molecular and turbulent transport terms and can be neglected if the flow is homogeneous. Hence for a homogeneous flow, the turbulent potential energy equation can be obtained by multiplying equation (2.31) with  $N^2(\partial\langle\rho\rangle/\partial z)^{-2}$  to get:

$$\frac{\partial E_P}{\partial t} = \frac{g}{\rho_o} \langle u'_j \rho' \rangle \delta_{j3} - N^2 \kappa_\rho \left\langle \frac{\partial\rho'}{\partial x_j} \frac{\partial\rho'}{\partial x_j} \right\rangle \left( \frac{\partial\langle\rho\rangle}{\partial z} \right)^{-2}. \quad (2.32)$$

In equation (2.32) the first term on the right hand side is the buoyancy flux ( $u'_j \delta_{j3}$  represents vertical velocity fluctuation  $w'$ ),  $B = g/\rho_o \langle w' \rho' \rangle$  and the second term is the potential energy dissipation  $\epsilon_{PE}$  which represents the irreversible conversion of turbulent potential energy to background potential energy and provides a measure of diapycnal mixing. It is evident that the buoyancy flux term links the turbulent kinetic energy evolution equation (equation 2.28) and the turbulent potential energy evolution equation (2.32).

## 2.6 Diapycnal mixing

In a stratified turbulent flow, mixing of fluid with different densities across the isopycnal (constant density) is termed as diapycnal mixing which is an irreversible process. Diapycnal mixing is strongly influenced by stratification in geophysical flows as more turbulent kinetic energy is needed to displace water over a strong density gradient. Small scale turbulent mixing is generally

represented by a turbulent (eddy) diffusivity. The diapycnal eddy diffusivity of mass is defined as

$$K_\rho = \frac{\epsilon_\rho}{\partial\langle\rho\rangle/\partial z}, \quad (2.33)$$

is the true measure of irreversible mixing of density (Venayagamoorthy & Stretch, 2010; Winters & D'Asaro, 1996).

Towards the context of measurement in oceanography with current (state-of-the-art) sensors,  $\epsilon_\rho$  is not a measurable quantity. But with small scale isotropic assumption,  $\epsilon$  and rate of dissipation of thermal variance,  $\chi$  can be measured in a vertical profile manner in the ocean. To obtain the vertical eddy diffusivity for oceanic flows, (Osborn, 1980) provided the following equation for homogeneous stationary turbulence,

$$K_\rho = \Gamma \frac{\epsilon}{N^2}, \quad (2.34)$$

where  $\Gamma = R_f/(1 + R_f)$  is the mixing coefficient and  $R_f$  is mixing efficiency defined in the following section (2.6.1). From the stationary and homogeneous scalar (temperature) transport equation, (Osborn & Cox, 1972) defined eddy diffusivity of temperature variance as

$$K_T = \frac{\chi}{2\partial\langle T\rangle/\partial z}. \quad (2.35)$$

## 2.6.1 Mixing efficiency

The flux Richardson number  $R_f$ , also known as the mixing efficiency is defined as the ratio of buoyancy flux,  $B = g/\rho_0\langle\rho'w'\rangle$  and rate of production of turbulent kinetic energy,  $P = \langle u'w'\rangle (d\langle U\rangle/dz)$  (section 2.5),

$$R_f = B/P. \quad (2.36)$$

The above equations are obtained by considering the simplest type of flow i.e., flow is stationary and homogeneous. Considering inhomogeneity in to flow Ivey & Imberger (1991) defined mixing efficiency as

$$R_f = B/B + \epsilon, \quad (2.37)$$

where,  $B + \epsilon$  represents the net mechanical energy required to sustain turbulent motions which include advection, production and transport of turbulent kinetic energy (equation 2.28). For an equilibrium condition or homogeneous case  $P = B + \epsilon$ . Both the above definitions of flux Richardson number or mixing efficiency contain counter gradient flux. It is not possible to separate the reversible (flux due to wave action in stratified flows) and irreversible (i.e. mixing: due to pure turbulent motion in stratified flows) fluxes. Whether the flow is stationary or not, the irreversible transfer of kinetic energy and density are still (locally) correctly represented by rate of dissipation of turbulent kinetic energy,  $\epsilon$  and rate of dissipation of density variance,  $\epsilon_\rho$ . Thus the flux Richardson number representing irreversible mixing is defined as

$$R_f = \frac{\epsilon_{PE}}{\epsilon_{PE} + \epsilon}, \quad (2.38)$$

where,  $\epsilon_{PE} = N^2 \epsilon_\rho (\partial \langle \rho \rangle / \partial z)^{-2}$  is the rate of dissipation of turbulent potential energy (eqn). This definition has been suggested by Peltier & Caulfield (2003) and Venayagamoorthy & Stretch (2010) from independent works. In a recent study, Venayagamoorthy & Koseff (2016) suggested that there is nearly no difference between any of the above three definitions of mixing efficiency for a stationary homogeneous shear dominated stratified turbulence defined with gradient Richardson number  $Ri_g \leq 0.25$ . With increase of stratification, irreversible flux Richardson number is the only positive definite definition representing diapycnal mixing. In the context of this thesis, we imply that  $R_f$  and  $\Gamma$  as irreversible mixing efficiency and irreversible mixing coefficient, respectively, unless otherwise mentioned. Thus,  $\Gamma$  can also be defined as  $\Gamma = \epsilon_{PE} / \epsilon$ . Note that  $\epsilon_{PE}$  and  $\epsilon$  are true measures of irreversible loss of energy.

## 2.6.2 Parameterization of $R_f$ or $\Gamma$

$\Gamma$  is typically considered to have a canonical constant value of 0.2 ( $R_f \approx 0.17$ ) (Osborn, 1980). It should be noted that the constancy of  $\Gamma$  has been the subject of extensive debate and a universal parameterization of  $\Gamma$  still remains elusive (Gregg *et al.*, 2018; Mater & Venayagamoorthy, 2014). Common non-dimensional parameters used for parameterization of mixing efficiency are, buoy-

ancy Reynolds number  $Re_b$ , gradient Richardson number  $Ri_g$  and turbulent Froude number  $Fr$ , defined as

$$Re_b = \epsilon/\nu N^2, \quad Ri_g = N^2/S^2 \text{ and } Fr = \epsilon/Nk, \quad (2.39)$$

where,  $\nu$  is the kinematic viscosity,  $S$  is the mean shear and  $k$  is the turbulent kinetic energy.

Direct numerical simulation of sheared stratified turbulence suggests that  $\Gamma \propto Re_b^{-1/2}$  for  $Re_b > \mathcal{O}(100)$ , corresponding to shear dominated or energetic flow (Salehipour & Peltier, 2015; Shih *et al.*, 2005). Similar scaling was found by Lozovatsky & Fernando (2012) for atmospheric flow but for higher range of  $Re_b > \mathcal{O}(10^4)$ . From experimental data Barry *et al.* (2001) suggested that  $\Gamma \propto Re_b^{-2/3}$  for  $Re_b > 300$ . Using a  $Re_b - Ri_g$  parameter space, Salehipour *et al.* (2016) found a non-monotonic relation between  $\Gamma$  and  $Re_b$ . Such a dependence is not surprising given the ambiguity inherent in  $Re_b$  which attempts to capture the competition between inertial, buoyancy and viscous forces. Hence, for  $Re_b$  based parameterizations, decrease in mixing coefficient with increase in  $Re_b$  can be considered as an artifact of low stratification.

From a scaling analysis, Maffioli *et al.* (2016) suggested that in the limit of high turbulent Froude number,  $\Gamma = \epsilon_{PE}/\epsilon \sim Fr^{-2}$  consistent with other experimental studies of Holford & Linden (1999); Ivey & Imberger (1991); Linden (1980); Strange & Fernando (2001). However in the limit of low  $Fr$  which represents strongly stratified fluid, Maffioli *et al.* (2016) found that  $\Gamma$  approaches a constant value of  $\sim 0.3$  decreasing from a peak value of  $\sim 0.5$  at  $Fr \sim \mathcal{O}(1)$ , inconsistent with the experimental results where  $\Gamma$  was found to decrease to zero in the limit of low  $Fr$  (Wells *et al.*, 2010). This is because, the experimental data have considered  $\Gamma = B/\epsilon$  which is the flux coefficient and Maffioli *et al.* (2016) considered the true irreversible mixing coefficient. Here, one should note that, the flux coefficient and the mixing coefficient behave similar only for weakly stratified flows (Venayagamoorthy & Koseff, 2016).

The irreversible flux Richardson number (or mixing coefficient) is also parameterized as a function of gradient Richardson number which shows that mixing efficiency increases with  $Ri_g$  in the shear dominated flow upto a critical value of  $Ri_g$  ( $\sim 0.25$ ) (Karimpour & Venayagamoorthy, 2014; Linden, 1984; Venayagamoorthy & Koseff, 2016) and approaches a constant value for high  $Ri_g$

regime (Karimpour & Venayagamoorthy, 2014). Though  $Ri_g$  based parameterizations are simple to use,  $Ri_g$  is an external parameter and hence, restricted to only shear driven turbulence. Considering the ambiguities inherent in single parameter formulations (Mater & Venayagamoorthy, 2014), multiparameter frame work has been proposed for parameterization of mixing based on both  $Re_b$  and  $Ri_g$  (Lucas & Caulfield, 2017; Salehipour *et al.*, 2016). Again  $Re_b = Fr^2 Re$  where  $Re$  is the turbulence Reynolds number (Ivey & Imberger, 1991). In the limit of high Reynolds number flow (with approximate constant order of  $Re$  as in most of the DNS simulations),  $Re_b \sim f(Fr^2)$ . It has been shown that bulk Richardson number,  $Ri_b$  (approximation of gradient Richardson number), is related to turbulent Froude number,  $Ri_b \sim Fr^{-2}$  as per classical parameterization of mixing based on idea of Turner (Maffioli *et al.*, 2016). Here, it is worth noting that  $Fr$  can be viewed as a competition of time scales (i.e. the turbulence time scale  $T_L = k/\epsilon$  to the buoyancy time scale  $N^{-1}$ ). Hence,  $Fr$  is a dynamic indicator of the local state of turbulence in a stably stratified flow. However,  $T_L$  is difficult to measure in the field.

Venayagamoorthy & Stretch (2006) showed that small-scale mixing does not directly depend on buoyancy time scale  $N^{-1}$  but rather on the turbulent kinetic energy decay time scale  $T_L$ . They proposed a model for the Lagrangian mixing term as

$$\kappa \nabla^2 \rho'(t) = -\gamma' T_L^{-1} \rho', \quad (2.40)$$

where  $\gamma' \sim 0.7$ . Brethouwer & Lindborg (2009) also suggested that the asymptotic behaviors of adiabatic dispersion depends on eddy turn over time and not on the buoyancy time  $N^{-1}$  contrary to the original suggestion of Pearson *et al.* (1983). But as noted previously,  $T_L$  is difficult to estimate in the field mainly due to challenges in estimating the turbulent kinetic energy.

## 2.7 Turbulence measurement in the ocean

Oceans are highly energetic with ubiquitous turbulence phenomenon with Reynolds number up to  $10^{10}$  in the upper ocean and surf zones (Thorpe, 2005). Understanding turbulence in the

ocean is necessary for modeling of oceanic flows. Measures of the effect of turbulence can be determined from momentum and/or scalar fluxes. The very first ocean turbulence measurements were conducted by H. Grant and his research group in 1950 using hot film anemometers which is only applicable in high turbulence flow regimes. Vertical free falling profilers were first used in late 1960s (Lueck *et al.*, 2002). Free falling profilers became popular since they are decoupled from ship motions and hence from ship induced noise. The basic components of instruments for oceanic measurements mainly consists of three parts: a sensor or probe to measure required physical parameter, electronic circuit to collect the signal from probe and store the data and a platform for smooth functioning of the probe in the ocean. Some widely used instruments for oceanic measurements are the CTD (Conductivity-Temperature-Depth) (figure 2.5a, 2.5b), VMP (Vertical Microstructure Profiler) (figure 2.5c) and ADCP (Acoustic Doppler Current Profiler) (figure 2.5d). The CTD and ADCP are usually shipboard (mounted or tethered) instruments while the VMP is typically a free-falling instrument.

The study of turbulent mixing in the ocean is very important for understanding the global ocean overturning circulation because of its influence on climate. Most of the turbulence measurements in the ocean suggest that the vertical eddy diffusivity is approximately  $10^{-5} m^2/s$  (Gregg, 1989), which is a factor of 10 smaller than the canonical mean vertical eddy diffusivity that maintains the global thermohaline circulation (Munk, 1966). Recently, Waterhouse *et al.* (2014) showed that the global-average diffusivity below 1000 *m* depth is  $O(10^{-4}) m^2/s$  based on microstructure observations.

### **2.7.1 CTD:**

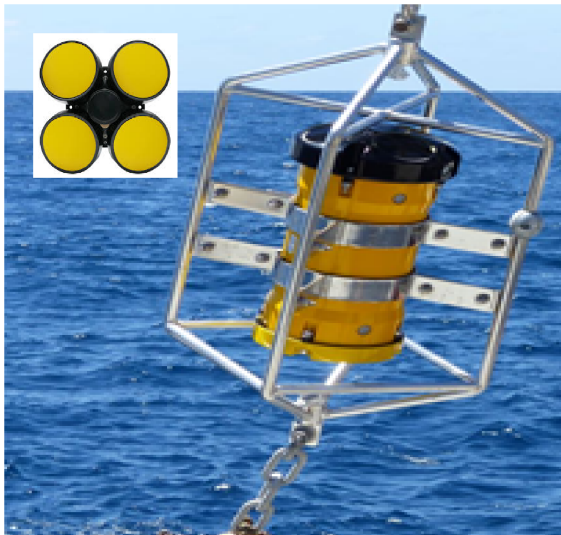
CTD is an acronym for Conductivity, Temperature, and Depth. CTD is a primary instrument used by oceanographers to measure physical, chemical and biological properties (salinity, temperature, pressure, dissolved oxygen, pH, fluorescence, nitrates water sample etc. ) of sea water to understand the processes in ocean. Here only physical properties are discussed. (Encyclopedia of Ocean Sciences, vol. 1, p. 579-588). CTD can be used in several thousand meters of water depth



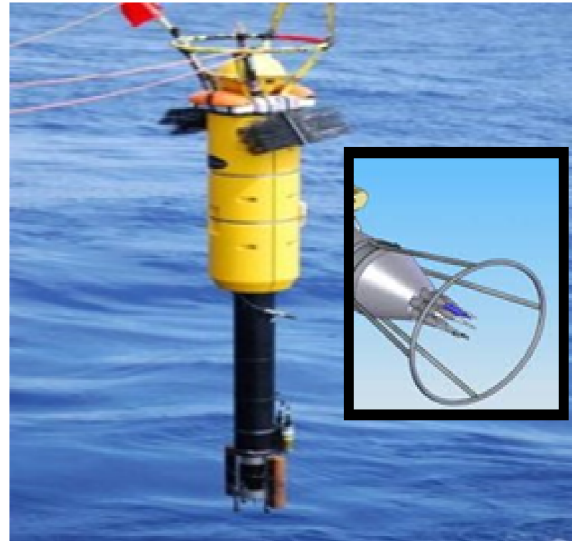
(a)



(b)



(c)



(d)

**Figure 2.5:** Pictures of commonly used instruments in the field of oceanography. (a): CTD Rosette, (b): UCTD (c) ADCP and (d): VMP

and withstands water pressure. For ship board CTD deployment and retrieval the ship needs to be completely stationary. CTD is generally lowered from ship to the maximum desirable depth. Then while retrieving back water samples are collected through the sampler bottles attached with CTD as shown in figure 2.5a, and other hydrographic properties are measured with attached sensors at desired interval of depths. Such setups of the CTD are also known as a CTD Rosette. On the other hand the use of underway CTD or UCTD (figure 2.5b) has increased in recent due to it being less

expensive but more importantly because it enables the measurement of conductivity, temperature and pressure in a moving ship (speed upto 13 knots, the ship speed in general goes up to 20 knots). The probe is simple to operate and data collections are done more rapidly in time compared to CTD Rosette. UCTD is generally used to study upper few hundreds of meters of the ocean (Rudnick & Klinke, 2007). The required data for our study of ocean turbulence measure from CTD for this study are pressure  $P$ , temperature  $T$  and salinity  $S$ .

### **2.7.2 ADCP:**

Acoustic Doppler Current Profiler (ADCP) measures ocean currents (velocity) using the principle of Doppler shift. ADCP has generally 4 (sometimes 5) acoustic transducers that emits and receives signal from four different directions allowing the instrument to measure current at different depth of an entire water column simultaneously (figure 2.5c). ADCPs can be bottom mounted (anchored to sea floor) with internal data logger or vessel mounted (shipboard). ADCP measures absolute water current not relative to ship, and can measure ocean current upto 1000 m depth depending type of frequency of the instrument. It measures small scale currents. The ADCP works by transmitting "pings" of sound at a constant frequency into the water. As the sound waves travel, they ricochet off particles suspended in the moving water, and reflect back to the instrument. Due to the Doppler effect, sound waves bounced back from a particle moving away from the profilers have a slightly lower frequency when they return. Particles moving toward the instrument send back higher frequency waves. The difference in frequency between the waves the profiler sends out and the waves it receives is called the Doppler shift. The instrument uses this shift to calculate how fast the particle and the water around it are moving (WHOI ocean instruments). In common practice the fine scale horizontal velocities are measured using an ADCP.

### **2.7.3 VMP:**

A VMP, which stands for Vertical Microstructure Profiler, is an untethered microstructure profiling system that, after being released, sinks to a pre-defined ocean depth. It collects data on the way down, through various sensors, meters, and probes, both in the nose cone of the instrument

and in the main body (figure 2.5d). After the VMP reaches the pre-defined depth, the instrument releases ballast weights so that it becomes positively buoyant and rises to the ocean surface. It is equipped with state-of-art microstructure velocity probes (shear probes), high-resolution temperature sensors (thermistors), and high-accuracy CTD sensors such that concurrent measurement of hydrographic and turbulence data are possible. Vertical microstructure profilers are expensive compared to CTD profiles. Measurements of turbulence in the deep ocean, particularly close to the bottom, are extremely sparse because of the difficulty and operational risk of obtaining deep profiles near the seafloor. A newly developed expendable instrument, the VMP-X (Vertical Microstructure Profiler Expendable) carries two microstructure shear probes to measure the fluctuations of vertical shear into the dissipation range and can profile down to a depth of 6000 m (Shang *et al.*, 2017). The shear probe and the thermistors measure small scale rate of dissipation of turbulent kinetic energy  $\epsilon$  and rate of thermal dissipation  $\chi$  respectively, based on the assumption of small scale isotropy given as

$$\epsilon = \frac{15}{2}\nu \left\langle \left( \frac{\partial u'}{\partial z} \right)^2 \right\rangle, \quad (2.41)$$

$$\chi = 6\kappa_T \left\langle \left( \frac{\partial T'}{\partial z} \right)^2 \right\rangle, \quad (2.42)$$

where,  $\nu$  is kinematic molecular viscosity and  $\kappa_T$  molecular thermal diffusivity.

## 2.8 Lagrangian dispersion and mixing

Study of statistical properties of Lagrangian particle trajectories is imperative if one wants to understand the phenomenon of mixing and dispersion in fluids. Lagrangian statistics give in-depth understanding of particle displacement or particle dispersion (Monin *et al.*, 1971; Yeung & Pope, 1989) and particle relative dispersion (Sawford, 2001) in a fluid in motion.

### 2.8.1 Lagrangian frame work

Lagrangian and Eulerian descriptions are two different approaches or frameworks to describe fluid motion. In a Lagrangian description, history of a fluid particle is obtained by keeping track

of the position vector  $\mathbf{r}$ <sup>3</sup> of the particle for all time  $t$  with reference to some initial time  $t_0$  with particle position  $\mathbf{r}_0$ . Hence in a Lagrangian framework, the position of a given particle at any time is function of the initial conditions. The position vector is given as

$$\mathbf{r} = \mathbf{r}(\mathbf{r}_0, t) \text{ where } \mathbf{r} = \mathbf{r}_0 \text{ when } t = t_0. \quad (2.43)$$

Hence, the velocity and acceleration of a fluid particle are simply partial derivatives with time given by

$$\mathbf{u} = \left( \frac{\partial \mathbf{r}}{\partial t} \right)_{\mathbf{r}_0} \text{ and } \mathbf{a} = \left( \frac{\partial^2 \mathbf{r}}{\partial t^2} \right)_{\mathbf{r}_0} = \left( \frac{\partial \mathbf{u}}{\partial t} \right)_{\mathbf{r}_0}. \quad (2.44)$$

On the contrary, in an Eulerian description, the fluid motion is studied within a fixed space (control volume) where fluid particles flow through. Here, the velocity vector  $\mathbf{u} = \mathbf{u}(\mathbf{r}, t)$  is therefore a function of time and of the space where the observation is made. The partial derivative therefore gives only local rate of change instead of the total rate of change obtained from the Lagrangian description. Hence, the Eulerian acceleration is given as

$$\mathbf{a} = \frac{D\mathbf{u}}{Dt} = \frac{\partial \mathbf{u}}{\partial t} + \mathbf{u} \cdot \nabla \mathbf{u}. \quad (2.45)$$

The majority of fluid mechanics problems are solved in an Eulerian framework since analysis using a Lagrangian framework is challenging and costly due to the need for tracking a large number of particles. However, Lagrangian analysis is a natural way to study dispersion in fluid flows. In DNS, the Eulerian velocity field is computed in a fixed domain (i.e. at each grid point in the computational mesh). Given the Eulerian velocity and any other related quantities such as the density field, the Lagrangian statistics can be computed by tracking the motions of an ensemble of fluid particles within the Eulerian velocity field. Lagrangian and Eulerian velocities are equal only when calculated at a particle position (where advection term is zero). The relationship of Lagrangian and Eulerian velocity field is given by

---

<sup>3</sup>Bold letter signifies vector representation,  $\mathbf{r}(x, y, z)$

$$\mathbf{u}(\mathbf{r}_0, t) = \mathbf{u}(\mathbf{r}(\mathbf{r}_0, t), t). \quad (2.46)$$

and instantaneous position of fluid particle is

$$\frac{\partial \mathbf{r}(\mathbf{r}_0, t)}{\partial t} = \mathbf{u}(\mathbf{r}_0, t). \quad (2.47)$$

## 2.8.2 Particle dispersion

The law of diffusion is about the average particle distribution at any instant of time initially concentrated at one point and is highly influenced by presence of both turbulence and stable stratification. A particle dispersion study would therefore provide fundamental insights on turbulent diffusion and ultimately mixing in stably stratified turbulent flows. Turbulent diffusion was studied mathematically in the seminal work by Taylor considering velocity auto correlation of particle with time and experimentally by Dobson and Richardson separately using a smoke plume (Taylor, 1921). In a continuous turbulent motion, mean square particle displacement  $\langle (\delta r)^2 \rangle$  or standard deviation of position of a single particle with uniform mean velocity is directly proportional to square of time for short time intervals and proportional to time at large times (Taylor, 1921). This is similar to Einstein's Brownian motion for molecular diffusion which shows an initial ballistic region ( $\sim t^2$ ) and a later diffusive region ( $\sim t$ ).

Csanady (1964) extended the work of Taylor (1921) for single particle dispersion to stratified fluid by considering random stochastic buoyant acceleration instead of pressure gradient and viscous force which was earlier suggested by Priestley (1959), in order to calculate net vertical movement of particles in a stably stratified fluid. Lagrangian and Eulerian velocities are the same for a particular particle position. Keeping this relation in mind mean square vertical displacement of a particle in stably stratified fluid for time,  $t \rightarrow \infty$  is given as (Csanady, 1964)

$$\langle z_w^2 \rangle = 2 \langle (w')^2 \rangle t \tau_L, \quad (2.48)$$

where  $\tau_L > 0$ , is Lagrangian time scale of turbulence,

$$\tau_L = \int_0^{\infty} R_w(t) dt, \quad (2.49)$$

with the Lagrangian vertical velocity temporal auto-correlation function  $R_w(t)$  given as

$$R_w(t) = \frac{\langle w'(t_0)w'(t_0 + t) \rangle}{\langle w'^2 \rangle}, \quad (2.50)$$

where  $w'$  is vertical velocity fluctuation,  $\langle z_w^2 \rangle$  is mean square vertical displacement,  $\langle (w')^2 \rangle$  is mean square vertical velocity fluctuation and  $t$  is time. This relation is obtained by considering large time Lagrangian vertical velocity auto correlation as a Markov process though turbulent diffusion is not purely a Markov process at least for early time. Some experimental results have shown that vertical particle dispersion at long time does not grow with time and the auto correlation function can not be neglected (Britter *et al.*, 1983) and plays dominant role in particle dispersion and equation 2.48 can be written as

$$\langle z_w^2 \rangle = 2\langle (w')^2 \rangle t\tau_L + \int_0^{\infty} tR_w(t) dt. \quad (2.51)$$

Once the mean square vertical particle dispersion is known, the vertical eddy diffusivity can be obtained for long time as

$$K_t \approx \langle z_w^2 \rangle / 2t \text{ or } K_t = \langle w^2 \rangle \tau_L. \quad (2.52)$$

Lagrangian velocity auto correlation is an important statistic that can be used to obtain the eddy diffusivity. Lagrangian integral time scale and Lagrangian velocity auto correlation functions are difficult to obtain theoretically and their relationships with corresponding Eulerian statistics are not clearly proven yet. Whether the Lagrangian integral time scale is larger than the Eulerian integral length scale or smaller is still unclear even for an unstratified turbulent flows (Dosio *et al.*, 2005). For unstratified turbulent flows suggestions have been given to use Lagrangian integral length scale  $L_L$  instead of Lagrangian integral time scale (Xia *et al.*, 2013) since it is easier to obtain from Lagrangian spatial auto correlation function by keeping track of particle position from the initial position. In this way eddy diffusivity is given as  $K_t = (\langle w^2 \rangle)^{1/2} L_L$ . This suggests that an appropriate length scale and velocity scale is required for estimation of eddy diffusivity.

Vertical diffusion can also be inferred from density fluctuation at a point. Pearson *et al.* (1983) studied statistically stationary stably stratified homogeneous flow using a stochastic Langevin model and derived root mean square vertical particle displacement from density transport equation as

$$\langle z_w^2 \rangle^{1/2} = \langle w \rangle / N (\zeta_z^2 + 2\gamma^2 Nt)^{1/2}, \quad (2.53)$$

where,  $\zeta_z^2$  is dimensionless parameter that depends on turbulent pressure gradient spectrum,  $\gamma$  is mixing coefficient which determines particle density change owing to small scale mixing,  $N$  is buoyancy frequency. Pearson *et al.* (1983) suggested that for intermediate time defined with buoyancy time  $Nt$ ,  $1 < Nt < \gamma^{-2}$  (when  $\gamma \ll 1$ ), root mean square vertical particle dispersion is constant ( $\langle z_w^2 \rangle^{1/2} \simeq w/N$ ) and for large time scale exhibits a diffusive regime. Lindborg & Brethouwer (2008) showed that for stratified flows with decaying turbulence, the mean square vertical particle displacement approaches constant value of  $2(E_p(0) + aE(0))/N^2$  when  $t \rightarrow \infty$ , where  $E_p(0)$  is initial mean potential energy,  $E(0)$  is initial total turbulent energy and  $a$  is the fraction of total initial turbulent energy that has been dissipated. But for stationary turbulence at long time, the mean square vertical particle dispersion approaches  $\langle \delta z^2 \rangle = (4E_p + 2\epsilon_p t)/N^2$  as function of time, where  $4E_p/N^2$  is the adiabatic dispersion (which does not contribute for net vertical diffusion), where  $E_p$  is mean potential energy and  $2\epsilon_p t/N^2$  is diabatic dispersion. The ratio of adiabatic and diabatic dispersion bear universal constant ratio ( $3\pi$ ). Adiabatic dispersion approaches a plateau at one eddy turn over time and diabatic dispersion dominates at 2 eddy turn over times and grows linearly with time. Vertical particle dispersion does not depend on buoyancy time  $N^{-1}$  but rather on the eddy turnover time  $T_L = k/\epsilon$ . Similar results for linear growth of vertical particle dispersion for decaying stably stratified turbulence is shown by Venayagamoorthy & Stretch (2006) and for single and particle pairs in stationary stratified flows has been shown for passive scalar by Aartrijk *et al.* (2008). It should be noted that as discussed earlier,  $T_L$  is difficult to estimate in the field.

In a stratified flow, vertical dispersion ceases while horizontal dispersion is quite similar to that observed in the unstratified counterpart. Further work on particle dispersion is warranted to gain fundamental insights on turbulent small-scale mixing in stably stratified flows.

## **2.9 Summary**

In this chapter, a discussion on the salient properties of turbulence in stably stratified flows has been presented to set the stage for the research that will be presented in subsequent chapters. In particular, the lack of robust parameterizations for mixing has been highlighted.

# Chapter 3

## Analysis of oceanic diapycnal mixing from microstructure measurements<sup>4</sup>

### 3.1 Introduction

Turbulent diapycnal mixing is the key component which controls global circulations and distribution of heat, mass and tracers in the ocean (Munk & Wunsch, 1998). Accurate estimation of diapycnal diffusivity is essential for understanding global heat and mass budget (Wunsch & Ferrari, 2004). One of the primary motivation of ocean microstructure measurements is to estimate the vertical fluxes of mass, heat and momentum across the isopycnal (constant density surfaces), associated with turbulent mixing. Commonly measurable turbulent quantities from microstructure profiles are the rate of dissipation of turbulent kinetic energy,  $\epsilon$  and the rate of dissipation of thermal variance  $\chi$ . As small scales are not directly resolved in numerical models, it is desirable to parameterize turbulent mixing accurately from these measurable quantities.

Direct measurement of turbulent fluxes are proven to be difficult and hence, the turbulent fluxes are often parameterized in large scale ocean and climate models by diascalar diffusivities and corresponding mean gradients. For example, the buoyancy flux is given as  $\langle \rho'w' \rangle = -K_\rho N^2$ , where  $K_\rho$  is the eddy diffusivity of mass and  $N^2 = \sqrt{(g/\rho_o)(\partial\langle\rho\rangle/\partial z)}$  is the buoyancy frequency that represents the background stratification through the mean density gradient  $\partial\langle\rho\rangle/\partial z$ . The big challenge in oceanography is to estimate diascalar diffusivity accurately from the data that are measured with current state-of-the-art instruments. Most of the turbulence measurements in the ocean suggest that the vertical eddy diffusivity is approximately  $10^{-5} \text{ m}^2/\text{s}$  (Gregg, 1989), which is a factor of 10 smaller than the canonical mean vertical eddy diffusivity (Munk, 1966)

---

<sup>4</sup>The research presented in this chapter is under preparation to be submitted in the Journal of Geophysical Research under the title "Microstructure measurements: Methodology to infer diapycnal mixing from microstructure data for oceanic flows" by A. Garanaik and S. K. Venayagamoorthy. The chapter is written in a collective "we" voice to acknowledge collaboration with Dr. S. K. Venayagamoorthy.

that is required to maintain the global thermohaline circulation. By compiling 5200 microstructure profiles, (Waterhouse *et al.*, 2014) suggested that the globally averaged diapycnal diffusivity below 1000  $m$  depth is  $\mathcal{O}(10^{-4}) m^2/s$  and above 1000  $m$  depth is  $\mathcal{O}(10^{-5}) m^2/s$  which are on average consistent with previously predicted diffusivity and provide an indication of the bulk statistics of mixing. It has been also noted that, distribution of diapycnal mixing is sparse varying in both location and depth as well as with time (Kunze *et al.*, 2006). Hence while the bulk statistics can provide a general overall idea of ocean mixing, they can not describe the governing parameters of diapycnal mixing. This requires proper diagnostics of diapycnal mixing and its subsequent parameterization through careful identification of the relevant turbulent regions.

The most commonly used model for diapycnal diffusivity is developed by Osborn (1980) for a homogeneous and stationary flow which recasts the diapycnal diffusivity as

$$K_\rho = \Gamma \frac{\epsilon}{N^2}, \quad (3.1)$$

where  $\Gamma = R_f/(1 - R_f)$  is a mixing coefficient and  $R_f$  is the flux Richardson number (also termed the mixing efficiency) which is a ratio of buoyancy flux ( $B$ ) to production of turbulent kinetic energy  $P$ ,  $\epsilon$  is the rate of dissipation of turbulent kinetic energy and  $N = \sqrt{(-g/\rho_o)(d\rho/dz)}$  is the buoyancy frequency.  $\Gamma$  is typically considered to have a canonical constant value of 0.2 ( $R_f \approx 0.17$ ) (Osborn, 1980). It should be noted that the constancy of  $\Gamma$  has been the subject of extensive debate and a universal parameterization of  $\Gamma$  still remains elusive (Gregg *et al.*, 2018; Mater & Venayagamoorthy, 2014).

Common parameterizations of  $\Gamma$  are expressed as functions of buoyancy (Gibson) Reynolds number  $Re_b = \epsilon/\nu N^2$ , where  $\nu$  is the kinematic viscosity. With the availability of microstructure data, the rate of dissipation of turbulent kinetic energy,  $\epsilon$  is available. The background stratification is typically extracted from CTD measurements and hence,  $Re_b$  can be readily computed from ocean data. This is the basic reason why  $Re_b$  based parameterization of  $\Gamma$  is popular even though they have no fidelity as they are not justified on physical grounds. Direct numerical simulation of sheared stratified turbulence suggest that  $\Gamma \propto Re_b^{-1/2}$  for  $Re_b > \mathcal{O}(100)$ , corresponding to shear

dominated or energetic flow (Salehipour & Peltier, 2015; Shih *et al.*, 2005). Similar scaling was found by Lozovatsky & Fernando (2012) for atmospheric flow, but for a higher range of  $Re_b > \mathcal{O}(10^4)$ . From experimental data, Barry *et al.* (2001) suggested that  $\Gamma \propto Re_b^{-2/3}$  for  $Re_b > 300$ . Osborn (1980) suggested constant canonical value of  $\Gamma$  is only acceptable for buoyancy driven flow which is defined as  $\mathcal{O}(1) < Re_b < \mathcal{O}(100)$  (Bouffard & Boegman, 2013; Maffioli & Davidson, 2016; Shih *et al.*, 2005). DNS study of Maffioli & Davidson (2016) found  $\Gamma$  can peak upto 0.5 and approach a constant value of 0.33 for strongly stratified fluid with  $Re_b \sim \mathcal{O}(10)$ . Oakey (1982) suggested  $0.05 < \Gamma < 0.47$  and Moum *et al.* (1989) suggested  $0.12 < \Gamma < 0.48$ . Laurent & Smitt (1999) argued that high mixing efficiency might be related to double diffusion. Parameterization of  $\Gamma$  as a function of gradient Richardson number  $Ri_g = N^2/S^2$ , (where  $S$  is background mean shear) shows that mixing efficiency increases with  $Ri_g$  in the shear dominated flow upto a critical value of  $Ri_g$  ( $\sim 0.25$ ) (Karimpour & Venayagamoorthy, 2014; Linden, 1984; Venayagamoorthy & Koseff, 2016) and approaches a constant value for high  $Ri_g$  regime (Karimpour & Venayagamoorthy, 2014; Venayagamoorthy & Koseff, 2016). The reliability of  $Ri_g$  based parameterization in the ocean depends on how efficiently the background shear and stratification are computed from the data.

With these ambiguities of current Parameterizations of mixing, it is not advisable to use a constant mixing efficiency throughout the ocean. The questions to ask is: whether a constant value for  $\Gamma$  ( $= 0.2$  or  $R_f = 0.17$ ) is justified in the upper ocean and in deep ocean influenced by topography, where water columns are already well mixed with very weak to no stratification? If not, does the mixing efficiency decrease in a universal way as a function of  $Re_b^{-1/2}$  from  $Re_b$  throughout the ocean? Current parameterizations still use  $R_f = 1/6$  considering that turbulent overturns loose 17% of their energy in raising the dense water (Olbers & Eden, 2013; Polzin, 2009). Because of the difficulty in accurately estimating mixing efficiency from field measurements and lack of deeper knowledge of their validity, this maximum value is being used (loosely) for  $R_f$  in shear induced turbulent mixing of stratified flows. Parameterization of mixing efficiency is generally obtained from controlled experiments and applied to the ocean globally. In this study, we focus on ambigu-

ities of  $Re_b$  based parameterization in the microstructure measurements. Field data analysis also faces challenges on how accurately the data are measured and how effectively data are analyzed. We also provide a brief discussion on different methodologies for ocean data analysis. In section 3.2, theoretical background is discussed for estimation of  $\Gamma$  from microstructure measurements. Section 3.3 provides a brief description of data used for this study. Methodology of data analysis is presented in section 3.4 followed by results and discussions in section 3.5. Concluding remarks are provided in section 3.6.

## 3.2 Theoretical background

The evolution equation of temperature variance in a stratified turbulent field is given as

$$\frac{\partial \langle T'^2 \rangle}{\partial t} + \langle U_i \rangle \frac{\partial \langle T'^2 \rangle}{\partial x_j} = \underbrace{-2 \langle u'_j T' \rangle \frac{\partial T}{\partial x_j}}_P + \underbrace{\kappa_T \frac{\partial^2 \langle T'^2 \rangle}{\partial x_j^2} - \frac{\partial \langle u'_j T'^2 \rangle}{\partial x_j}}_T - \underbrace{2 \kappa_T \left\langle \frac{\partial T'}{\partial x_j} \frac{\partial T'}{\partial x_j} \right\rangle}_\chi, \quad (3.2)$$

where  $\langle \rangle$  represents statistical average,  $T'$  is the small scale temperature fluctuation,  $\kappa_T$  is the molecular diffusivity of heat,  $u'_i$  is the small scale velocity fluctuation,  $U_i$  is the mean velocity and  $i, j = 1, 2, 3$ . The first term on right hand side of the equation 3.2 is the production of temperature variance ( $P$ ). The 2<sup>nd</sup> and 3<sup>rd</sup> terms are molecular and turbulent transport terms ( $T$ ) respectively and the last term is the rate of dissipation of temperature variance ( $\chi$ ). For a homogeneous flow, the transport terms can be neglected. Assuming stationary and equilibrium flow, equation 3.2 simplifies to  $P = \chi$ . In the oceanographic context, data acquisitions are done by vertical profile measurements as stratification is also predominant in the vertical direction. Hence, for 1D homogeneous, stationary flow

$$\langle w' T' \rangle \frac{\partial T}{\partial z} = -\frac{\chi}{2}. \quad (3.3)$$

The vertical temperature flux  $\langle w' T' \rangle$  is related to the down-gradient of mean temperature. By invoking the gradient diffusion hypothesis (Pope, 2000),  $\langle w' T' \rangle = -K_T \frac{\partial \langle T \rangle}{\partial z}$ , where  $K_T$  is the

vertical eddy (turbulent) diffusivity of heat.

$$K_T = \frac{\chi/2}{(\partial\langle T \rangle/\partial z)^2}. \quad (3.4)$$

The value of  $\chi$  can be measured in the ocean using vertical microstructure profiler with the assumption of small scale isotropy. Background temperature gradient is obtained from CTD profiles. This model was developed by Osborn & Cox (1972) for obtaining turbulent diffusivity in ocean from measurable quantities. This method suffers, when temperature gradients are very small.

Osborn (1980) derived the model for vertical eddy mass diffusivity (eq: 3.1) from the equation of evolution of turbulent kinetic energy ( $k$ ). Turbulent kinetic energy is the sum of the isotropic Reynolds stress terms as  $k = \frac{1}{2}\langle u_i^2 \rangle$ . The evolution equation of  $k$  is obtained from the momentum equations of the fluctuating velocity field  $u'_i$ ,

$$\begin{aligned} \frac{Dk}{Dt} = \frac{\partial k}{\partial t} + \langle U_j \rangle \frac{\partial k}{\partial x_j} = & \underbrace{-\langle u'_i u'_j \rangle \frac{\partial \langle U_i \rangle}{\partial x_j}}_P - \underbrace{\nu \langle \frac{\partial u'_i}{\partial x_j} \frac{\partial u'_i}{\partial x_j} \rangle}_\epsilon - \underbrace{\frac{g}{\rho_0} \langle \rho' u'_j \rangle \delta_{i3}}_B \\ & + \underbrace{\nu \frac{\partial^2 k}{\partial x_j^2} + \frac{\partial \langle k u'_j \rangle}{\partial x_j}}_T - \frac{1}{\rho_0} \frac{\partial \langle u'_i p' \rangle}{\partial x_j}, \end{aligned} \quad (3.5)$$

where,  $\nu$  is the molecular kinematic viscosity,  $\delta_{i3}$  is Kronecker delta<sup>5</sup> and is equal to unity for vertical momentum equation and zero for horizontal momentum equations. The first three terms in right hand side of equation (3.5) are production of turbulent kinetic energy  $P$ , rate of dissipation of turbulent kinetic energy  $\epsilon$  and buoyancy flux  $B$  respectively. The last term is pressure diffusion which is very small compared to other terms. The 3<sup>rd</sup> and 4<sup>th</sup> terms are molecular viscous transport and turbulent transport respectively. For one dimensional statistically homogeneous and stationary turbulent flow, equation 3.5 can be simplified to

---

<sup>5</sup> $\delta_{ij} = 1$  (if  $i = j$ ) and  $\delta_{ij} = 0$  (if  $i \neq j$ ) for  $i, j = 1, 2$  and  $3$

$$\underbrace{\langle u'w' \rangle}_{P} \frac{\partial U}{\partial z} = -\epsilon - \underbrace{\frac{g}{\rho_0} \langle \rho'w' \rangle}_{B}. \quad (3.6)$$

The ratio of buoyancy flux to production is defined as the flux Richardson number,  $R_f (= B/P)$ , also known as the mixing efficiency. By deduction,  $B/\epsilon = \Gamma$ , where  $\Gamma = R_f/(1 - R_f)$  is considered as mixing coefficient. Vertical density flux is related to down-gradient of mean density. Invoking the gradient diffusion hypothesis, eddy diffusivity of mass is defined as

$$K_\rho = -\frac{\rho'w'}{\partial \langle \rho \rangle / \partial z} = \frac{B}{N^2} \quad (3.7)$$

or

$$K_\rho = \Gamma \frac{\epsilon}{N^2}, \quad (3.8)$$

where  $N^2 = (-g/\rho_0)(\partial \langle \rho \rangle / \partial z)$  is the buoyancy frequency. Deriving eddy diffusivity of mass in the manner above way is helpful in oceanography as both  $\epsilon$  and  $N$  can be measured using vertical microstructure profiles and CTD respectively. According to Osborn model of diffusivity,  $\Gamma = 0.2$  or  $R_f = 0.17$ .

For a turbulent flow, eddy diffusivity of mass and temperature and the other scalars should be same as the differences in molecular diffusion are equivalently compensated by differences in fluctuating gradients. With this concept for a turbulent flow,  $K_T = K_\rho$ . From equations 3.4 and 3.8, Oakey (1982) derived the mixing coefficient  $\Gamma$  as

$$\Gamma = \frac{\chi N^2}{2\epsilon(\partial \langle T \rangle / \partial z)^2}. \quad (3.9)$$

All the parameters of equation 3.9 are measurable in oceanic flows using microstructure profiler and CTD. Considering the data which have all these parameters measured concurrently, we can find better assessment of parameterization of  $\Gamma$  from field measurements. The mixing efficiency can be derived from mixing coefficient as

$$R_f = \frac{\Gamma}{1 + \Gamma}. \quad (3.10)$$

### 3.3 Data considered

A variety of sensors are generally used in a research cruise. The Conductivity-Temperature-Depth (CTD) sensor is the most common type instrument for hydrographic data collection. For small scale turbulent data measurements, vertical microstructure profiler (VMP) is used with shear probes (for  $\epsilon$ ) and thermistors (for  $\chi$ ). For the measurement of oceanic currents, Acoustic Doppler Current Profilers (ADCP) are employed to measure fine scale horizontal velocities. Detailed descriptions of these instruments were provided in chapter 2.

For the present study, we have considered the microstructure data which has all sensors attached to one instrument to provide us with the hydrographic data ( $P, S, T$ ), turbulence data ( $\chi, \epsilon$ ) and ocean velocity data ( $u, v$ ) measured concurrently. That means, the vertical microstructure profiler occupying ADCP, CTD, shear and thermistor probes all together were used for data collection. This approach eliminates any uncertainty associated with time and location mismatch of measurement which is unavoidable if data are measured with different instruments. The microstructure data considered for our study are obtained from NSF-funded microstructure database (<https://microstructure.ucsd.edu>). This database provides a compilation of various datasets obtained from microstructure profiles provided by data owners (PIs), capable of measuring smallest scales of oceanic turbulence. Data are archived in NETCDF files at  $1m$  bin resolution which can be extracted easily using software like MATLAB and PYTHON. The variables saved are time, depth, pressure, temperature, salinity, latitude, longitude, dissipation rate of turbulent kinetic energy  $\epsilon$  and if available, dissipation rate of thermal variance  $\chi$ . Out of all 31 documented datasets, only, BBTRE96, BBTRE97, EXITS1, EXITS2, EXITS3, GEOTRACES, GRAVILUCK, MIXET1, MIXET2, NATRE, SPAM1 and SPAM2 have hydrographic and turbulent parameters. From personal communication with PIs, we have BBTRE, NATRE and IWISE data sets with complete required hydrographic data, turbulence data and velocity data. From a research collaboration with AirSea Interactions in the Northern Indian Ocean (ASIRI), we have glider data with all above

mentioned variables measured at 0.5  $m$  vertical resolution. ASIRI is an international research effort (2013 – 17) aimed at understanding and quantifying coupled atmosphereocean dynamics of the Bay of Bengal (BoB) with relevance to Indian Ocean monsoons (Wijesekera *et al.*, 2016). For our analysis, we have considered BBTRE, IWISE and BoB data.

IWISE (The Internal Waves In Straits Experiment) was conducted at 250 km wide Luzoin strait of South China sea. This site is considered to be one of the most energetic internal wave environment in the world ocean (Laurent *et al.*, 2011). As the salinity was un-pumped in the CTD for IWISE data set, salinity was obtained from microstructure temperature and a fit for T-S (temperature-Salinity) was obtained from a separate deployment CTD and it has been shown that these data can be considered robust for further analysis as described in (Mater *et al.*, 2015). A total of 67 vertical profiles are considered with an average depth of 1000  $m$  with 9 profiles measuring till 1600  $m$  depth. Turbulence levels are significantly enhanced in this site. The BBTRE97 (Brazil Basin Tracer Release Experiment) took place near the Brazil basin north of south Atlantic ocean in spring 1997. The data consists of 89 profiles out of which 69 profiles are used in this study. Additional information about the data and experiments can be found in (Polzin *et al.*, 1997). The 3rd data set considered here is collected at the Bay of Bengal of Indian ocean in the year of 2013 as a part of ASIRI experiments (Shroyer *et al.*, 2016). Total of 300 profiles are considered which ranged up to a depth of the upper 150  $m$ .

## 3.4 Methodology

### 3.4.1 Equation of states and T-S plots

The real T-S relationships of the waters of the ocean plotted on the  $T - S$  or  $\theta - S$  ( $T/\theta$ -temperature, S-salinity of sea water) diagram serve as the immediate indicator of thermohaline conditions. The analysis of the  $T - S$  relationships, together with the field expressing the equation of state of sea water, allows taking into account the most important factors that determine the nature of the transformation and interaction of different waters. The density of sea water is function of depth, temperature and salinity. Density is not directly obtained from instruments but computed

from equation of state using Gills method by using GSW Oceanographic Toolbox (McDougall & Barker, 2011). Oceanic data analysis is conducted with potential temperature and potential density to reduce the effect of adiabatic expansion/compression due to pressure as the pressure in the ocean increases with depth. For every 33 feet or 10 m depth of water, the pressure increases by 1 bar (source: NOAA). Salinity has negligible pressure dependence. For all further analysis temperature is always potential temperature  $\theta$ , density is always potential density  $\sigma$  and salinity is always the measured salinity unless mentioned otherwise. From a  $T - S$  plot, it can be found that density is either a function of temperature or salinity or both. From figure 3.1a and 3.1b, For the bulk part of the flow depth, show that,  $\sigma = f(\theta)$  for IWISE data and  $\sigma = f(\theta, S)$  for BBTRE data.  $T - S$  plot of BoB data shows that in upper 20 – 30 m, salinity plays major role in determining density but for water column below 60 m, density is strictly a function of temperature (figure 3.4).

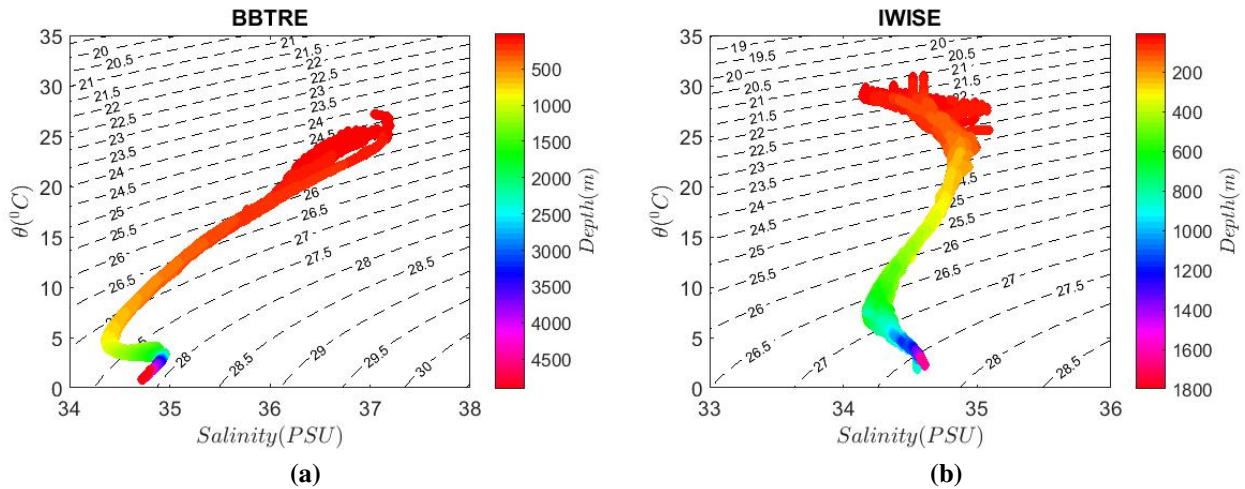


**Figure 3.1:** T-S plot for (a) BBTRE and (b) IWISE with depth in color bar. Density difference from  $1000 \text{ kg/m}^3$  are shown in dashed contour lines.

For the analysis of overturns, potential temperature is generally considered as proxy for potential density (Mater *et al.*, 2015; Smyth *et al.*, 2001). This is because, the measurements of salinity are not usually reliable. In such cases, density is obtained from depth, temperature and a constant salinity. When  $\theta$  is used instead of  $\sigma$  in the study of overturns, overturns are identified by resorting

$\theta$  profiles, not  $\sigma$  profiles. Thorpe (1977) originally proposed the method for identifying overturn patches using temperature profiles. But that experiment was conducted in a lake, where the stratifying agent is only temperature not salinity. If a overturn is identified from  $\theta$  profiles for a water column where density is influenced by both temperature and salinity, it might lead to different statistics of patches compared to that obtained from density sorted profiles. For our study, we have considered the data which have pumped salinity or the salinity from microstructure has been corrected from the corresponding CTD values to provide a better assessment of patch analysis based on both  $\theta$  sorting and  $\sigma$  sorting methods.

### 3.4.2 Bin-wise vs patch-wise analysis

Considering the fact that, hydrographic and turbulent measurements are made coincidentally from a field campaign, there are probably a number of ways to make inferences on oceanic mixing, each subjected to its own specific set of assumptions. Data available for the study of ocean mixing are the rate of dissipation of turbulent kinetic energy  $\epsilon$  (from shear microstructure), rate of thermal dissipation  $\chi$  (from temperature microstructure), temperature, depth and salinity (from CTD), velocity (from ADCP). A discussion on how these instruments collect data is described in chapter 2. Here we have outlined two plausible approaches for data analysis. First approach uses is bin-wise analysis and the second one is based on patch-wise analysis. Data are collected from research vessels as vertical profiles with some time and space interval between each vertical profile.

Bin-wise method is easier given that, data is measured at certain vertical resolutions, e.g., 1  $m$  intervals (For all data considered here, vertical resolution is 0.5  $m$ ). The profiles are averaged over some selected depth windows (called bins). The selection criteria for bin size is very subjective and different studies have used different bin sizes with some acceptable but not universal arguments. For example, Merrifield *et al.* (2016) analyzed the values of  $\epsilon$ ,  $\chi$ ,  $\partial T/\partial z$  and  $N^2$  by taking ensemble average over each 100  $m$  bin for their study of enhanced diapycnal mixing at Drake passage. The 95% confidence intervals based on bootstrap method were calculated over a 10 or 20  $m$  bin assuming as an approximated value for Ozmidov length scale (Ozmidov, 1965) which is considered

as largest overturning length scale. Here the gradients were obtained for each point of data measurements. To obtain fine scale gradients, Laurent & Smitt (1999) used a slope of a linear fit over 5  $m$ -segment, centered at each 0.5  $m$  interval. The 5  $m$  segment was chosen considering a suitable trade off between the need of high vertical resolution and statistically reasonable regression estimation. In bin-wise method, the back ground gradients are not obtained from the sorted profile but from some averaging over selected windows which is ambiguous as it might result in negative buoyancy frequency due to unstable regions. Generally large enough bin size is selected to smear the effects of unstable regions. Again turbulence in ocean is intermittent or sporadic and turbulent mixing is patchy (Dunckley *et al.*, 2012). Though a bin-wise approach can provide statistics of bulk quantities in ocean, this method is not very useful for developing/testing parameterizations of mixing.

On the other hand, patch-wise analysis provides better insights into the dynamics of the flow. In this method turbulent patches are determined from Thorpe sorting method (Thorpe, 1977) by identifying overturn regions. The background gradients of temperature or density are obtained from adiabatically sorted profiles resulting in statistically stable configuration. An overturn represents the available potential energy, part of which gets converted to turbulent kinetic energy, when the overturn collapses. Several studies have been conducted though patch-wise data analysis. The primary goal for identifying a turbulent patch is to estimate the rate of dissipation of kinetic energy  $\epsilon$ , indirectly from Thorpe length scale,  $L_T$  (in absence of expensive microstructure instruments) (Dillon, 1982; Ferron *et al.*, 1998). Recently, it was shown that  $L_T$  scales with larger (outer) scales of turbulence and not with the small isotropic scales (Mater *et al.*, 2013). For a weakly stratified regime,  $L_T$  scales with  $L_{k\epsilon}$ , the inertial length scale, where  $k$  is turbulent kinetic energy. Still, patch-wise analysis has many more applications including identification of age of turbulence (Smyth *et al.*, 2001). Methodology for identifying patches and background stratification are discussed in following sections.

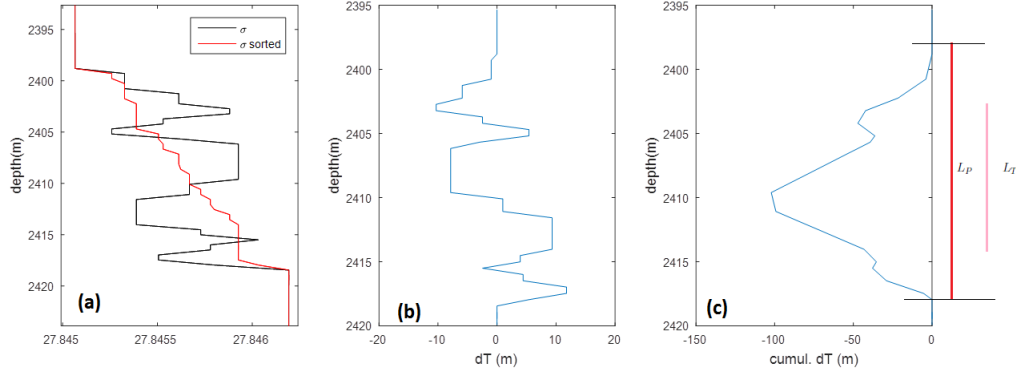


**Figure 3.2:** Example showing identification of a turbulent patch based on density sorted profile.

### 3.4.3 Identification of turbulent patch- Thorpe resorting method

Turbulent patches in a vertical profile of density are obtained by Thorpe sorting method (Thorpe, 1977), which involves resorting of the instantaneous potential density ( $\sigma$ ) profiles to a minimum available potential energy state such that, the potential density profile becomes gravitationally stable ( $\sigma_{sorted}$ ) as shown in figure 3.2(a). For a given depth, Thorpe displacement,  $dT = z_i - z_{sorted}$  is calculated from difference between the instantaneous depth  $z_i$  of data point for potential density and the sorted depth to which the sample has moved from  $z_i$  in order to obtain a stable profile. If there is no unstable region,  $dT = 0$  (see figure 3.2(b)). For an individual overturn,  $dT$  is large and negative at upper boundary of the overturn and gradually increases with depth (depth positive) and becomes large and positive towards bottom boundary of the overturn. In the example patch shown in figure 3.2, single overturning region is identified with multiple non zero consecutive  $dT$  regions as on overall whole region is unstable which is shown by cumulative  $dT$  ( $\sum dT$ ) in figure 3.2(c). For individual overturn, the Thorpe overturning scale is obtained from the root mean square of  $dT$  of each point inside the patch and patch length is identified from zero crossing of cumulative  $dT$ . Thorpe length scale is defined as  $L_T = \langle dT^2 \rangle^{1/2}$ . Here one should notice that the Thorpe length scale ( $L_T$ ) is not necessarily equal to the maximum size of the patch ( $L_P$ ). The following procedures are followed to identify a turbulent patch. The potential temperature and potential density

are filtered with smoothing algorithm provided by Gargett & Garner (2008) with threshold value for temperature set at  $0.0005\text{ }^{\circ}\text{C}$  and threshold value for density as  $0.0001\text{ kg/m}^3$  to eliminate any instrumental noise (Mater *et al.*, 2015). Thorpe scale threshold is considered as  $1\text{ m}$  and  $L_T < 1\text{ m}$  are discarded. The lower 25 percentile of  $\chi$  data were discarded and if patch average  $\chi$  or  $\epsilon$  are found to be zero or with not enough data points inside a patch, those patches are not considered for this study.

### 3.4.4 Background gradients

For a bin-wise analysis, background gradients are generally obtained by two different methods. Firstly, gradients are obtained by taking central difference or forward difference of consecutive data points and then taking ensemble average of gradients over certain user defined depth size or bin size (Smyth & Moum, 2013). The second method involves selecting a user defined bin size first and then fitting the data over the bin by a least square method. The slope of the line gives the gradient (Laurent & Smitt, 1999). In both the methods, uncertainties associated with bin size can result in different gradient values. For example, Smyth & Moum (2013) computed gradient Richardson number,  $Ri_g = N^2/S^2$  where  $N$  is buoyancy frequency and  $S$  is shear, by taking differences of density and velocity values in adjacent  $2\text{ m}$ ,  $4\text{ m}$ ,  $8\text{ m}$  and  $16\text{ m}$  bins and found different distributions for  $Ri_g$  in the limit of low stratification or in the regime of shear driven flow.

For patch-wise method, the gradients for each individual patch of density and temperature are the background gradients against which overturning occurs. The patches are obtained from sorted potential temperature and sorted potential density. Since disturbance occurs against estimation of Buoyancy frequency  $N^2$  which is a measure of stratification, gradients (temperature and density) must be calculated over a depth range enclosing particular event (Dillon, 1982). For density sorted turbulent patches, some of the patches have zero temperature gradient or very small ( $< 10^{-7}$ ) temperature gradients which are neglected from further calculations.

Density gradients are necessary to find background stratification as buoyancy frequency is given by mean density gradient.  $N^2 = -g/\rho_0 (\partial\langle\rho\rangle/\partial z)$ . Here we have considered three methods

to calculate the value of  $N$ , namely  $N_{bulk}$  for bulk gradient of patch,  $N_{2pt}$  for bulk gradient of patch and  $N_{ls}$  for least square method of gradient of patch depending how the density gradients are obtained. For  $N_{2pt}$ , after obtaining a turbulent patch as described in section 3.4.3, the density at top and bottom boundary of the patch is found from sorted density profiles. As the overturn works against a background stratification, calculating background stratification from stable sorted profile is more reasonable. Obtaining top and bottom boundary value of density, the gradient is calculated by the difference of these two values over the patch length (Moum, 1996). In  $N_{ls}$  method, a turbulent patch is identified, the density at each point inside the patch are identified and then are fitted with a least square method, the slope of which is considered as background gradient. Smyth *et al.* (2001) suggested the  $N_{bulk}$  method for better representation of bulk background stratification which is insensitive to patch boundaries (as multiple patches can form a single over turn, figure 3.2 (a)) This method assumes that the Ellison length scale,  $L_E = \langle \rho'^2 \rangle^{1/2} / \partial \langle \rho \rangle / \partial z$ , where  $\rho'$  is the density difference between instantaneous profile and adiabatically resorted profile (Ellison, 1957) and the Thorpe length scale,  $L_T$  (Thorpe, 1977) are equal such that the bulk density gradient is obtained as  $\partial \langle \rho \rangle / \partial z_{bulk} = \langle \rho'^2 \rangle^{1/2} / L_T$ . There are significant evidences showing  $L_E \approx L_T$  (Ivey & Imberger, 1991; Mater *et al.*, 2013).

While sorting a density profile, it is logical to tag corresponding temperature of that point as these are properties of fluid. Temperature gradients are also obtained similar way to density gradients using the three corresponding methods over the patch.

One of the parameter to estimate the strength of stratification is gradient Richardson number defined as  $Ri_g = N^2 / S^2$ . Different methods to obtain background stratification,  $N$ , is discussed above. To our knowledge there is no definite method to obtain velocity gradient to find shear for the patches. For bin-wise method shear is obtained from differences of velocity over consecutive points and summation is taken over desired bins. But for patch-wise analysis, finding the mean shear for a given patch size remains a challenge. Here we have highlighted two methods. First approach uses a patch-average shear and the second approach uses a patch-across shear as shown in figure 3.3. The patch average shear,  $S_{avg}$ , is obtained by taking average of shear at each point

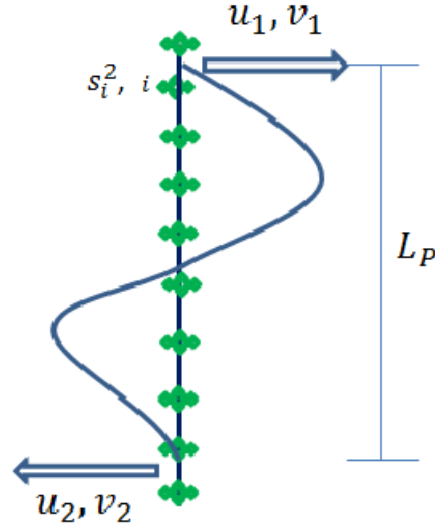


**Figure 3.3:** A schematic showing mechanism of shear.

$S_i^2$ , defined as

$$S_{avg} = \sqrt{\frac{1}{n} \sum S_i^2} = \sqrt{\frac{1}{n} \sum \left( \left( \frac{\partial u_i}{\partial z} \right)^2 + \left( \frac{\partial v_i}{\partial z} \right)^2 \right)}, \quad (3.11)$$

where,  $u_i$  and  $v_i$  are the horizontal velocities at each point  $i$  in the patch and  $\partial z$  represents the depth between consecutive points and  $n$  represents number of points in the patch. The question to ask is, how average shear over a patch represents a background shear which drives the overturn? We proposed a different definition of shear by considering that the shear or the velocity gradient that can drive the overturn should create a couple from the top and bottom velocity. Let  $u_1$  and  $v_1$  be the velocities at top boundary of the patch and  $u_2$  and  $v_2$  be the velocities at bottom end of the patch. The patch length is represented as  $L_P$ . Now the shear across the patch is defined as

$$S_{across} = \sqrt{\left( \frac{u_2 - u_1}{L_P} \right)^2 + \left( \frac{v_2 - v_1}{L_P} \right)^2}. \quad (3.12)$$

We have tested all three types of background stratification and two types of shear for different regimes of ocean in section 3.5.

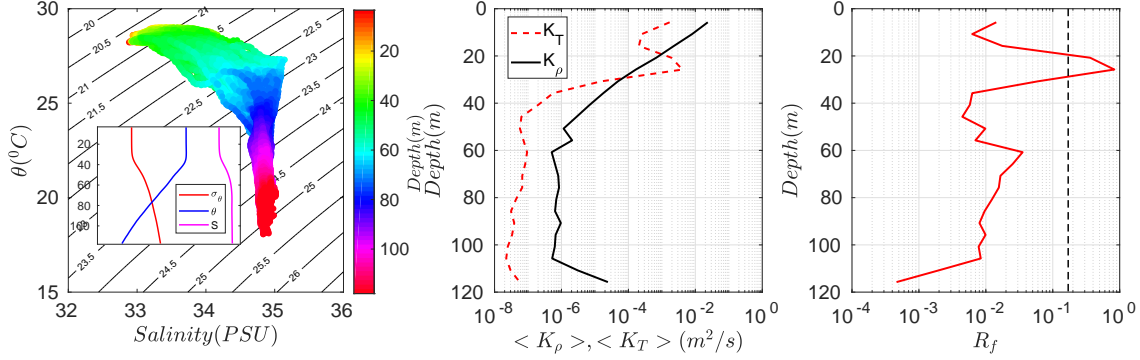


**Figure 3.4:** The left panel is showing T-S plot with depth of measurement in color bar for BoB data with an inset plot of average vertical profiles of potential temperature  $\theta$ , potential density  $\sigma_\theta$  and salinity (S). The middle panel presents the average vertical profile of eddy diffusivity of temperature  $K_T$  (3.4) and mass  $K_\rho$  (3.8). The right panel average vertical profile of mixing efficiency (3.10). Vertical line corresponds to  $R_f = 0.17$ . Here average signifies the average over all measured profiles. For better visualization average vertical profiles are shown with 5m depth average values.

## 3.5 Results

### 3.5.1 Traditional approach: Bin-wise analysis with $\Gamma = 0.2$

The traditional way of data analysis in the ocean is conducted through bin analysis. Figure 3.4 and 3.5 show the bin-wise turbulent data analysis for BoB data. The vertical profiles are obtained by ensemble average of all the 300 profiles measured. Gradients are obtained from central difference method in each profile. The plots (except  $T - S$ ) show 5 m depth average values for better visualization.  $K_T$  and  $K_\rho$  values are obtained for each data point as per equations 3.4 and 3.8, respectively.  $K_\rho$  is obtained with  $\Gamma = 0.2$ . The mixing efficiency is obtained from actual data as per equation 3.9 and shown in plot 3.4.

For the upper ocean (0 – 20 m), the flow is highly energetic as evident from the value of  $\epsilon$  in figure 3.5(a) which is  $\sim 10^{-7} \text{ m}^2/\text{s}^3$ . The background  $\epsilon$  in ocean is generally considered  $\sim 10^{-10} \text{ m}^2/\text{s}^3$ . The stratification in this regime is very low (figure 3.5(b)). In this regime, mixing efficiency  $R_f$  is definitely low (0.001) as there is nothing to mix.  $\Gamma = 0.2$  over predicts the mixing in highly energetic upper ocean mixed layer. Again below  $\sim 50 \text{ m}$ ,  $\Gamma = 0.2$  also over predicts the mixing. In this region even though the stratification is stronger compared to the upper ocean, there is less

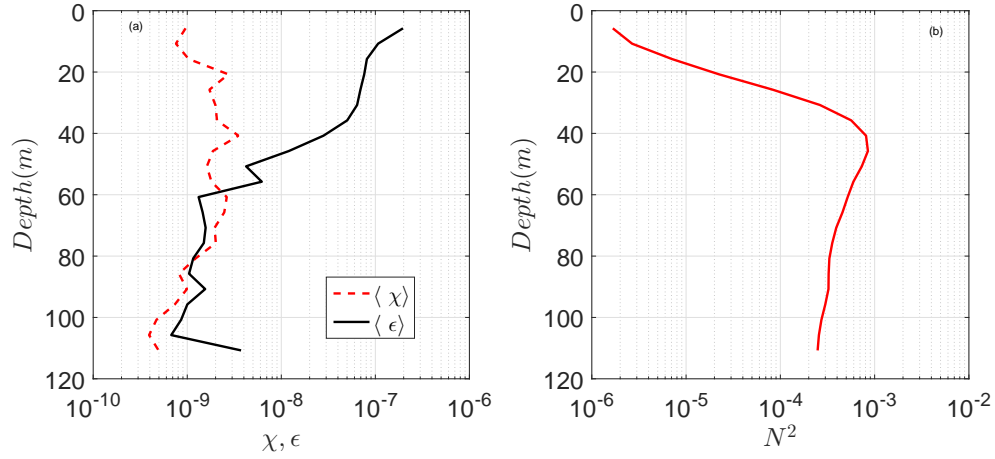


**Figure 3.5:** (a) Average vertical profiles of  $\chi$  ( $^0C/s$ ) and  $\epsilon$  ( $m^2/s^3$ ) (b) the average background stratification.

energy to mix the fluid.  $\Gamma = 0.2$  can be considered to provide efficient results only for thermocline regime provided turbulent energy is higher than the background.

Two major conclusions can be derived from these results. firstly,  $\Gamma = 0.2$  does not predict the right eddy diffusivity in most part of the ocean. Secondly, bin-wise analysis can present an overall structure of the ocean but does not identify the physics of overturns on unstable regions.

### 3.5.2 Patch statistics: temperature sorted vs density sorted

In this section the patch statistics obtained from density sorted profiles are compared with those obtained from temperature sorted profiles for BBTRE and IWISE data. Figure 3.1a and 3.1b shows the  $T - S$  plots for BBTRE and IWISE data respectively. From visual inspection of these two plots it is clear that the density in BBTRE site is a function of both salinity and temperature (except 1000 – 1700 m, salinity intrusion) and density in IWISE site can be considered to be a function of temperature only as the salinity changes are negligible. Hence, these two data sets are selected for our study to provide an insight into the justification of substitution of potential temperature for potential density is the patch analysis. This is an important issue, because the water mass overturn is created if heavy fluid moves up and lighter fluid moves down. Temperature sorted profiles might not represent an overturn if density of water is compensated by salinity. Figure 3.6 shows data analysis for patch statistics for IWISE data and figure 3.7 for BBTRE data. For IWISE data,

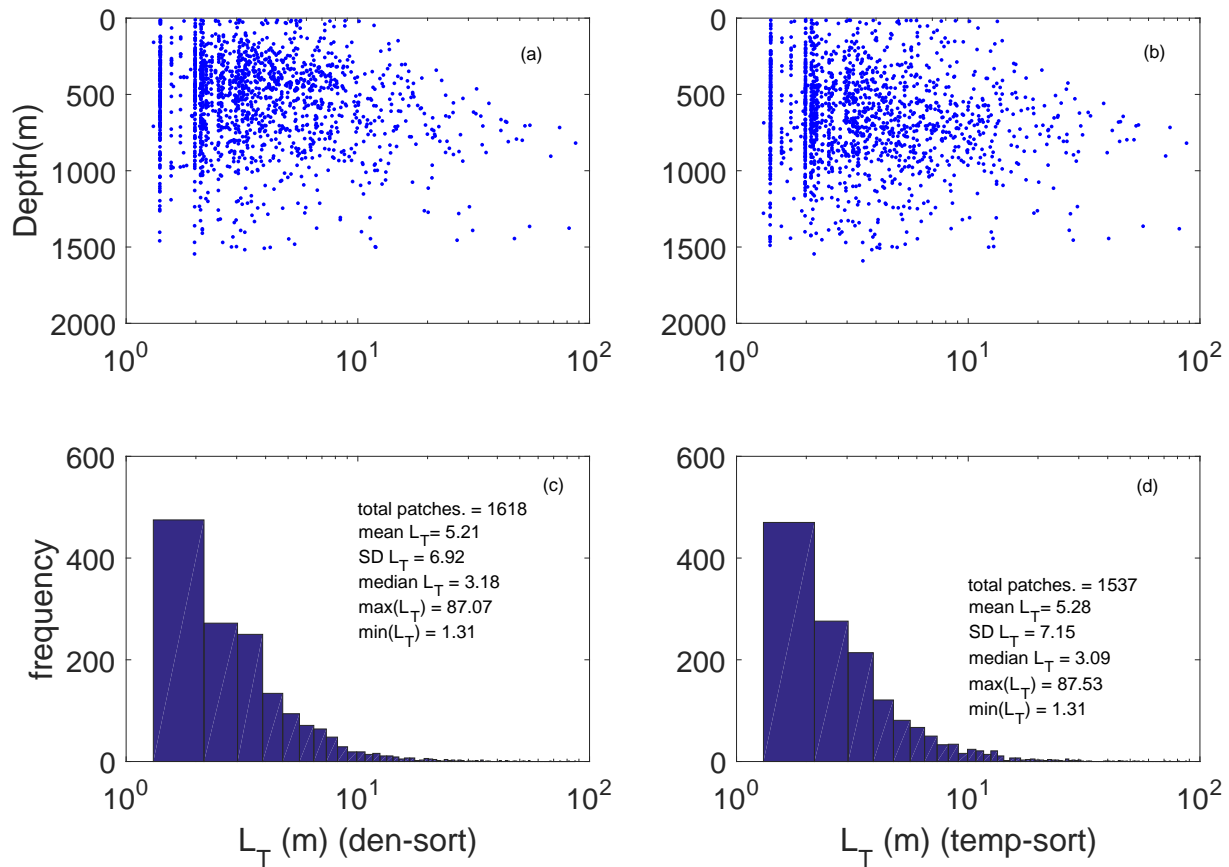


**Figure 3.6:** (a) Density sorted Thorpe length scales for all the profiles of IWISE through out the depth (b) Temperature sorted Thorpe length scale for all the profiles of IWISE throughout the depth. (c) Histogram of density sorted  $L_T$  with patch statistics for IWISE, (d) Histogram of temperature sorted  $L_T$  with patch statistics for IWISE.

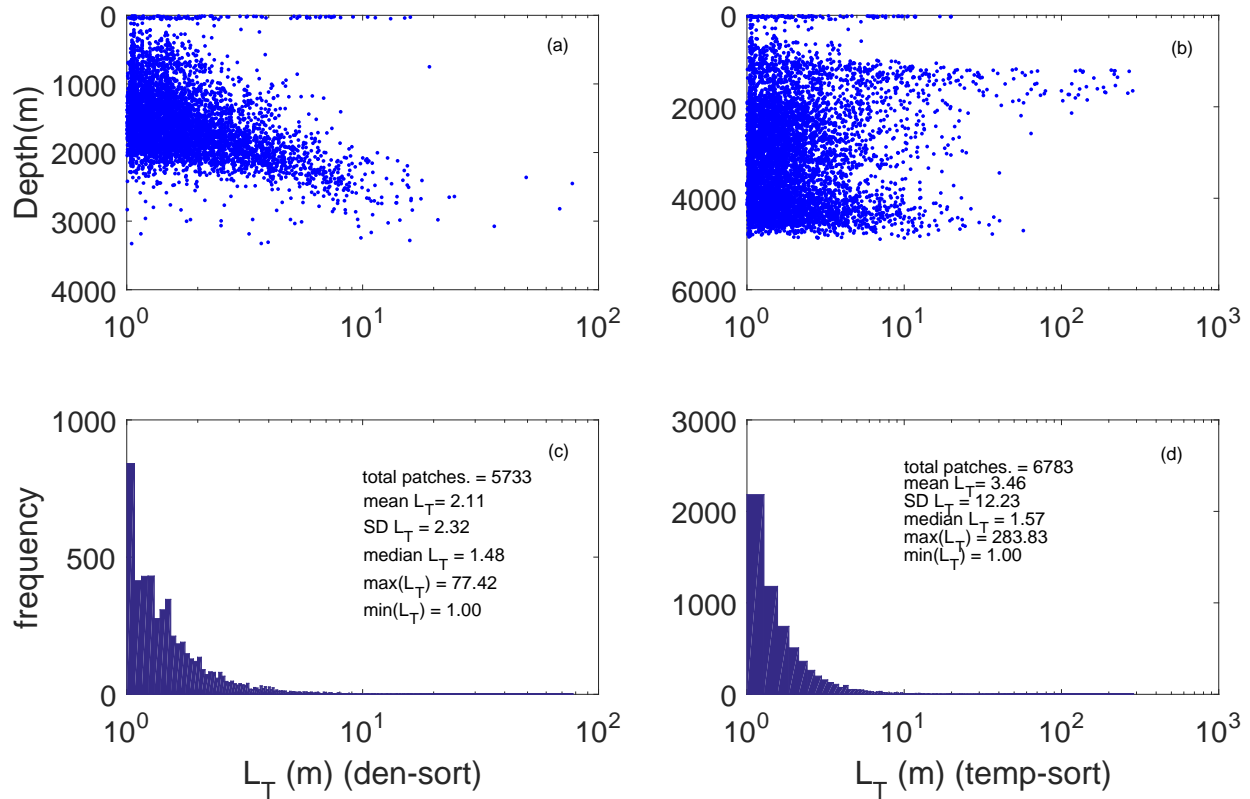


**Figure 3.7:** (a) Density sorted Thorpe length scales for all the profiles of BBTRE through out the depth (b) Temperature sorted Thorpe length scale for all the profiles of BBTRE throughout the depth. (c) Histogram of density sorted  $L_T$  with patch statistics for BBTRE, (d) Histogram of temperature sorted  $L_T$  with patch statistics for BBTRE.

density is mostly a function of temperature hence both the sorting methods provide similar patch statistics. Figure 3.6 shows that the distribution of patches throughout the depth can be considered collocated. The maximum  $L_T$  is also same for both approaches which is  $\sim 87$  m. Now, for the BBTRE data set,  $L_T$  obtained from density sorted profiles and temperature sorted profiles show significant difference in patch statistics as evident from figure 3.7. The big patches in 1000 – 1700 m depth of BBTRE data obtained through temperature sorting method are ambiguous. The cause might be salinity intrusion.

Figure 3.8 shows the relation of Thorpe length scale  $L_T$  and Patch size  $L_P$  for both temperature sorted and density sorted profiles of both the data sets. For the temperature sorted patches,  $L_P = 3L_T$  consistent with literature. But for density sorted patches,  $L_P$  are much larger than  $L_T$ . This is

possible because, the overturn region can consist of multiple small patches where the fluid particles have to move a shorter distance to achieve an adiabatically stable profile, compared to the size of the whole overturn. Some data points which show  $L_P < L_T$  in figure 3.7, are discarded further as we have considered only those patches, for which water moves within the patch in order to obtain a stable background profile. Also, further analysis, we have considered density sorted patches. Only data from clearly defined thermocline and deep ocean regions are considered for further analysis to overcome the effects of wind driven upper ocean and topography influenced bottom ocean data. The BBTRE data from 1000 – 1700  $m$  are also discarded to eliminate the probability of double diffusion due to salinity intrusion (Laurent & Smitt, 1999). For a well mixed region (upper ocean and bottom boundary of ocean) mixing efficiency is low. For double diffusion region, high mixing efficiency is obtained which is not a result of turbulent mixing. All data considered for this study do not have double diffusion regions.

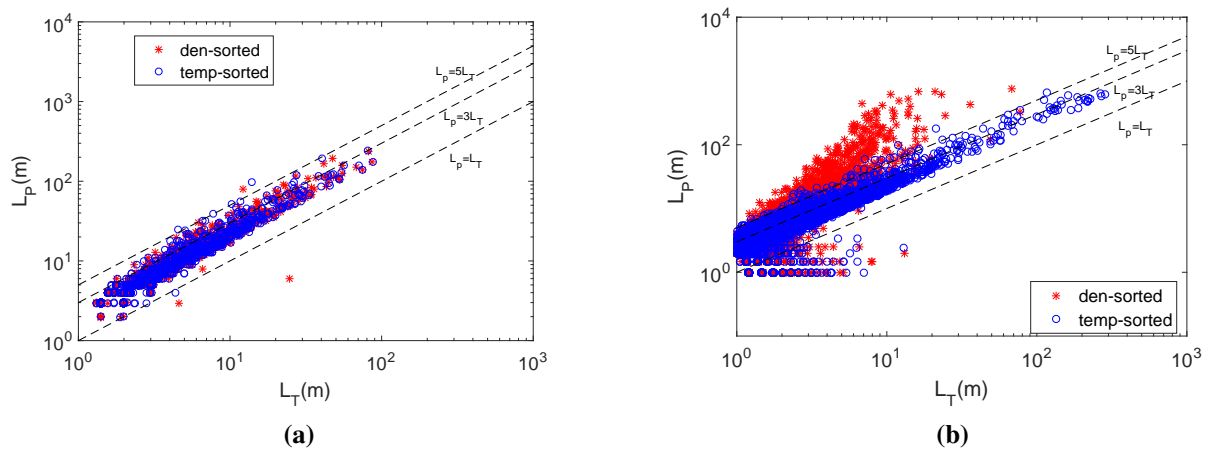


**Figure 3.8:** A comparative study of Thorpe length  $L_T$  and patch length  $L_P$  for corresponding patches for (a) IWISE data (b) BBTRE data.

### 3.5.3 Background stratification

In this section, the statistics of background stratification are discussed for all three different methods of computing  $N$  as discussed in section 3.4.4. Figure 3.9 shows the statistics for  $N_{2pt}$ ,

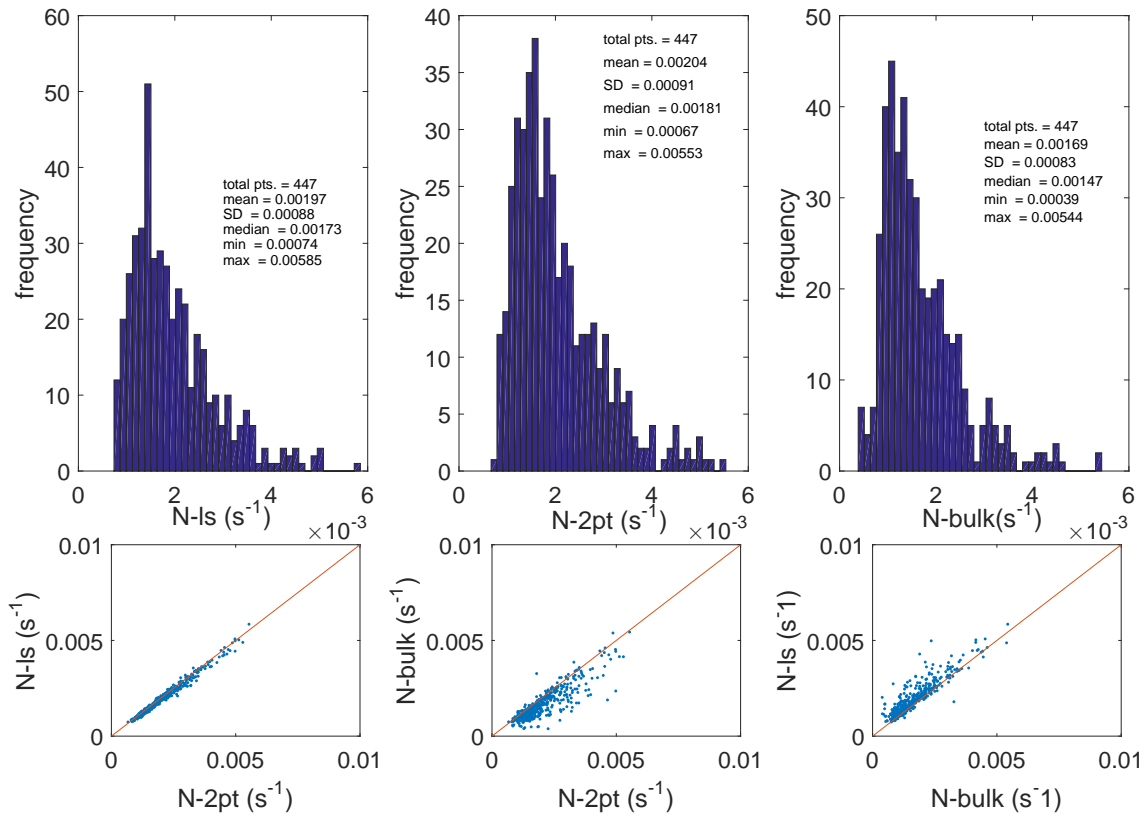


**Figure 3.9:** Statistics of background stratification obtained from different methods for BBTRE thermocline data.

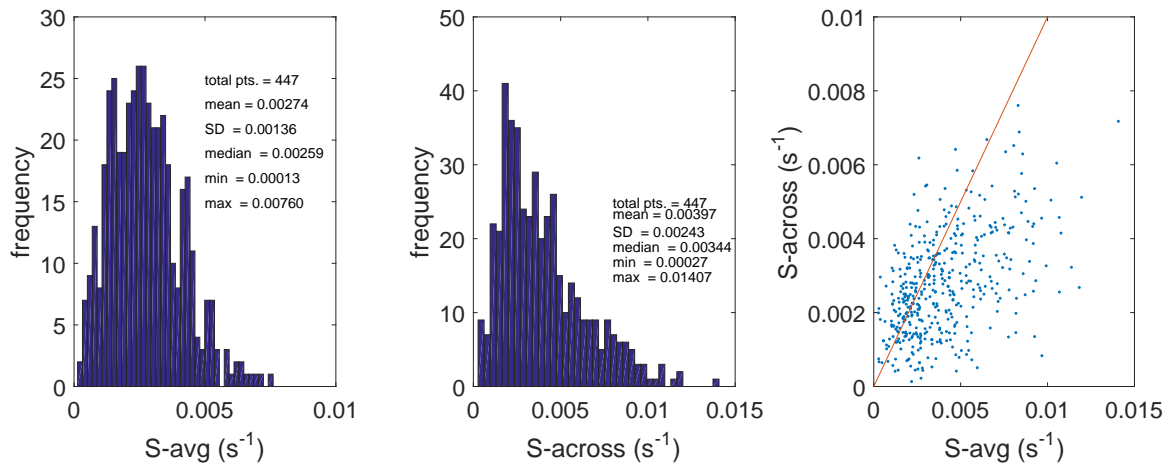


**Figure 3.10:** Statistics of background shear obtained from different methods for BBTRE thermocline data.

$N_{bulk}$  and  $N_{ls}$  and their comparisons for patches of BBTRE thermocline region. This plot is a representation of all other data (not shown here). It is evident from figure 3.9 that buoyancy frequency obtained from  $N_{2pt}$  and  $N_{ls}$  are in good agreement.  $N$  obtained from bulk method underpredicts the values from other two methods. As  $N_{2pt}$  and  $N_{ls}$  are no different, we have considered only  $N_{2pt}$  and  $N_{bulk}$  for further analysis.

### 3.5.4 Background shear

Statistics of the background shear obtained from both the methods described in section 3.4.4 are plotted in figure 3.10 for BBTRE thermocline region for the same patches shown in figure 3.9. The shear obtained from patch-across and patch-average methods provide completely different statistics. Hence, the values used to define background shear has significant effect in determining gradient Richardson numbers.

### 3.5.5 Ambiguity of $Re_b$ based parameterization of mixing efficiency, $R_f$

In section 3.1, we have provided a brief overview concerning mixing efficiency and its parameterizations. The commonly used parameterization suggest that mixing efficiency decreases with buoyancy Reynolds number  $Re_b$  with a relation  $R_f \propto Re_b^{-1/2}$ , for the energetic regime,  $Re_b > \mathcal{O}(100)$  and  $R_f$  is constant with a value of 0.16 (similar to Osborn model) in the buoyancy driven regime ( $7 < Re_b < 100$ ), (Barry *et al.*, 2001; Maffioli & Davidson, 2016; Shih *et al.*, 2005). We have shown the statistics of  $R_f$  with  $Re_b$  for the field data in figures 3.11 and 3.12. We have analysed the mixing efficiency by dividing the vertical profiles into two broad categories, thermocline and deep ocean region as the ocean energetics are different in these two regimes. Thermocline is generally very strongly stratified than the deep ocean. Here we have considered  $N_{bulk}$ , corresponding bulk temperature gradient, patch average  $\chi$  and patch average  $\epsilon$  to compute  $R_f$  and  $Re_b$  for each individual density sorted patches. The scatter plots of all the patches together do not provide any information. Hence, we have divided the data into small bins and used statistical arithmetic mean of those bins in the plots. The number of data points in each bin are also shown in the figure. We have discarded the bin if there are less than 10 points. The statistical average data

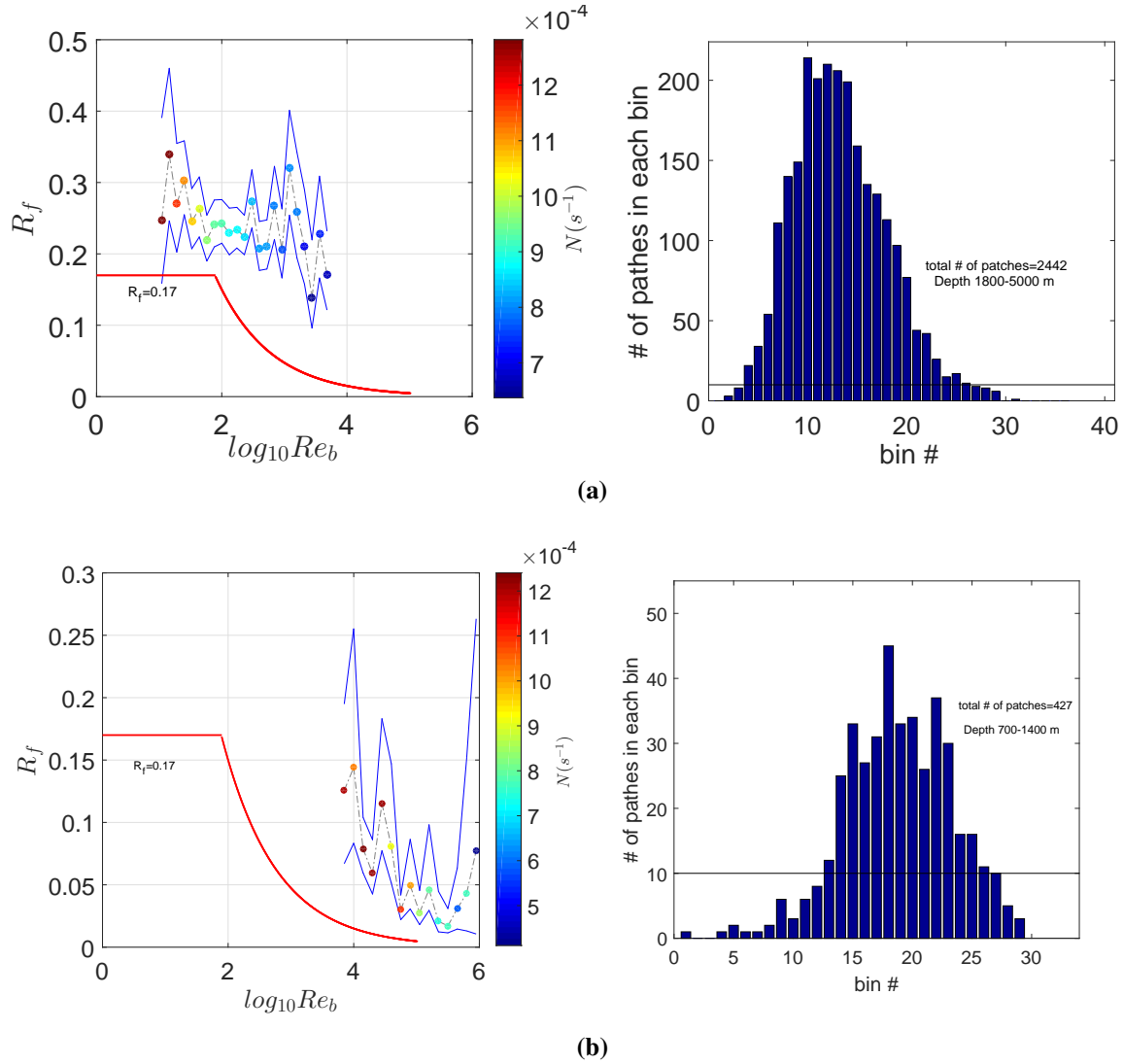


**Figure 3.11:** Left panel: Variation of mixing efficiency with buoyancy Reynolds number ( $Re_b = \epsilon/\nu N^2$ ) in deep ocean region for (a) BBTRE data (b) IWISE data.  $N = N_{bulk}$ . The red solid line shows the parameterization of  $R_f$  as per Shih *et al.* (2005). Blue boundary lines suggest 95 CI. Right panel: Distribution of patches over different bins considered to obtain left panel mean data.

are shown with 95% confidence interval obtained through a bootstrap method. Figure 3.11a shows that for deep ocean region, BBTRE data exhibits a higher value of  $R_f$  than 0.17 and figure 3.11b shows that IWISE data exhibits a lower value of  $R_f$  compared to the canonical value 0.17. For both cases,  $R_f$  decreases with  $Re_b$  but at higher value of  $Re_b$  ( $\mathcal{O}(10^3)$  for BBTRE and  $\mathcal{O}(10^4)$  for IWISE). IWISE site is a highly energetic site and the  $Re_b$  values are very high which corresponds to weak stratification and strong turbulence resulting in low values of mixing efficiency. The de-

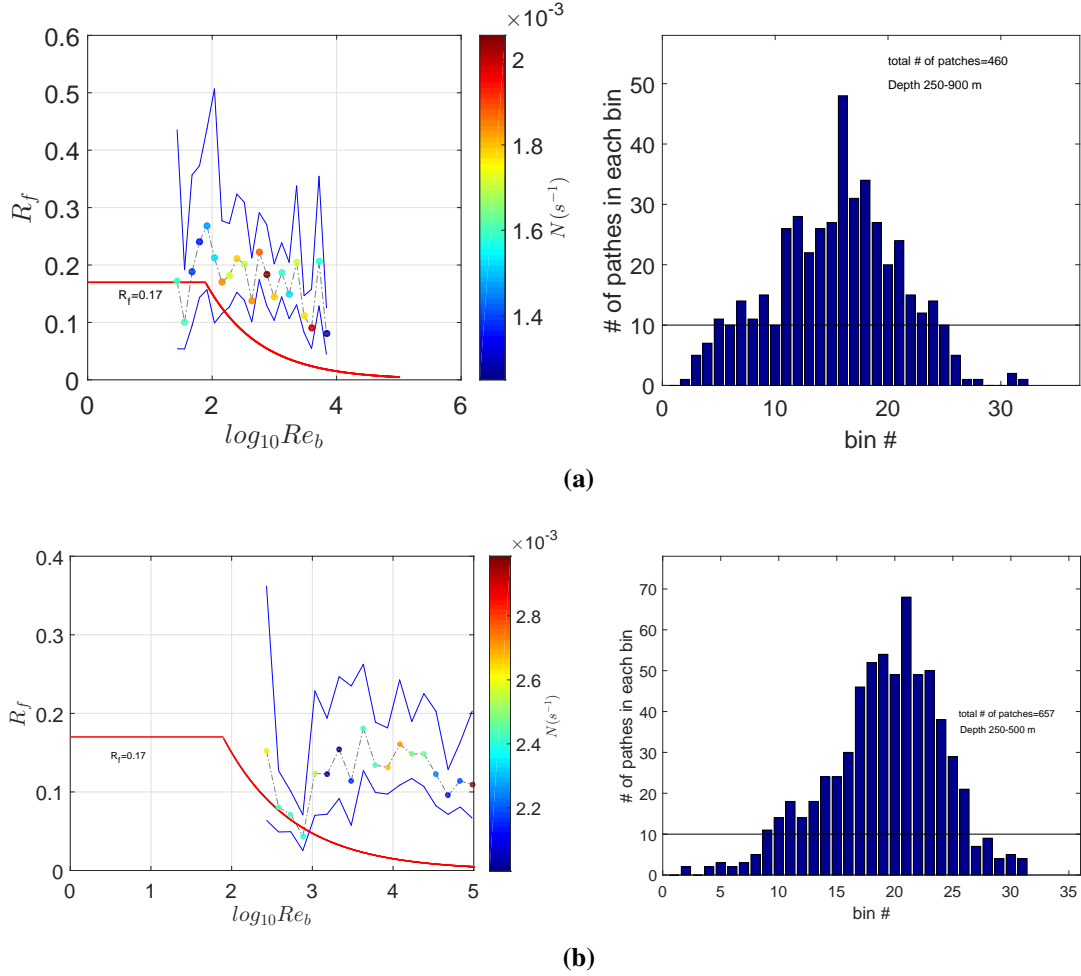


**Figure 3.12:** Left panel: Variation of mixing efficiency with buoyancy Reynolds number ( $Re_b = \epsilon/\nu N^2$ ) in thermocline region for (a) BBTRE data (b) IWISE data.  $N = N_{bulk}$ . The red solid line shows the parameterization of  $R_f$  as per Shih *et al.* (2005). Blue boundary lines suggest 95% CI. Right panel: Distribution of patches over different bins considered to obtain left panel mean data.

crease of  $R_f$  is due to decrease in stratification as evident from figure. Color bar displaying values of  $N$  signifies the strength of stratification. Now for thermocline data, figure 3.12 shows that  $R_f$  is relatively constant and insignificant to change of  $Re_b$ . We can argue that this might be possible as thermocline is strongly stratified. If there is any mixing due to breaking of the internal waves, these regions restratify quickly then maintaining the vertical structure. So, for the patches where  $Re_b$  value indicates strong turbulence in thermocline region a constant mixing efficiency of 0.17 might be appropriate but is not limited to  $7 < Re_b < 100$  as suggested by Shih *et al.* (2005) from direct numerical simulation data.

### 3.5.6 Mixing efficiency and gradient Richardson number

In this section, we have shown variation of mixing efficiency as a function of gradient Richardson number. Gradient Richardson number is a non dimensional parameter to determine relative strength of background stratification and background shear in a shear dominated flow. This is defined as  $Ri_g = N^2/S^2$ , where  $N^2$  is the buoyancy frequency and  $S^2$  is the shear. The existing parameterizations suggest that for shear dominated regime, ( $Ri_g \sim 0.25$ ), mixing efficiency increases with  $Ri_g$ . This is justified as when  $Ri_g = 0$ , i.e., there is no stratification,  $R_f$  should go to zero as there is nothing to mix. With increase of stratification  $R_f$  gradually increases. The relation of  $R_f$  and  $Ri_g$  for  $Ri_g < 0.25$  is robust and shown by various studies (Ivey & Imberger, 1991; Karimpour & Venayagamoorthy, 2014; Linden, 1984; Lozovatsky & Fernando, 2012; Venayagamoorthy & Koseff, 2016). There is no substantial evidence regarding the relation of  $R_f$  in the limit of high  $Ri_g$ . Does high values of  $Ri_g$  represents strongly stratified flows, or is it artifact for low stratification over low shear? From DNS data analysis, Karimpour & Venayagamoorthy (2014) showed that  $R_f = 0.25[1 - \exp(-7Ri_g)]$  such that mixing efficiency increases with  $Ri_g$  upto a value of 0.25 and then asymptotes to a constant value at  $Ri_g \sim O(1)$  similar to other results (Canuto *et al.*, 2001; Lozovatsky & Fernando, 2012; Mellor & Yamada, 1982). Here we have presented variation of  $R_f$  as a function of  $Ri_g$  for various data where shear is obtained from two different methods as described in section 3.4.4 and are shown in figures 3.13 and 3.14 respectively. The patch statistics are obtained in similar ways as in figure 3.11 and 3.12. The values of  $R_f$  and  $Ri_g$  are qualitatively similar when the background stratification is obtained by either  $N_{2pt}$  or  $N_{bulk}$  method (figures 3.13 and 3.14).

Figure 3.13a and 3.14a show that  $R_f$  increases with  $Ri_g$  in shear dominated regime similar to other findings, approaches a constant value, and then decreases with  $Ri_g$  for  $Ri_g \sim O(10)$ . The decrease of mixing efficiency is a result of low stratification as shown by the values of  $N$  in color bar. The constant values are different for both the data sets. This type of trend is possible if shear is calculated as patch-across shear ( $S_{across}$ ). When shear is calculated by patch-averaging, ( $S_{avg}$ ), the trend of  $R_f$  and  $Ri_g$  is different as evident from figures 3.13b and 3.14b, where mixing efficiency

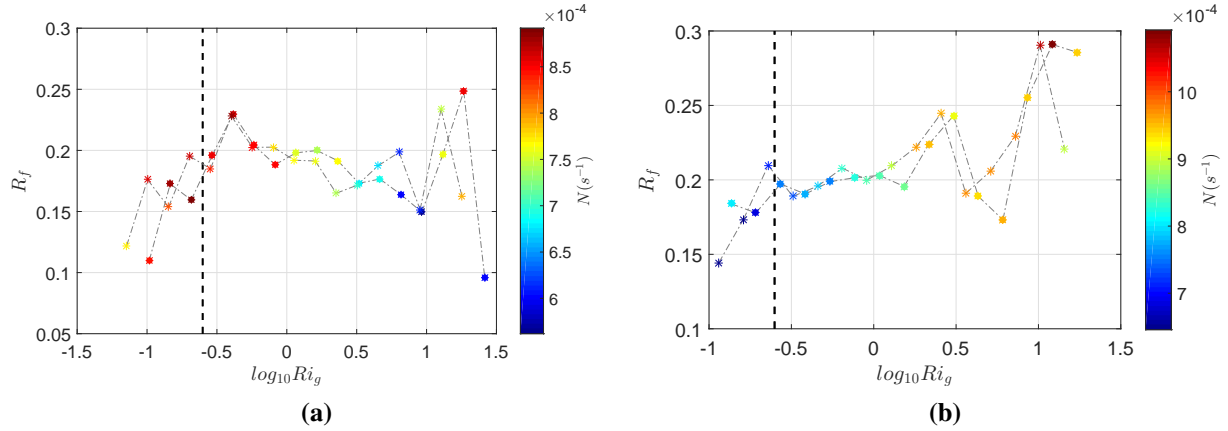


**Figure 3.13:** Variation of mixing efficiency with gradient Richardson number ( $Ri = N^2/S^2$ ) for BBTR deep ocean data. (a) Patch-across shear (b) Patch-average shear. Solid circle:  $N_{2pt}$ , star:  $N_{bulk}$ . Vertical line corresponds to  $Ri = 0.25$ .

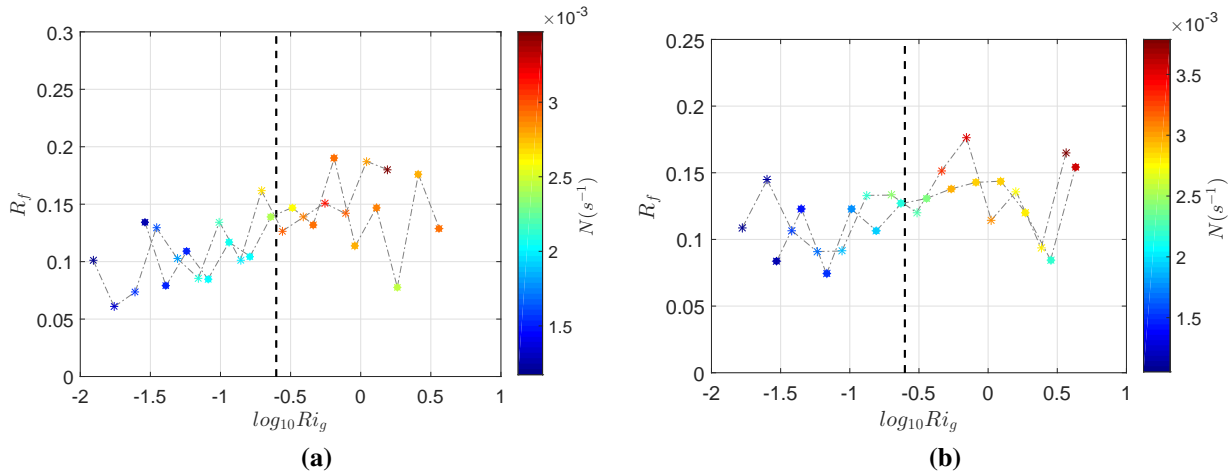


**Figure 3.14:** Variation of mixing efficiency with gradient Richardson number ( $Ri_g = N^2/S^2$ ) for IWISE thermocline data. (a) Patch-across shear (b) Patch-average shear. Solid circle:  $N_{2pt}$ , star:  $N_{bulk}$ . The dashed vertical line corresponds to  $Ri_g = 0.25$ .

shows an increasing trend in full spectrum of  $Ri_g$ . At this stage we can only conclude that the methodology of data analysis is crucial for parameterizing mixing with field data and can not be overlooked. We can not conclude with confidence which method of computing  $Ri_g$  is correct. From a reasoning analysis, shear obtained from  $S_{across}$  is better justified.

### 3.6 Concluding remarks

In this study, we have used field data for the analysis of mixing efficiency and its parameterization with most commonly used parameters  $Re_b$  and  $Ri_g$ . We have shown that the traditional canonical value of constant mixing efficiency does not necessarily hold in different parts of the ocean. Further it is shown that the  $Re_b$  based parameterizations are not universal. In order to test the validity of shear based parameterizations, further study is required with different flow conditions where  $Ri_g$  has a higher range. We have also proposed a new method for obtaining the background shear of overturning region. Further investigations using a diversified field data sets along with high resolution direct numerical simulation data of sheared stratified turbulence are required in order to validate proposed methods for estimation of mean shear.

# Chapter 4

## Assessment of small scale anisotropy in stably stratified turbulent flows using direct numerical simulations<sup>6</sup>

### 4.1 Introduction

Accurate estimation of small scale turbulent mixing is essential for understanding the dynamics of density stratified geophysical flows such as in the oceans and in the atmosphere. For example, the small scale fluxes due to mixing impacts the meridional overturning circulation, global climate, ocean heat budget, ocean productivity etc. The effect of small scale mixing is generally parameterized in terms of a turbulent (eddy) diffusivity,  $K_\rho$  in large scale ocean and climate models and hence such models are highly sensitive to such parameterizations (Richards *et al.*, 2009). The present study focuses on the small scale dynamics using direct numerical simulations (DNS), to assess the goodness of isotropy assumption for stratified flows that is widely used in *in situ* measurements of turbulent quantities.

Direct measurement of eddy diffusivity is not feasible in the ocean due to internal wave induced fluctuations that are prevalent in stably stratified turbulence. Therefore, the standard practice in oceanography is to infer the vertical eddy diffusivity,  $K_\rho$  indirectly from measurable small scale turbulent quantities such as the rate of dissipation of turbulent kinetic energy ( $\epsilon$ ), using the Osborn model (Osborn, 1980), or from the rate of dissipation of scalar (density) variance ( $\epsilon_\rho$ ), using the Osborn & Cox model (Osborn & Cox, 1972). The natural question to ask is how accurately are  $\epsilon$  and  $\epsilon_\rho$  measured in the ocean? This is because, the true value of  $\epsilon$  requires nine mean

---

<sup>6</sup>The research presented in this chapter is nearing submission to Physics of Fluid under the title "Assessment of small scale anisotropy in stably stratified turbulent flows using direct numerical simulations" by A. Garanaik and S. K. Venayagamoorthy. The chapter is written in a collective "we" voice to acknowledge collaboration with Dr. S. K. Venayagamoorthy.

square fluctuating velocity gradients and the true value of  $\epsilon_\rho$  requires three mean square fluctuating scalar gradients. Simultaneous measurements of all the components are not possible in the ocean with current (state-of-the-art) micro-structure sensors. As a consequence, it is common practice to measure dissipation quantities using one or two spatial gradients of the fluctuating quantities invoking Kolmogorov's small scale isotropy hypothesis (§4.2), which is generally applicable to high Reynolds number flows (Kolmogorov, 1941). So the extension of local isotropic assumption to oceanic stratified flows where the turbulence is sporadic in nature and the Reynolds numbers are not always sufficiently high to justify isotropy at small scales, is definitely questionable. The buoyancy forces cause large scale anisotropy in stably stratified turbulent flows and small scales are also expected to be anisotropic especially at lower Reynolds number flow conditions that are often possible in the deep ocean. A number of studies, however, have shown evidence of strong anisotropy in fluctuating strain rates for stratified turbulence from *in situ* measurements (Gargett *et al.*, 1984; Yamazaki & Osborn, 1990), laboratory experiments (Fincham *et al.*, 1996; Thoroddsen & Atta, 1992) and numerical simulations (Brethouwer *et al.*, 2007; Godeferd & Staquet, 2003; Smyth & Moum, 2000) as well as in fluctuating density (scalar) fields (Smyth & Moum, 2000; Sreenivasan, 1991). The small scale anisotropy generally develops faster than the large scale anisotropy in stratified turbulence (Thoroddsen & Atta, 1992; Wingstedt *et al.*, 2015).

Gargett *et al.* (1984) suggested a threshold value of buoyancy Reynolds number  $Re_b \approx 200$  above which small scales are isotropic. The buoyancy Reynolds number is defined as  $Re_b = \epsilon/(\nu N^2)$ , where  $N$  is the buoyancy frequency and  $\nu$  is the kinematic viscosity. From a DNS of sheared stratified turbulence, Smyth & Moum (2000) also found a similar result that shows departure from isotropy only for  $Re_b < 10^2$ . Note that, in the oceanic thermocline,  $Re_b$  is generally  $\leq 200$  and hence, the effects of stratification contributing towards small-scale anisotropy cannot be overlooked. Again, the measurements of Gargett *et al.* (1984) included only three orthogonal turbulent velocity components and the local isotropy assumption was in-built in the evaluation of the frequency response of the instruments (Thoroddsen & Atta, 1992). Though the DNS data used in Smyth & Moum (2000) has all the nine velocity gradients and all the three scalar gradients, the

simulations were at lower values of initial Richardson number  $\leq 0.12$ , representative of weakly stratified flow conditions. DNS data of Itsweire *et al.* (1993) show that estimates of dissipation rates obtained from isotropic formulas can be erroneous by a factor of 2 – 4 even for  $50 < Re_b < 650$ . Using the assumptions of axis-symmetry about vertical axis and semi-isotropic turbulence, Yamazaki & Osborn (1990) and Thoroddsen & Atta (1992) have estimated rates of dissipation of turbulent kinetic energy in separate experiments using two cross stream gradients. The modern vertical microstructure profilers measure the vertical gradients of horizontal velocities ( $u_z$  and  $v_z$ ) which are the dominant velocity gradients in a vertically stratified flow (Godefert & Staquet, 2003). Ward *et al.* (2014) used a new Air-Sea Interaction profiler with two shear probes orientated at  $90^\circ$  to each other which can provide simultaneous measurements of two orthogonal components but such measurements are limited to maximum depth of 100 m.

The hypothesis of local isotropy supposes that all small scale statistics are isotropic. A proper verification of the local isotropy hypothesis is not possible (as yet) from laboratory experiments or field measurements due to the limited number of velocity gradients that can be measured. As a result, different values of  $Re_b$  have been reported in the literature at which different components of spatial gradients approach the state of isotropy (Brethouwer *et al.*, 2007; Osborn & Lueck, 1985; Smyth & Moum, 2000; Thoroddsen & Atta, 1992; Yamazaki & Osborn, 1990). Given the complexity and difficulties associated with measurement of small scales, it is not surprising that there is no consensus on what is the right parameter of choice for quantifying departure from isotropy and there is no universal parameterization of degree of isotropy. We note here that, even though it is convenient to use  $Re_b$ , it might not be the best parameter to use due to ambiguity of its physical interpretation (Gargett, 1988; Mater & Venayagamoorthy, 2014). In fact, the turbulent Froude number is the fundamental parameter which determines the dynamical coupling between stratification and fluctuating motions (Sarkar, 2003).

To get a clear understanding of departure from isotropy in small scale stratified turbulence, a high-resolution DNS study of decaying stratified turbulence was conducted. Results are discussed in terms of the turbulent Froude number defined as  $Fr = \epsilon / (NE_k)$  where,  $E_k$  is the turbulent

kinetic energy. Theoretical background of small scale isotropy assumption is discussed in §4.2. In §4.3, we provide a brief description of the numerical simulations. Results are discussed in §4.4 and concluding remarks are given in §4.5.

## 4.2 Theoretical background of small scale isotropy

In this section, an overview of the small scale isotropy assumption is discussed for estimation of the rate of dissipation of turbulent kinetic energy and the rate of dissipation of scalar variance. The concept of small scale or local isotropy postulated by Kolmogorov (1941) is crucial for modern turbulence theory. According to this hypothesis, in a sufficiently high Reynolds number flow, the directional information of the large scales are lost during the transfer of energy from large to small scales and the statistics of small scales are therefore universally isotropic (independent of coordinate orientations). This implies that the spatial gradients of dissipation quantities are related to each other and that any one component is sufficient to estimate the exact values of the dissipation as described below.

The rate of dissipation of turbulent kinetic energy,  $\epsilon$  is generally defined as

$$\epsilon = \nu \left\langle \frac{\partial u_i}{\partial x_j} \left( \frac{\partial u_i}{\partial x_j} + \frac{\partial u_j}{\partial x_i} \right) \right\rangle, \quad (4.1)$$

where the angle bracket,  $\langle \rangle$  represents the ensemble average,  $u_i$  is the fluctuating velocity vector,  $\nu$  is the kinematic viscosity and  $i, j = 1, 2, 3$ . The rate of dissipation of density variance is defined as,

$$\epsilon_\rho = \kappa \langle (\partial \rho / \partial x_i)^2 \rangle, \quad (4.2)$$

where  $\rho$  is the fluctuating density and  $\kappa$  is the molecular diffusion. It is evident from the above equations that the exact estimation of  $\epsilon$  (4.1) requires nine spatial velocity gradient components while that of scalar dissipation (4.2) requires three spatial scalar gradients. The following relationships can be established between the mean square turbulent velocity gradients by virtue of local isotropy (Pope, 2000; Taylor, 1935).

$$\langle u_x^2 \rangle = \langle v_y^2 \rangle = \langle w_z^2 \rangle. \quad (4.3)$$

$$\langle u_y^2 \rangle = \langle u_z^2 \rangle = 2\langle u_x^2 \rangle. \quad (4.4)$$

$$\langle u_y v_x \rangle = \langle v_z w_y \rangle = \langle u_z w_x \rangle = -\frac{1}{2}\langle u_x^2 \rangle. \quad (4.5)$$

Here, the notation  $u_x$  refers to the gradient of the fluctuating u velocity with respect to the x (horizontal) direction. With the relations described in 4.3, 4.4 and 4.5, the isotropic rate of dissipation of turbulent kinetic energy  $\epsilon_{iso}$  can be obtained from any one velocity gradient, as shown in equation 4.6.

$$\begin{aligned} \epsilon_{iso}/\nu &= 15\langle u_x^2 \rangle = 15\langle v_y^2 \rangle = 15\langle w_z^2 \rangle = 7.5\langle u_y^2 \rangle = 7.5\langle u_z^2 \rangle \\ &= 7.5\langle v_x^2 \rangle = 7.5\langle v_z^2 \rangle = 7.5\langle w_x^2 \rangle = 7.5\langle w_y^2 \rangle. \end{aligned} \quad (4.6)$$

Similarly, the isotropic density dissipation rate,  $\epsilon_{\rho_{iso}}$  can be obtained from any scalar gradient by noting that,  $\langle \rho_x^2 \rangle = \langle \rho_y^2 \rangle = \langle \rho_z^2 \rangle$  as

$$\epsilon_{\rho_{iso}}/\kappa = 3\langle \rho_x^2 \rangle = 3\langle \rho_y^2 \rangle = 3\langle \rho_z^2 \rangle. \quad (4.7)$$

### 4.3 Direct numerical simulations

Direct Numerical simulation (DNS) provides full description of turbulent flow field ranging from energy containing large eddy scale ( $\mathcal{L}$ ) to small dissipative Kolmogorov scale ( $\eta$ ) without involving any parameterization of small-scale physics. The numerical simulations for our study were carried out using pseudo-spectral DNS code developed by Riley *et al.* (1981) for stably stratified homogeneous turbulent flows. A cubical periodic domain with dimension  $2\pi$  with  $512^3$  grid points was considered for all simulations. The turbulent flow was initialized with a Gaussian isotropic three dimensional solenoidal velocity field and allowed to evolve and decay under the influence of a constant background stratification. The mean shear was zero for all the simulations and the

only large scale anisotropy considered was vertical stable stratification. Flow was characterized with an initial Reynolds number of 1000 defined as  $Re_0 = u_0 L_0 / \nu$ , where  $u_0$  is the initial velocity scale and  $L_0$  is the initial length scale. Background stratification was characterized with an initial Richardson number, defined as  $Ri_0 = (N L_0 / u_0)^2$ , where  $N$  is the buoyancy frequency. Four DNS simulations were performed for the present study with  $Ri_0 = 0.01, 0.1, 1.0$  and  $10$ , respectively, for a duration of  $5L_0/u_0$  in order to investigate the effects of weakly stratified to strongly stratified condition on the small scales of turbulence. The value of  $k_{max}\eta$  (corresponding to maximum dissipation) varied from 1.41 to 1.6 for  $Ri_0 = 0.01$  to  $Ri_0 = 10$  respectively, where  $k_{max}$  is the maximum wave number. This criteria ensures that the resolution was sufficient to resolve the smallest scales of dissipation (Yeung *et al.*, 1995). The molecular Prandtl number  $Pr = \nu/\kappa = 1$  for all the simulations to ensure accurate resolution of the dissipative scales of the density (scalar) field. Similar to the simulations performed by Mater *et al.* (2013), after the first eddy turnover period,  $1L_0/u_0$ , the dissipation peaks and begins to decay. This is interpreted as a signature of fully developed turbulence. Hence, initial transients prior to this time were ignored in this study.

## 4.4 Results and discussions

### 4.4.1 Flow dynamics

In this section, we present an analysis into the energetics of the flow to help understand the development of anisotropy in strongly stratified flows. Figure 4.1 shows the evolution of kinetic energy  $E_k$  and potential energy  $E_p$  for  $Ri_0 = 0.01, 0.1, 1$  and  $10$  with respect to time  $t$ , non-dimensionalized by  $L_0/u_0$ . These results are equivalent to previously published results using DNS of lower resolutions (Riley *et al.*, 1981; Venayagamoorthy & Stretch, 2006). The initial  $E_p$  was set to zero for all the simulations.  $E_p$  gradually increases to a peak value by gaining energy from  $E_k$  and eventually, all energy decays under the influence of stratification. The energy conversion from  $E_k$  to  $E_p$  is more for higher stratification. This is because, with increase of stratification the vertical buoyancy flux dominates the flow by reducing more of turbulent kinetic energy in vertical direction. For an isotropic or nearly isotropic flow, there is an equal contribution of all the three

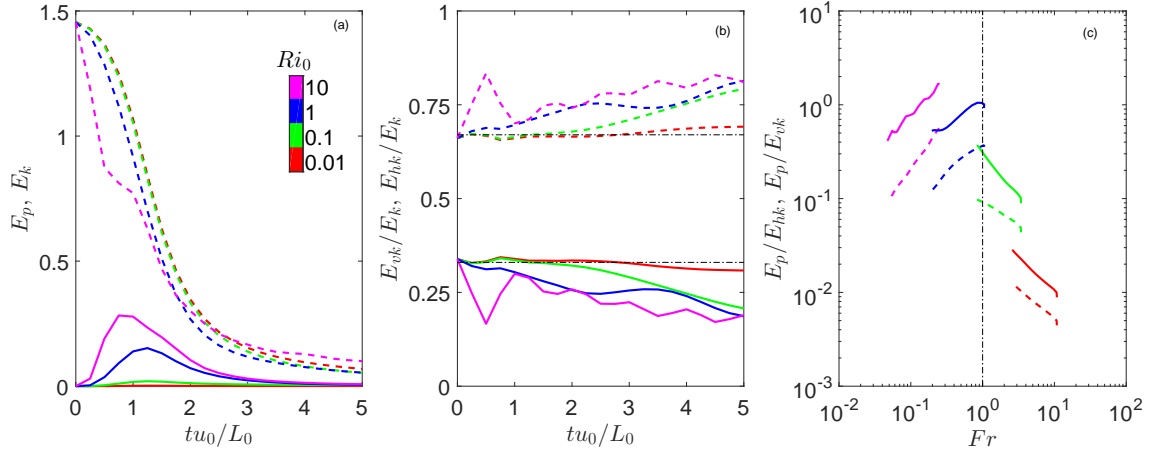


**Figure 4.1:** (a) The time evolution of kinetic energy,  $E_k$ , (dashed line) and potential energy,  $E_p$ , (solid line). (b) The ratio of horizontal kinetic energy to total kinetic energy,  $E_{hk}/E_k$ , (dashed line) and the ratio of vertical kinetic energy to total kinetic energy,  $E_{vk}/E_k$ , (solid line). (c) The ratio of potential energy to horizontal kinetic energy,  $E_p/E_{hk}$ , (dashed line) and the ratio of potential energy to vertical kinetic energy,  $E_p/E_{vk}$  (solid line) with turbulent Froude number,  $Fr$ . The color indicates different values of initial Richardson number ( $Ri_0$ ).

velocity components towards  $E_k$ . This implies that the ratio of vertical kinetic energy  $E_{vk}$  to total kinetic energy  $E_k$  is  $1/3$  and the ratio of horizontal kinetic energy  $E_{hk}$  to  $E_k$  is  $2/3$ . Note that the horizontal kinetic energy includes both horizontal velocity components. The ratio  $E_{hk}/E_k$  and  $E_{vk}/E_k$  are plotted in figure 4.1 (b) for all simulations with respect to non-dimensional time. For strong vertical stratification, the vertical motions are attenuated due to restoring buoyancy forces creating anisotropy in stably stratified flows. Hence, the ratio,  $E_{vk}/E_k$  decreases and  $E_{hk}/E_k$  increases with increase of stratification (figure 4.1b). That is, for any instant of time, most of the turbulent kinetic energy resides in the horizontal directions and the energy distribution is not equal in all the directions as in the case an isotropic (unstratified) flow. The loss of vertical kinetic energy contributes towards the increase of the potential energy. Figure 4.1 (c) shows the ratio  $E_p/E_{hk}$  and  $E_p/E_{vk}$  with respect to turbulent Froude number. For weakly stable flows,  $Fr > \mathcal{O}(1)$ , the conversion of kinetic energy to potential energy is relatively small compared to that of strongly stable flows,  $Fr < \mathcal{O}(1)$ . Generally, the potential energy is transferred towards small scale more efficiently than the kinetic energy and higher rate of transfer of potential energy towards small scale leads to decrease of vertical kinetic energy (Godefert & Staquet, 2003). With increase of

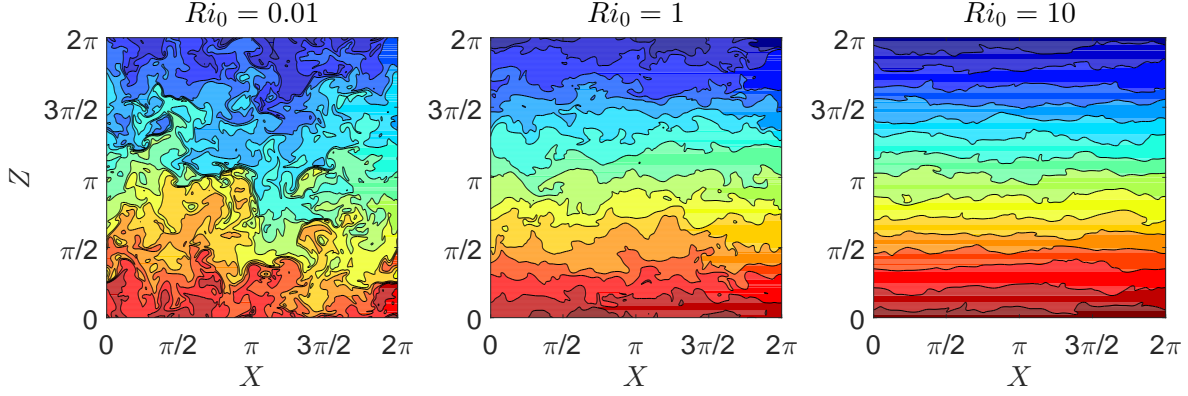


**Figure 4.2:** Snapshot (2D) of instantaneous density instability at eddy turnover time 5 in the  $X$ - $Z$  plain (at  $Y = \pi$ ) where,  $Z$  is the vertical axis along which linear stratification is imposed. Color from red to blue indicates heavy to lighter fluid respectively. Stratification increases from left panel to right. Black lines indicate isopycnals.

stratification, more vertical kinetic energy gets converted to potential energy, which dominates the smallest dynamical scales and the small scale statistics are expected to be anisotropic. The question is, under what conditions does the isotropy assumption breaks down for the small scale statistics in a stratified fluid?

A visualization of fluctuating density field on a vertical plain is shown in figure 4.2, for three different initial Richardson numbers,  $Ri_0 = 0.01, 1$  and  $10$  representing weak, moderate and strong stratification respectively, at  $5L_o/u_o$ . For low stratification ( $Ri_0 = 0.01$ ) the vertical density perturbation is significant but with increase of stratification the vertical motion diminishes as described above and the emergence of horizontal layers is apparent.

#### 4.4.2 Anisotropy of rate of dissipation of turbulent kinetic energy ( $\epsilon$ )

All the nine individual isotropic dissipation components (4.6) normalized by the true rate of dissipation of turbulent kinetic energy (4.1) are shown in figure 4.3, as a function of turbulent Froude number ( $Fr$ ). The color bar represents the buoyancy Reynolds number ( $1 < Re_b < 10^5$ ). We have not considered any data with  $Re_b < 1$  as in that regime, turbulent motions are nearly absent and  $\epsilon$  is obtained from vertical shearing (Brethouwer *et al.*, 2007). Also, all the data presented are for  $tu_o/L_o > 1$  to exclude the pre-turbulent stage. When the local isotropy

assumption is valid, the ratio of isotropic dissipation components to the true dissipation should be approximately unity. As shown in figure 4.3, for  $Fr > 1$ , the dissipation rates obtained using the isotropic assumption are close to the true dissipation rate. However, as soon as the stratification becomes relatively strong, i.e.,  $Fr \sim \mathcal{O}(1)$ , there is a clear signature of departure from isotropy. Significant departure from isotropy is noticeable in the strongly stable regime ( $Fr < \mathcal{O}(1)$ ). One can argue that the small scale anisotropy can be a artifact of lower Reynolds number. In our simulations  $Re \sim \mathcal{O}(10^3)$ . Sarkar (2003) also showed that the anisotropy of small dissipative scales can not be an artifact of low Reynolds number, rather stable stratification is the cause of dominance of fluctuating vertical shear irrespective of direction of mean shear.

For  $Fr < \mathcal{O}(1)$ , statistically,  $\langle u_z^2 \rangle \approx \langle v_z^2 \rangle$ ,  $\langle u_x^2 \rangle \approx \langle v_y^2 \rangle$ ,  $\langle u_y^2 \rangle \approx \langle v_x^2 \rangle$ ,  $\langle w_x^2 \rangle \approx \langle w_y^2 \rangle$ , because of axis-symmetry about vertical direction in the shear-free vertically stratified turbulence (figure 4.3). These relations of mean square velocity gradients also satisfy the isotropic initial conditions for inviscid and non-diffusive flow (Rehmann & Hwang, 2005). Our results suggest that the nature of anisotropy in the small scales depends on the direction about which the gradients of velocity are determined, i.e., the vertical derivatives over predict the true dissipation and the streamwise derivatives under predict the true dissipation similar to the results of Godefert & Staquet (2003). Rate of dissipation of turbulent kinetic energy obtained by  $\langle u_z^2 \rangle$  or  $\langle v_z^2 \rangle$  can overestimate the true rate of dissipation upto 40% in the limit of  $Re_b \approx 10$  and the over prediction can be by a factor of 2 for  $Re_b \approx 1$ . Similarly, dissipation obtained by  $\langle u_y^2 \rangle$  can underestimate true dissipation upto 35% and by  $\langle u_x^2 \rangle$  upto 15% for  $Re_b \approx 10$ . Itsweire *et al.* (1993) found similar results for sheared stratified flows. Rehmann & Hwang (2005) suggested that the isotropic component  $7.5\nu\langle v_z \rangle$  is better to estimate true  $\epsilon$  which predicts the dissipation value within 8% error in sheared and less than 15% error in shear-free stratified flow. But our results suggest that error associated with vertical gradient of horizontal velocity is maximum and horizontal gradients of horizontal velocity (cross-stream gradients) is minimum to estimate true  $\epsilon$  in strongly stable regime.

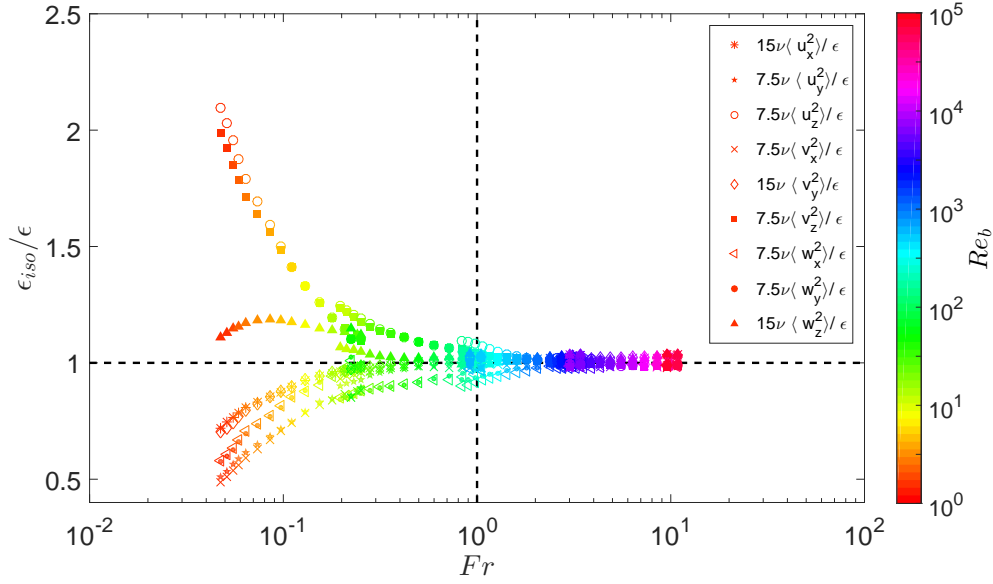


**Figure 4.3:** Contributions of each isotropic dissipation components to the true rate of dissipation of turbulent kinetic energy  $\epsilon$ , normalized by  $\epsilon$ .

#### 4.4.3 Anisotropy of rate of dissipation of density variance ( $\epsilon_\rho$ )

Figure 4.4 shows that the three isotropic density dissipation rates as given by (4.7) normalized by true rate of dissipation of density variance given by (4.2) as a function of turbulent Froude number. Similar the results for  $\epsilon$  as shown in figure 4.3, it is evident that all the scalar gradients are nearly isotropic for  $Fr > 1$ . Departure from isotropic is significant in strongly stable flows where  $Fr < \mathcal{O}(1)$ . Due to axis symmetry,  $\langle \rho_x^2 \rangle \approx \langle \rho_y^2 \rangle$  in strongly stable regime. The vertical gradient component ( $3\kappa\langle \rho_z^2 \rangle$ ) over estimates the true scalar dissipation by 40% and horizontal gradients of density ( $3\kappa\langle \rho_x^2 \rangle$  and  $3\kappa\langle \rho_y^2 \rangle$ ) underestimate the true density dissipation by 35% for  $Re_b \approx 10$ . The over estimation of density dissipation could be upto a factor of 2 if the vertical gradient of density is used to estimate the true density dissipation is commonly done in practice from field measurements.

#### 4.4.4 Inferring true dissipation from oceanic measurements

It is common to estimate  $\epsilon$  from  $\langle u_z^2 \rangle$  and/or  $\langle v_z^2 \rangle$  in the field. Figure 4.3 clearly shows that vertical gradients of horizontal velocity fluctuations over predict the true rate of dissipation. We

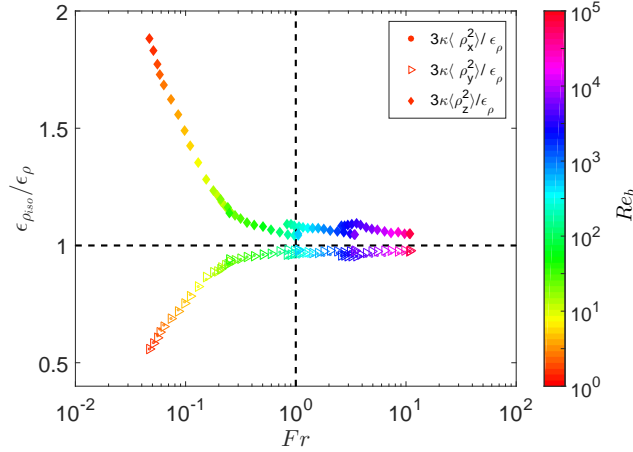


**Figure 4.4:** Contributions of each isotropic density dissipation components to the true rate of dissipation of density variance  $\epsilon_\rho$ , normalized by  $\epsilon_\rho$ .

denote estimates as  $\epsilon(1D)$  and the true value using all components of spatial gradients as  $\epsilon(3D)$ . The parameters that readily measurable in the ocean are  $\epsilon(1D)$ ,  $Re_b(1D)$ .  $\epsilon(3D)$  can be inferred from the above mentioned measurable quantities through a simple empirical relation that is obtained from the DNS results and shown in equation 4.8.

$$\frac{\epsilon(3D)}{\epsilon(1D)} = 1 - \exp(-a \log(Re_b)) \quad (4.8)$$

Here  $a$  is the constant which is 1.3 for the present dataset and  $Re_b$  is the 1D buoyancy Reynolds number. Figure 4.5 shows the ratio of  $\epsilon(3D)$  to  $\epsilon(1D)$  as a function of  $Re_b(1D)$ . The color bar shows the true  $Fr$  for reference. It is clear that the isotropy assumption is valid for  $Re_b(1D) \gtrsim \mathcal{O}(10^3)$ .

## 4.5 Concluding remarks

Direct numerical simulations were performed for the assessment of local isotropy of dissipative scales for stably stratified flows. It is shown that estimation of rate of dissipation of turbulent kinetic energy ( $\epsilon$ ) and density variance ( $\epsilon_\rho$ ) can be obtained using the isotropic assumption for  $Fr \gtrsim \mathcal{O}(1)$ . There is a clear departure from isotropy for  $Fr < \mathcal{O}(1)$  which depicts the strongly

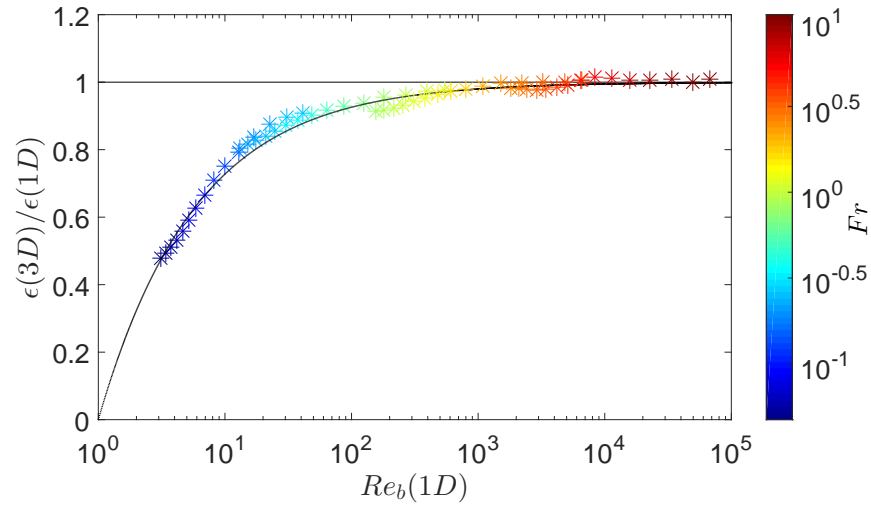


**Figure 4.5:** Ratio of  $\epsilon(3D)$  to  $\epsilon(1D)$  varying with  $Re_b(1D)$ . The horizontal line shows that the isotropy assumption is valid. The dashed line shows the empirical relation as provided in 4.8.

stable flows. The present study does not consider the effect of mean shear which might change the behavior of each isotropic component, but our finding suggests that turbulent Froude number is the fundamental parameter which describes the departure from isotropy. We have also suggested that true dissipation can be obtained from available measured isotropic dissipation using microstructure instruments through an empirical relation.

# Chapter 5

## Some new insights for inferring diapycnal diffusivity in stably stratified turbulence<sup>7</sup>

### 5.1 Introduction

Accurate prediction of diapycnal (irreversible) mixing of density is crucial for the understanding and modeling of many physical processes in the ocean and atmosphere. For example, accurate parameterization of diapycnal mixing is essential for getting the right overall mass and energy balances in ocean circulation models and thus has direct implications for climate variability predictions (Gregg, 1987; Munk & Wunsch, 1998). Despite the prevalence of a number of studies on this topic, our understanding of small-scale irreversible mixing in stratified turbulence remains limited due to a number of challenges such as the complexity associated with geophysical flows and the lack of consensus on the right choice of parameter(s) for quantifying mixing in stratified flows.

It is common practice to use a turbulent (eddy) diffusivity to quantify diapycnal mixing using the gradient-diffusion hypothesis (Pope, 2000) as

$$K_\rho = -\frac{\langle \rho' w' \rangle}{d\langle \rho \rangle / dz}, \quad (5.1)$$

where  $\langle \rho' w' \rangle$  is the turbulent density flux and  $d\langle \rho \rangle / dz$  is the mean (background) density gradient. For homogeneous and stationary turbulence, the diapycnal diffusivity defined in equation 5.1 can be written as

$$K_\rho = \frac{\epsilon_\rho}{(d\langle \rho \rangle / dz)^2}, \quad (5.2)$$

---

<sup>7</sup>The research presented in this chapter is under review in the Journal of Fluid Mechanics under the title "Some new insights for inferring diapycnal diffusivity in stably stratified turbulence" by A. Garanaik and S. K. Venayagamoorthy. The chapter is written in a collective "we" voice to acknowledge collaboration with Dr. S. K. Venayagamoorthy.

where  $\epsilon_\rho$  is the rate of dissipation of density variance (a detailed discussion on the derivation can be found in Venayagamoorthy & Stretch, 2010). Direct measurements of turbulent density fluxes (and hence diapycnal diffusivity as shown in (5.1)) are difficult in the ocean due to the intermingling of internal waves with turbulence in strongly stratified flows. As a result, a number of indirect techniques are commonly used in praxis in oceanography to infer heat and momentum fluxes. For example, the popular Osborn (1980) model recasts the diapycnal diffusivity given by (5.1) or (5.2) as

$$K_\rho = \Gamma \frac{\epsilon}{N^2}, \quad (5.3)$$

where  $\Gamma = R_f/(1 - R_f)$  is a mixing coefficient and  $R_f$  is the flux Richardson number (also termed the mixing efficiency) which is a ratio of buoyancy flux to production of turbulent kinetic energy,  $\epsilon$  is the rate of dissipation of turbulent kinetic energy and  $N = \sqrt{(-g/\rho_o)(d\langle\rho\rangle/dz)}$  is the buoyancy frequency. In the ocean,  $\epsilon$  can be measured directly using a vertical microstructure profiler,  $N$  is obtained using a Conductivity-Temperature-Depth (CTD) profiler, and  $\Gamma$  is typically considered to have a canonical constant value of 0.2 (Osborn, 1980). It should be noted that the constancy of  $\Gamma$  has been the subject of extensive debate and numerous studies, and a universal parameterization for  $\Gamma$  still remains elusive (Mater & Venayagamoorthy, 2014). Furthermore, direct (microstructure) measurements of  $\epsilon$  assume isotropy of small scales which is highly questionable given the strong anisotropic effects introduced by buoyancy in strongly stratified flows (Itsweire *et al.*, 1993; Smyth & Moum, 2000). In the absence of microstructure measurements, indirect estimates of  $\epsilon$  are commonly obtained in practice by assuming a one to one relationship between the Thorpe length scale  $L_T$ , which is readily obtained from CTD measurements (Thorpe, 1977) and the Ozmidov length scale defined as  $L_O = (\epsilon/N^3)^{1/2}$  (Ozmidov, 1965). In a recent study, Mater *et al.* (2013) found that  $L_T$  and  $L_O$  are equivalent only when the turbulent Froude number ( $Fr = \epsilon/(Nk)$ , where  $k$  is the turbulent kinetic energy) is of order unity. In the light of these issues, it is clear that there is a critical need for simple and robust models for diapycnal mixing that are physically based. This is the primary motivation for the work presented in this paper.

In a stratified flow, a relevant ‘mixing’ length scale is the Ellison length scale ( $L_E$ ) (Ellison, 1957) defined as

$$L_E = \frac{\langle \rho'^2 \rangle^{1/2}}{\partial \langle \rho \rangle / \partial z}, \quad (5.4)$$

where  $\langle \rho'^2 \rangle^{1/2}$  is root mean square density fluctuation and  $\partial \langle \rho \rangle / \partial z$  is the background density gradient. Similarly, if it is assumed that the appropriate velocity scale is the vertical (fluctuating) velocity  $w'$ , then, it follows from dimensional reasoning that the diapycnal diffusivity should scale as

$$K_\rho^m \sim w' L_E, \quad (5.5)$$

where the superscript  $m$  is used to differentiate the modeled diffusivity from the true diffusivity given by (5.2). The question that is immediately apparent is how good is this simple model in predicting the true diapycnal mixing in a stably stratified turbulent flow? It is reasonable to hypothesize that in a weakly stratified turbulent flow (i.e. for  $Fr \gtrsim 1$ ) where buoyancy effects are not likely to be dominant, this scaling should yield a reasonable prediction for the turbulent diffusivity given that both  $L_E$  and  $w'$  are arguably the representative turbulent mixing length and velocity scales, respectively. On the other hand, in the strongly stratified regime ( $Fr < 1$ ), the hypothesis would be that this scaling should breakdown due to the dominance of buoyancy effects. These hypotheses are tested using high resolution direct numerical simulation (DNS) data. In what follows, a brief description of the DNS is first provided in §5.2. This is followed by testing of the simple scaling given in (5.5) and a theoretical development of a new refined model to (5.5) in §5.3. §5.4 includes introduction of new Reynolds number practical to oceanography. Concluding remarks are given in §5.5.

## 5.2 Numerical method

Direct numerical simulations (DNS) of homogeneous stably stratified turbulence were performed as part of this study using the pseudo-spectral code developed by Riley *et al.* (1981). A cubical periodic flow domain with dimensions of  $2\pi$  with  $512^3$  grid points was used for all simula-

tions. The flow was initialized with a Gaussian isotropic and solenoidal velocity field and allowed to evolve under the effect of a constant background stratification. Flow was characterized with an initial Reynolds number of 1000 defined as  $Re_0 = u_0 L_0 / \nu$ , where  $\nu$  is the kinematic viscosity,  $u_0$  is the initial velocity scale and  $L_0$  is the initial length scale. Background stratification was characterized with an initial Richardson number, defined as  $Ri_0 = (NL_0/u_0)^2$ , where  $N$  is the buoyancy frequency. The molecular Prandtl number  $Pr = \nu/\kappa = 1$  for all simulations in order to ensure accurate resolution of the smallest scalar (density) scales. For the present study four DNS runs were performed with  $Ri_0 = 0.01, 0.1, 1.0$  and  $10.0$ , respectively, in order to represent weakly stable to strongly stable flows. However, in order to explore the temporal variance in the flow characteristics, the turbulent Froude number  $Fr$  is used in this study. The duration of all simulations was  $5L_0/u_0$ . Similar to the simulations performed by Mater *et al.* (2013), after approximately the first eddy turnover period,  $1L_0/u_0$ , the dissipation peaks and begins to decay. This is considered as a signature of fully developed turbulence. Hence initial transients prior to this time were ignored in this study.

### 5.3 Theoretical development of a new model for diapycnal diffusivity

The predicted diapycnal diffusivity  $K_\rho^m$  given by (5.5) versus the true diapycnal diffusivity  $K_\rho$  given by (5.2) are shown in figure 5.1. Note the diffusivities are non-dimensionalized using the molecular diffusivity  $\kappa$ . The color bar in figure 5.1(a) shows the turbulent Froude number  $Fr$  while that in figure 5.1(b) shows the buoyancy Reynolds number  $Re_b = \epsilon/\nu N^2$ . Note that  $Re_b$  (also sometimes referred to as the turbulence activity parameter) is a commonly used mixing parameter in oceanography. In this study, all the data presented are for  $Re_b > \mathcal{O}(1)$  and as such molecular effects are excluded. It can be seen from Figure 5.1(a) that the predicted diffusivities using the proposed simple model agrees remarkably well with the true diffusivities for  $Fr \gtrsim 1$ . This is more evident in figure 5.1(b) where the ratio of the predicted to the true diffusivities  $K_\rho^m/K_\rho$  is plotted as a function of  $Fr$ . However, as hypothesized, it is apparent that this simple model begins to

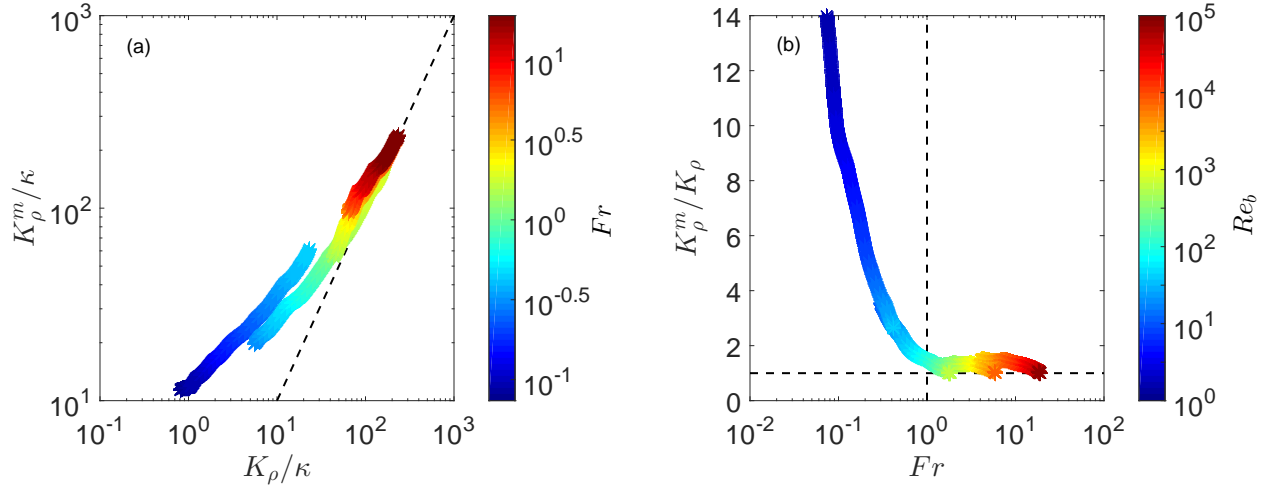


**Figure 5.1:** (a) Comparison of nondimensional model eddy diffusivity given by (5.5) with the nondimensional true eddy diffusivity given by (5.2). The dashed line shows the one to one comparison line. (b) Ratio of proposed eddy diffusivity to true eddy diffusivity as a function of the turbulent Froude number  $Fr$ .

breakdown for  $Fr < 1$  and significantly overpredicts (by at least an order of magnitude) the exact diffusivity especially for  $Fr \ll 1$ . The natural follow-on question is whether there is a physically based correction to (5.5) that can be used to predict the correct diffusivity in the strongly stable regime (i.e.  $Fr < 1$ )? In what follows, new scaling arguments are presented to resolve this question.

### 5.3.1 Diapycnal diffusivity in the regime of strongly stratified turbulence

$$(Fr < 1)$$

The diapycnal diffusivity in a stratified turbulent flow as defined in (5.2) can be also be expressed in terms of the rate of dissipation of turbulent (available) potential energy ( $\epsilon_{PE}$ ) as

$$K_\rho = \frac{\epsilon_\rho}{(d\langle\rho\rangle/dz)^2} = \frac{\epsilon_{PE}}{N^2}, \quad (5.6)$$

where  $\epsilon_{PE} = N^2\epsilon_\rho(\partial\langle\rho\rangle/\partial z)^{-2}$ . At this point, given the form of the simple model proposed in (5.5), it is both instructive and insightful to recast the diapycnal eddy diffusivity given in (5.6) in terms of a diapycnal length scale  $L_d$ , and a diapycnal velocity scale  $w_d$  as follows

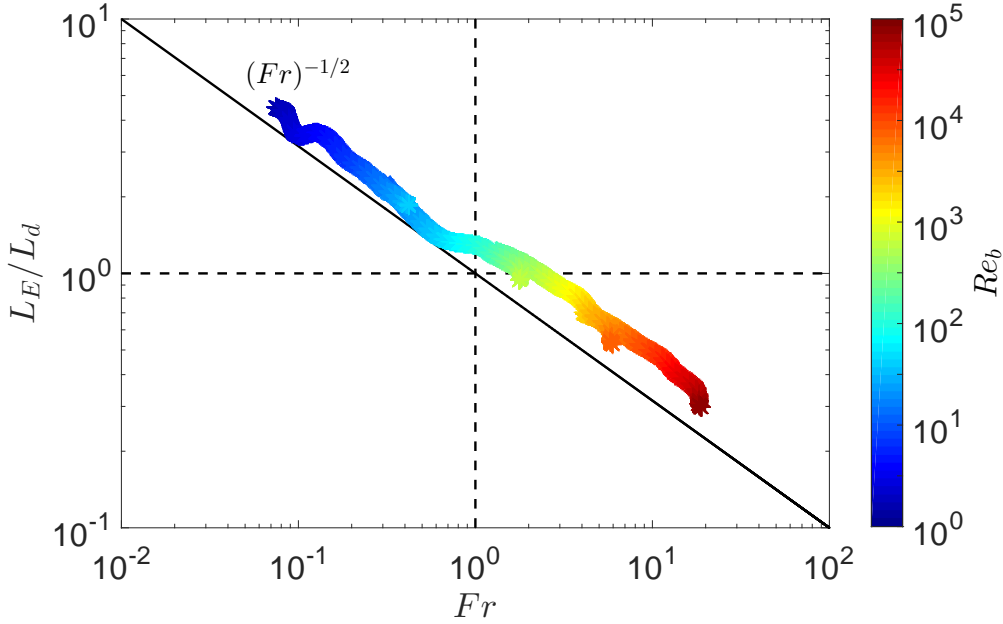


**Figure 5.2:** The ratio of Ellison length scale  $L_E$  to the diapycnal length scale  $L_d$  as a function of the turbulent Froude number,  $Fr$ .

$$K_\rho = \frac{\epsilon_{PE}}{N^2} = \underbrace{\left(\frac{\epsilon_{PE}}{N^3}\right)^{1/2}}_{L_d} \underbrace{\left(\frac{\epsilon_{PE}}{N}\right)^{1/2}}_{w_d}. \quad (5.7)$$

$L_d$  is in an analogous form to the Ozmidov length scale  $L_O$  (previously defined) but it is distinct in the sense that it is an inner length scale that truly represents the diapycnal mixing length scale in a stably stratified turbulent flow. In a similar vein,  $w_d$  represents the velocity scale associated with irreversible mixing in a stably stratified flow.

In strongly stratified flows, both  $L_E$  and  $w'$  are contaminated by adiabatic motions from internal waves which leads to the significant overprediction of the diapycnal diffusivity (i.e. false mixing) as shown in figure 5.1. A quantitative assessment of this overprediction is possible by determining the relationships between the length scales  $L_E$  and  $L_d$ , and velocity scales  $w'$  and  $w_d$ , respectively. First, consider the ratio of the Ellison length scale  $L_E$  to the diapycnal length scale  $L_d$  given by

$$\frac{L_E}{L_d} = \frac{\langle \rho'^2 \rangle^{1/2}}{\partial \langle \rho \rangle / \partial z} \bigg/ \left( \frac{\epsilon_{PE}}{N^3} \right)^{1/2}, \quad (5.8)$$

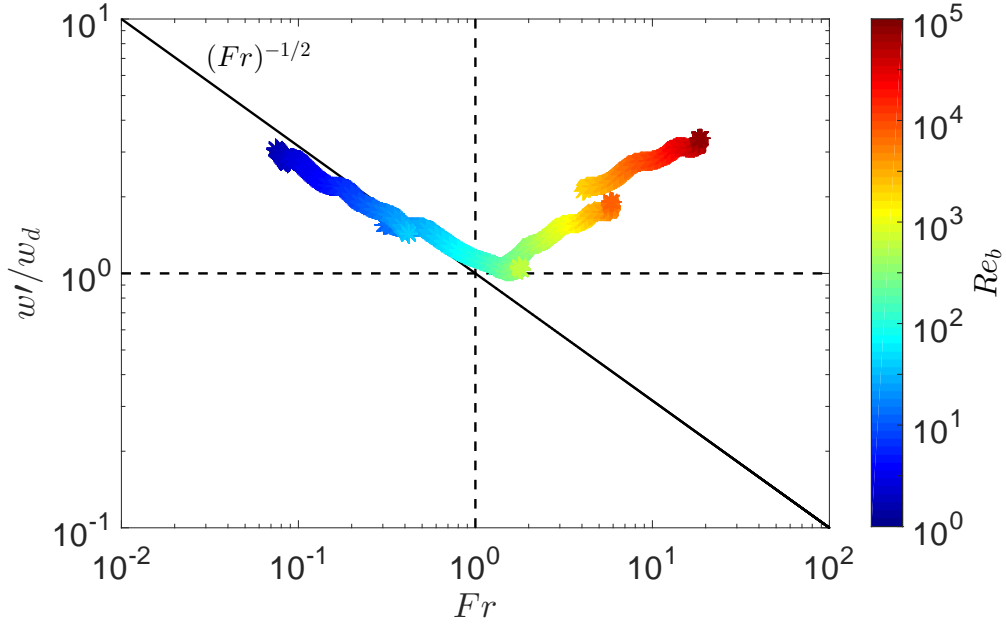


**Figure 5.3:** The ratio of vertical velocity fluctuation  $w'$  to the diapycnal velocity  $w_d$  as a function of the turbulent Froude number,  $Fr$ .

which on simplification gives

$$\frac{L_E}{L_d} = \left( \frac{\langle \rho'^2 \rangle}{\epsilon_\rho} N \right)^{1/2}. \quad (5.9)$$

The term  $\langle \rho'^2 \rangle / \epsilon_\rho$  on the right hand side of (5.9) is the density (scalar) decay time scale,  $T_\rho$ . It is plausible to assume that in a turbulent flow,  $T_\rho$  should scale with the turbulent kinetic energy decay time scale  $T_L = k/\epsilon$ . It is worth noting here that this assumption has been deemed to be reasonable in earlier works by Venayagamoorthy & Stretch (2006) and Stretch & Venayagamoorthy (2010). Hence, (5.9) simplifies further to

$$\frac{L_E}{L_d} \sim (Fr)^{-1/2}, \quad \text{for } Fr < 1. \quad (5.10)$$

Equation (5.10) implies that the Ellison length scale needs to be dampened by a factor of  $(Fr)^{1/2}$  in order for it to mimic the true diapycnal (mixing) length scale  $L_d$  in the strongly stratified regime ( $Fr < 1$ ). The validity of this scaling argument is tested using the DNS data as shown in figure 5.2. Our DNS data is high resolution decaying turbulence as described in the §5.2. To test the validity

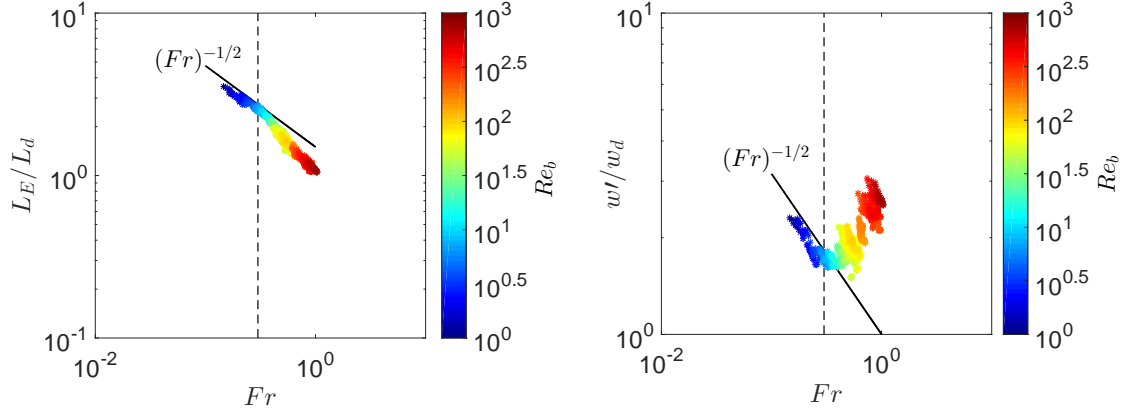


**Figure 5.4:** a: similar to fig 5.2, b: similar to fig 5.3 for sheared DNS data of Shih *et al.* (2005).

of proposed scaling argument for a broader range of flow, we have also tested equation (5.10) for DNS of sheared stratified turbulence obtained from Shih *et al.* (2005) in figure 5.4 (a). Their data set is limited to  $0.1 < Fr < 1$  with lower resolution but contains mean shear in the flow. Shih *et al.* (2005) data show a transition from weakly stratified turbulence and strongly stratified turbulence at a turbulent Froude number of approximately 0.3.. It is clear from figure 5.2 and figure 5.4 (a) that (5.10) provides a reasonable correction to  $L_E$  and thus can be used to obtain estimates of the true diapycnal length scale  $L_d$  for  $Fr < 1$ .

Next, consider the ratio  $w'/w_d$  given by

$$\frac{w'}{w_d} = \frac{w'}{(\epsilon_{PE}/N)^{1/2}}, \quad (5.11)$$

which on simplification gives

$$\frac{w'}{w_d} = \frac{w' \partial \langle \rho \rangle / \partial z}{(N \epsilon_\rho)^{1/2}}. \quad (5.12)$$

Now, in a density stratified fluid, it is reasonable to argue that density perturbations are generated by the vertical advection of the background density field (for a detailed discussion see Kundu *et al.*, 2016). Hence, this implies that  $w' \partial \langle \rho \rangle / \partial z \sim \rho' N$ . Substitution of this relation into (5.12) yields

$$\frac{w'}{w_d} \sim \left( \frac{\langle \rho'^2 \rangle}{\epsilon_\rho} N \right)^{1/2}. \quad (5.13)$$

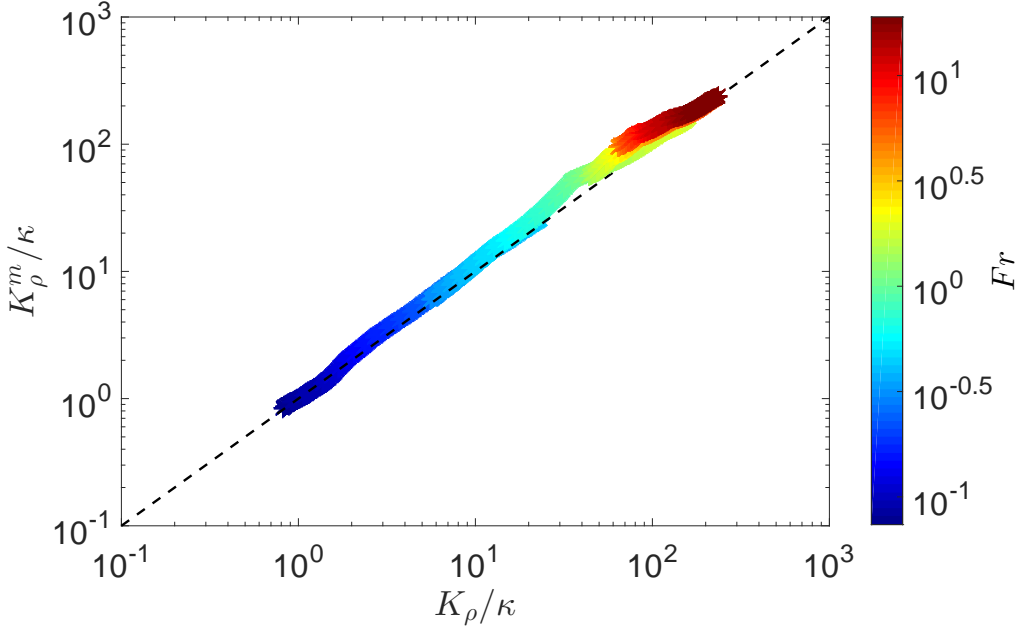


**Figure 5.5:** Comparison of predicted diapycnal diffusivity using the refined model given by (5.15) with the true diapycnal diffusivity given by (5.2). The dashed line shows the one-to-one comparison line.

The right hand side of (5.13) is identical to its counterpart in (5.9) and hence it follows directly that

$$\frac{w'}{w_d} \sim (Fr)^{-1/2}, \quad \text{for } Fr < 1. \quad (5.14)$$

In a similar manner to the Ellison length scale, (5.14) implies that the vertical velocity scale  $w'$  needs to be dampened by a factor of  $(Fr)^{1/2}$  in order for it to mimic the true diapycnal (mixing) velocity scale  $w_d$  in the strongly stratified regime ( $Fr < 1$ ). The validity of this scaling argument is again tested using the DNS data as shown in figure 5.3. The scaling argument is also tested for Shih *et al.* (2005) data in figure 5.4 (b). It is evident from figure 5.3 and figure 5.4 (b) that (5.14) provides a remarkably good correction to  $w'$  and hence can be used to obtain estimates of the true diapycnal velocity scale  $w_d$  for  $Fr < 1$  which is valid for both decaying and sheared stratified turbulence.

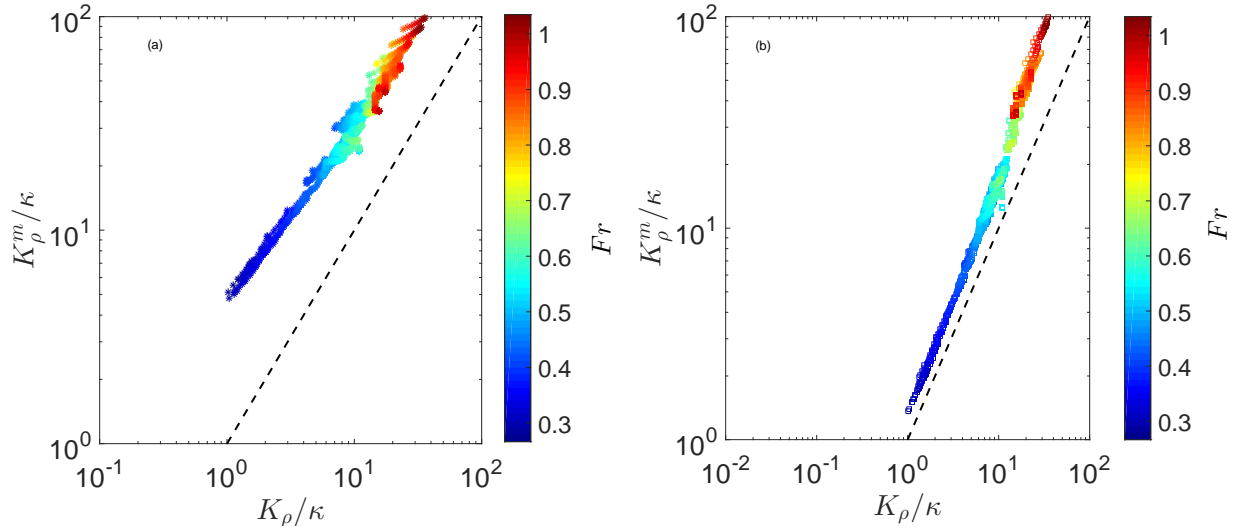


**Figure 5.6:** a:similar to fig 5.1(a), b:similar to fig 5.5 for sheared DNS data of Shih *et al.* (2005)

### 5.3.2 New model for diapycnal diffusivity

Given the scaling arguments presented in §5.3.1, it is straightforward to refine the simple model proposed in (5.5) to predict the true diffusivity across the full spectrum of the  $Fr$  number space as follows:

$$\begin{aligned}
 K_\rho^m &\sim w' L_E, & \text{for } Fr \geq \mathcal{O}(1), \\
 K_\rho^m &\sim (w' L_E) \times Fr, & \text{for } Fr < \mathcal{O}(1),
 \end{aligned}
 \tag{5.15}$$

Figure 5.5 shows a plot of the modeled diffusivities as predicted by (5.15) versus the true diffusivities given by (5.2) using DNS data. The agreement is remarkable across the whole  $Fr$  space. Figure 5.6 (a) shows a plot similar to figure 5.1 (a) for Shih *et al.* (2005) data. For this data set we do not see the one to one collapse of true diffusivity and modeled diffusivity proposed in 5.5 and shown in figure 5.1, in the limit of weakly stratified turbulence ( $Fr \sim 1$ ). This is because the data of Shih *et al.* (2005) has a limited  $Fr$  range and also the simulations are of low resolution to resolve full spectrum of flow. Nonetheless, for strongly stratified fluid, the proposed modeled diffusivity (5.15) with scaling arguments, shows a remarkable agreement with the true diffusivity as shown in

figure 5.6 (b). This is not surprising given the excellent agreements found for the scaling results presented in (5.10) and (5.14) as seen in figures 5.2 & 5.4 (a) and 5.3 & 5.4 (b), respectively.

## 5.4 Towards field application

Modeled diffusivities as predicted by (5.15) are in good agreement with the true diffusivities as discussed in the previous section. This method neither relies on a parameterization of mixing efficiency  $\Gamma$  nor needs a correction for small scale rate of dissipation of turbulent kinetic energy,  $\epsilon$  due to anisotropic effects introduced in the strongly stratified fluid, in order to infer diapycnal diffusivity as in equation 5.3. The proposed model depends on two basic fundamental parameters for stratified turbulence,  $w'$  and  $\rho'$  or  $L_E$ . In the ocean,  $\langle \rho'^2 \rangle^{1/2}$  and  $d\langle \rho \rangle / dz$  are obtained from instantaneous density profiles measured using CTD. The general practice in oceanography is to measure horizontal velocities using fine scale instrument like ADCP. Though the measurement of vertical velocity  $w'$  is scarce, we can not overlook the importance of vertical velocity for ocean dynamics which directly affects the vertical transport of mass and momentum. Several studies have been done that focus on the importance and measurement of vertical velocity in the ocean using natural buoyant floats (D'Asaro 2001) and pressure transducers (Moum, 1990). Thurnherr (2011) suggested a method to obtain vertical velocity from CTD/LADCP data with an higher accuracy of 0.5 cm/s. It is also shown that small scale dissipation can be parameterized from fine scale vertical kinetic energy (Thurnherr *et al.*, 2015). In theory, it is thus possible to measure  $w'$  and hence, the proposed new method can be used to infer diapycnal diffusivity in the ocean if the dynamic state of the flow can be identified. That is, a diagnostic assessment is required to determine if a given flow is in the weakly (high  $Fr$ ) or strongly (low  $Fr$ ) stratified flow regime.

Estimation of turbulent kinetic energy  $k$  in the ocean is challenging and hence the determination of the  $Fr$  is problematic. Here, we propose a method for inferring turbulent Froude number from measurable quantities. A new Reynolds number based on  $w'$  and  $L_E$  can be written as:

$$Re_O = \frac{w' L_E}{\nu}. \quad (5.16)$$

We denote this as the overturn Reynolds number.

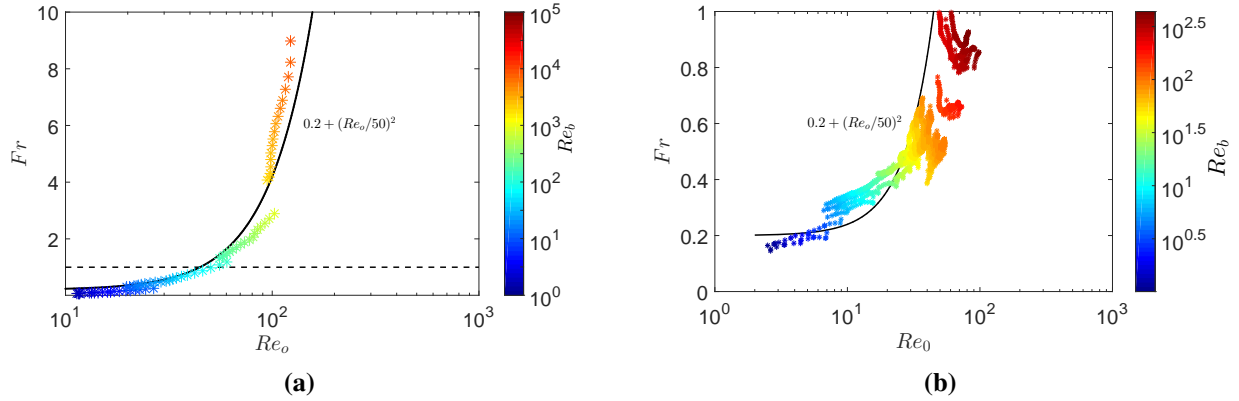


**Figure 5.7:** Turbulent Froude number as a function of overturn Reynolds number.

A plot for  $Fr$  versus  $Re_O$  for decaying DNS and sheared DNS data is shown in the figure 5.7a and 5.7b, respectively. The range of  $Fr$  for decaying turbulence is one order higher than that in sheared DNS data. We have fitted a curve for decaying DNS data as shown in the figure 5.7a, and tested that fit for the sheared DNS data, in order to provide a relation between these two non-dimensional parameters such that  $Fr$  can be inferred from  $Re_O$ . According to the fit  $Fr = 0.2 + (Re_O/Re_{Oc})^2$ , where  $Re_{Oc} = 50$  for present data. Figure 5.7a shows that,  $Re_O$  increases rapidly for  $Fr \leq 1$  and approaches a constant value of order 100 for  $Fr > 1$ . This transition is shown to occur at critical value of  $Re_O$  (denoted as  $Re_{Oc}$ ), corresponding to  $Fr \sim \mathcal{O}(1)$ . Of course, we admit that this proposition needs further verification with high resolution sheared data and field data which are as yet not available.

## 5.5 Concluding remarks

Scaling arguments have been presented in this study to propose a new model for the prediction of diapycnal mixing in stably stratified turbulence. To the best knowledge of the authors, this is the first time such a model has been proposed using a novel representation of the diapycnal diffusivity as a product of a diapycnal (mixing) length scale  $L_d$  and a diapycnal velocity scale  $w_d$  as shown

in (5.7). Comparisons of relevant scaling results that were developed using physical arguments and the model prediction for the diapycnal diffusivities with the exact diffusivities using high resolution DNS data (both decaying and sheared stratified turbulence) show remarkable agreement. A simple and robust scaling result based on the turbulent Froude number  $Fr$  for mixing in stably stratified turbulent flows is evident from the analysis presented in this study. It is expected that these results will provide a useful platform for developing practical parameterizations for the turbulence closure problem in large scale numerical models for stratified flows as well as for the inference of diapycnal mixing from field measurements. However, such extensions require further research work. We have proposed a practical method for parameterizing the turbulent  $Fr$  in terms of an overturn Reynolds number  $Re_0$  to enable the adoption of this new (and robust) model for inferring diapycnal mixing in the ocean.

# Chapter 6

## A practical recipe for parameterization of mixing in oceanic flows <sup>8</sup>

### 6.1 Introduction

Two major practical challenges for improved prediction of diapycnal mixing in geophysical flows are: (I) finding the best parameterization for irreversible mixing efficiency and (II) parameterizing the mixing efficiency using measurable quantities. The goal of this study is to address these challenges.

Direct measurements of turbulent density flux (and hence diapycnal diffusivity) is difficult in the ocean due to the intermingling of internal waves with turbulence in strongly stratified flows. As a result, a number of indirect techniques are commonly used in praxis in oceanography to infer heat and momentum fluxes. For example, the popular Osborn (1980) model recasts the diapycnal diffusivity for a homogeneous and stationary flow as

$$K_\rho = \Gamma \frac{\epsilon}{N^2}, \quad (6.1)$$

where  $\Gamma = R_f/(1 - R_f)$  is a mixing coefficient and  $R_f$  is the mixing efficiency,  $\epsilon$  is the rate of dissipation of turbulent kinetic energy and  $N = \sqrt{(-g/\rho_o)(d\langle\rho\rangle/dz)}$  is the buoyancy frequency. Following the work of Peltier & Caulfield (2003) and Venayagamoorthy & Stretch (2010),  $\Gamma$  and  $R_f$  considered for this study are irreversible mixing coefficient ( $\Gamma = \epsilon_{PE}/\epsilon$ ) and irreversible mixing efficiency ( $R_f = \epsilon_{PE}/(\epsilon_{PE} + \epsilon)$ ), respectively, where  $\epsilon_{PE}$  is the rate of dissipation of potential energy. In the light of the discussions presented on mixing efficiency in section 2.6.2 and in chapter

---

<sup>8</sup>The research presented in this chapter will be submitted to the Journal of Fluid Mechanics under the title "Utility of Thorpe and Ozmidov length scales to infer state of turbulence and mixing efficiency in geophysical flows" by A. Garanaik and S. K. Venayagamoorthy. The chapter is written in a collective "we" voice to acknowledge collaboration with Dr. S. K. Venayagamoorthy.

3 it is clear that a robust parameterization for  $\Gamma$  (or  $R_f$ ) is lacking and therefore highly desirable. It should be noted that stably stratified flows can be divided into roughly three flow regimes, depending on the values of the turbulent Froude number ( $Fr = \epsilon/Nk$ , where  $k$  is the turbulent kinetic energy): weakly stratified ( $Fr \gg \mathcal{O}(1)$ ), moderately stratified ( $Fr \sim \mathcal{O}(1)$ ) and strongly stratified ( $Fr \ll \mathcal{O}(1)$ ) regimes, respectively. A key objective of this research is to determine using scaling arguments the dependence between the mixing efficiency and the turbulent Froude number for all three regimes. Here, it is worth noting that  $Fr$  can be viewed as a competition of time scales (i.e. the turbulence time scale  $T_L = k/\epsilon$  to the buoyancy time scale  $N^{-1}$ ). Hence,  $Fr$  is a dynamic indicator of the local state of turbulence in a stably stratified flow. However,  $T_L$  is difficult to measure in the field. Hence, a second key objective is to formulate a relationship to obtain  $Fr$  from measurable quantities in the field.

In what follows a formulation for the mixing efficiency in stably stratified turbulence is presented using scaling arguments in section 6.2. A brief description of data considered is given in section 6.3. Results are discussed including validation of proposed scaling in section 6.4 and concluding remarks are presented in section 6.5.

## 6.2 Theoretical analysis

First, scaling arguments to highlight the fundamental relationship between mixing coefficient ( $\Gamma$ ) and turbulent Froude number ( $Fr$ ), through a consideration of the energetics of the flow is discussed. Second, it is shown that the turbulent Froude number can be inferred from two most fundamental and measurable length scales in the oceanic flows namely Ozmidov length ( $L_O$ ) and Ellison (or alternatively Thorpe,  $L_T$ ) length scale ( $L_E$ ).

### 6.2.1 Scaling argument for $\Gamma$ as a function of $Fr$

As discussed previously, the turbulent Froude number, defined as  $Fr = \epsilon/Nk$  is the most relevant parameter to describe flow dynamics in a stratified turbulent flow. In the limit of high  $Fr$ , considering a balance between advection and background stratification in the buoyancy equation,

Maffioli *et al.* (2016) have shown that  $\Gamma \sim Fr^{-2}$ . And in the limit of high  $Fr$ ,  $\Gamma$  tends to be constant. Here we have used a different scaling analysis, that considers dominant time scales governing the fluid flow for weakly stratified, moderately stratified and strongly stratified turbulence as described below. This is because, the transition between weakly stratified regime and strongly stratified regime does not happen at one single value. There is an intermediate regime in between which is moderately stratified, where both stratification and turbulence are important.

### 6.2.1.1 In the limit of weak stratification $Fr \gg \mathcal{O}(1)$

For a weakly stratified fluid or in the limit of high  $Fr$ , it is clear that, density acts as a passive scalar and does not have a significant contribution towards diapycnal mixing (Holford & Linden, 1999). The flow dynamics is mostly influenced/controlled by the turbulent time scale,  $T_L = k/\epsilon$ . The vertical displacement of the fluid particle  $L_{disp} \sim w'T_L$ , where  $w'$  is the vertical velocity. From this the density fluctuation  $\rho' \sim w'T_L \frac{\partial \langle \rho \rangle}{\partial z}$ , where  $\partial \langle \rho \rangle / \partial z$  is the background density gradient. Hence, the buoyancy flux  $B = \frac{g}{\rho} \langle \rho' w' \rangle \sim \frac{g}{\rho} w^2 T_L \frac{\partial \langle \rho \rangle}{\partial z} = w^2 N^2 T_L$ , where  $N^2 = \frac{g}{\rho} \frac{\partial \langle \rho \rangle}{\partial z}$  is the buoyancy frequency. The turbulent kinetic energy ( $k$ ) scales as  $\sim w^2$  and the rate of dissipation of turbulent kinetic energy  $\epsilon$  scales as  $\sim w^2/T_L$ . With this information, the mixing coefficient can be derived as,

$$\Gamma = \frac{B}{\epsilon} = \frac{\epsilon_{PE}}{\epsilon} \sim \frac{w^2 N^2 T_L^2}{w^2} \sim (NT_L)^2 = (Nk/\epsilon)^2 = Fr^{-2}. \quad (6.2)$$

This relation is identical to that found from direct numerical simulations (Maffioli *et al.*, 2016) and experimental data (Wells *et al.*, 2010) for weakly stratified turbulent flow.

### 6.2.1.2 In the limit of moderate stratification $Fr \sim \mathcal{O}(1)$

For a moderately stratified turbulent flow, the buoyancy has already taken effect in the flow dynamics and at the same time, the effect of turbulence has not completely gone. So both the buoyancy time scale  $N^{-1}$  and turbulent time scale  $T_L$  control the flow dynamics. Vertical displacement of fluid particle  $L_{disp} \sim w/N$  and the density fluctuation  $\rho' \sim \frac{w'}{N} \frac{\partial \langle \rho \rangle}{\partial z}$ . The buoyancy flux  $B = \frac{g}{\rho} \langle \rho' w' \rangle$ , scales as  $\sim \frac{g}{\rho} \frac{w^2}{N} \frac{\partial \langle \rho \rangle}{\partial z} = w^2 N$ . The rate of dissipation of turbulent kinetic energy then scales as  $\sim w^2/T_L$ . It then follows that,

$$\Gamma = \frac{B}{\epsilon} = \frac{\epsilon_{PE}}{\epsilon} \sim \frac{w^2 N}{w^2/T_L} \sim (NT_L)^1 = (Nk/\epsilon)^1 = Fr^{-1}. \quad (6.3)$$

### 6.2.1.3 In the limit of strong stratification $Fr \ll \mathcal{O}(1)$

In the limit of strong stratification, effect of non dissipative internal waves are strong. Most of the buoyancy flux occurs in first buoyancy period and most of the energy is dissipated within one buoyancy time period so that  $\epsilon \sim w^2/N^{-1}$ . Following the argument of moderately stratified case, vertical displacement of fluid particle  $L_{disp} \sim w/N$  and  $\rho' \sim \frac{w'}{N} \frac{\partial \langle \rho \rangle}{\partial z}$ . The buoyancy flux  $B = \frac{g}{\rho} \langle \rho' w' \rangle$ , scales as  $\sim \frac{g}{\rho} \frac{w^2}{N} \frac{\partial \langle \rho \rangle}{\partial z} = w^2 N$ . Hence, the mixing efficiency scales as

$$\Gamma = \frac{\epsilon_{PE}}{\epsilon} \sim \frac{w^2 N N^{-1}}{w^2} = constant \sim Fr^0. \quad (6.4)$$

Maffioli *et al.* (2016) have shown that this constant value approaches 0.33. Shih *et al.* (2005) found that the constant value of mixing coefficient is 0.2. Our data shows a higher value. Regardless of the exact value, it appears that mixing efficiency should be a constant in the limit of strong stratification.

## 6.2.2 Inferring $Fr$ from Ozmidov and Thorpe length scales

The turbulent Froude number ( $Fr$ ) is a dynamic parameter that can be used to diagnose the state of turbulence in a stably stratified flow. It should be noted that the proposed scaling for  $\Gamma$  (as shown in the section 6.2.1) requires the determination of  $Fr$  which is difficult to quantify directly in the ocean. Here, we propose a novel breakthrough to estimate  $Fr$  using measurable length scales in oceanic flows.

A fundamental length scale that provides a measure of overturning length scale is the well known Ellison length scale (Ellison, 1957) defined as

$$L_E = \frac{\langle \rho'^2 \rangle^{1/2}}{\partial \langle \rho \rangle / \partial z}, \quad (6.5)$$

where  $\rho'$  is the turbulent density fluctuation,  $\partial\langle\rho\rangle/\partial z$  is the mean background density gradient and  $\langle\rangle$  represents ensemble average. Conceptually,  $L_E$  is obtained from three dimension resorting of instantaneous density profile to a state of minimum potential energy (Winters *et al.*, 1995), but in the context of oceanography, instantaneous density is measured by dropping vertical profilers from a research vessel. In the limit of available one dimensional vertical profiles, statistically  $L_E$  represents the largest overturn of the flow and gives an indication of the available potential energy per unit mass. A similar and relatively simpler kinematic length scale obtained from instantaneous density profiles is the Thorpe length scale,  $L_T$  (Thorpe, 1977). In a statistical sense, both  $L_T$  and  $L_E$  represent a measure of the vertical distance traveled by fluid parcels in order to achieve an equilibrium position through adiabatically resorting. So that, for one dimensional vertical profiles, both  $L_T$  and  $L_E$  should be equivalent. From low resolution DNS, Itsweire *et al.* (1986) found good agreement between  $L_T$  and  $L_E$  for weakly stratified flows. From high resolution DNS data we have also found that  $L_T$  and  $L_E$  are in excellent agreement for all the range of stratification similar to the results of Mater *et al.* (2013).

Another length scale that is often used to represent the size of eddy in stratified turbulence was suggested by Ozmidov (1965) through a dimensionally constructed length scale known as Ozmidov length scale ( $L_O$ ) that is defined as

$$L_O = (\epsilon/N^3)^{1/2}, \quad (6.6)$$

where,  $N = \left(\frac{g}{\rho} \frac{\partial\langle\rho\rangle}{\partial z}\right)^{1/2}$  is the buoyancy frequency,  $\epsilon$  is the rate of dissipation of turbulent kinetic energy.  $L_O$  is the length scale at which inertial forces balance the buoyancy forces, in such a way that  $L_O$  represents the largest (isotropic) eddy unaffected by buoyancy.

The ratio of these two length scales has been used to denote the age of a turbulent event (Smyth *et al.*, 2001). Mater *et al.* (2013) suggested that  $L_T$  and  $L_O$  are equivalent only for turbulent Froude number of order one. Here, we delve further to show that the ratio of  $L_T/L_O$  or more explicitly,  $L_E/L_O$  is not only a signature of age of turbulence but more importantly, is a quantitative

representation of the strength of stratification in a turbulent flow similar to the concept of a turbulent Froude number. A quantitative relationship between  $L_E/L_O$  and  $Fr$  can be derived as follows.

The ratio of the Ellison length scale to the Ozmidov length scale can be written as

$$\frac{L_E}{L_O} = \frac{\langle \rho'^2 \rangle^{1/2} N^{3/2}}{(\partial \langle \rho \rangle / dz) \epsilon^{1/2}} = \frac{\langle \rho'^2 \rangle^{1/2}}{\epsilon^{1/2}} \left( \frac{g}{\rho} \right) \left( \frac{g}{\rho} \frac{\partial \langle \rho \rangle}{\partial z} \right)^{-1/4} = \frac{\langle \rho'^2 \rangle^{1/2} g}{\epsilon^{1/2} \rho} N^{-1/2}. \quad (6.7)$$

In the limit of strong stratification,  $\frac{g}{\rho} \langle \rho'^2 \rangle^{1/2}$  represents a gravitational acceleration term which can be expected to scale with velocity scale  $k^{1/2}$  and time scale  $N^{-1}$ , such that

$$\langle \rho'^2 \rangle^{1/2} \frac{g}{\rho} \sim wN \sim k^{1/2} N. \quad (6.8)$$

Thus, for strongly stratified regime  $Fr < O(1)$ , the length scale ratio can be written as

$$\frac{L_E}{L_O} \sim \frac{k^{1/2} N}{\epsilon^{1/2} N^{1/2}} = (kN/\epsilon)^{1/2} = Fr^{-1/2}. \quad (6.9)$$

This simplifies to

$$Fr \sim (L_E/L_O)^{-2} \sim (L_T/L_O)^{-2}. \quad (6.10)$$

Now, for a weakly stratified turbulent flow or in the limit of high Froude number  $Fr > O(1)$ , the Thorpe length scale as well as the Ellison length scale should scale with the isotropic turbulent length scale  $L_{k\epsilon} = k^{3/2}/\epsilon$  (Ivey & Imberger, 1991; Luketina & Imberger, 1989; Mater *et al.*, 2013).

Thus,

$$L_E \sim L_T \sim L_{k\epsilon} = k^{3/2}/\epsilon. \quad (6.11)$$

With this information, the length scale ratio,  $L_E/L_O$ , for a weakly stratified flow can be written as,

$$\frac{L_E}{L_O} \sim \frac{k^{3/2}/\epsilon}{\epsilon^{1/2}/N^{3/2}} = (kN/\epsilon)^{3/2} = Fr^{-3/2}, \quad (6.12)$$

which translates to

$$Fr \sim (L_E/L_O)^{-2/3} \sim (L_T/L_O)^{-2/3}. \quad (6.13)$$

Given that both  $L_T$  and  $L_O$  are measurable in the ocean using CTD and microstructure profilers, equations 6.10 and 6.13 provide a novel scaling to estimate  $Fr$  for the first time in the field. The scaling arguments presented for both  $\Gamma$  and  $Fr$  are tested using three independent DNS datasets in what follows.

### 6.3 Data considered

Direct Numerical simulation (DNS) provides full description of turbulent flow field ranging from energy containing large eddy scale ( $\mathcal{L}$ ) to small dissipative Kolmogorov scale ( $\eta$ ) without involving any parameterization of small-scale physics. Here we have considered three independent DNS data sets to test the veracity of our proposed scaling for  $\Gamma$  and  $Fr$  for different flow conditions. The first dataset is from our own simulations of decaying homogeneous stably stratified turbulence. The second data set represents forced stably stratified turbulence (Maffioli *et al.*, 2016). The third data set includes effect of shear in DNS of sheared stably stratified turbulence (Shih *et al.*, 2005). Brief detail of these simulations and datasets are given next.

Decaying DNS: The numerical simulations for our study were carried out using pseudo-spectral DNS code developed by Riley *et al.* (1981) for stably stratified homogeneous turbulent flows. A cubical periodic domain with dimension  $2\pi$  with  $512^3$  grid points was considered for all simulations. The turbulent flow was initialized with a Gaussian isotropic three dimensional solenoidal velocity field and allowed to evolve and decay under the influence of a constant background stratification. The mean shear was zero for all the simulations and the only large scale anisotropy considered was vertical stable stratification. Flow was characterized with an initial Reynolds number of 1000 defined as  $Re_0 = u_0 L_0 / \nu$ , where  $u_0$  is the initial velocity scale and  $L_0$  is the initial length scale. Background stratification was characterized with an initial Richardson number, defined as  $Ri_0 = (NL_0/u_0)^2$ , where  $N$  is the buoyancy frequency. Four DNS simulations were performed for the present study with  $Ri_0 = 0.01, 0.1, 1.0$  and  $10$ , respectively, for a duration of  $5L_0/u_0$  in order to investigate the effects of weakly stratified to strongly stratified condition on the small scales of turbulence. The value of  $k_{max}\eta$  (corresponding to maximum dissipation) varied

from 1.41 to 1.6 for  $Ri_0 = 0.01$  to  $Ri_0 = 10$  respectively, where  $k_{max}$  is the maximum wave number. This criteria ensures that the resolution was sufficient to resolve the smallest scales of dissipation (Yeung *et al.*, 1995). The molecular Prandtl number  $Pr = \nu/\kappa = 1$  for all the simulations to ensure accurate resolution of the dissipative scales of the density (scalar) field. At the first eddy turnover period,  $1L_0/u_0$ , the dissipation peaks and begins to decay. This is interpreted as a signature of fully developed turbulence. Hence, initial transients prior to this time were ignored in this study.

Forced DNS: These data were obtained from high resolution direct numerical simulations of linearly stratified fluid with constant buoyancy frequency. A body force is included in the Boussinesq momentum equation to simulate stationary turbulence. They have considered different size of grid for this study with isotropic forcing for most of the cases and 2D vortical forcing for 5 simulations to achieve a strongly stratified regime with buoyancy Reynolds number  $> 10$ . For details of simulations refer to Maffioli *et al.* (2016). Data from 17 simulations are used to test the scaling results.

Sheared DNS: These data were obtained from direct numerical simulations of Navier-Stokes equations for homogeneous, sheared, stratified turbulent flows using pseudo-spectral method on a  $128^3$  grid with periodic boundary conditions. Even though the resolution is much smaller than the resolution of our DNS, we have considered this data set to include the influence of shear which is very common in geophysical flows. For detail of the code and simulations see, Shih *et al.* (2005). A total of 36 simulations are used in the present study. All data considered for our study correspond to a shear time,  $St > 6$  to ensure that the simulations are fully developed.

## 6.4 Results

### 6.4.1 Mixing coefficient ( $\Gamma$ ) as a function of turbulent Froude number ( $Fr$ )

Figure 6.1 shows the mixing coefficient  $\Gamma$  as a function of turbulent Froude number for decaying and forced DNS data. The buoyancy Reynolds number ( $Re_b$ ) is shown in color bar. Here, two observations are noteworthy. First, the buoyancy Reynolds number does ( $Re_b$ ) not play any role

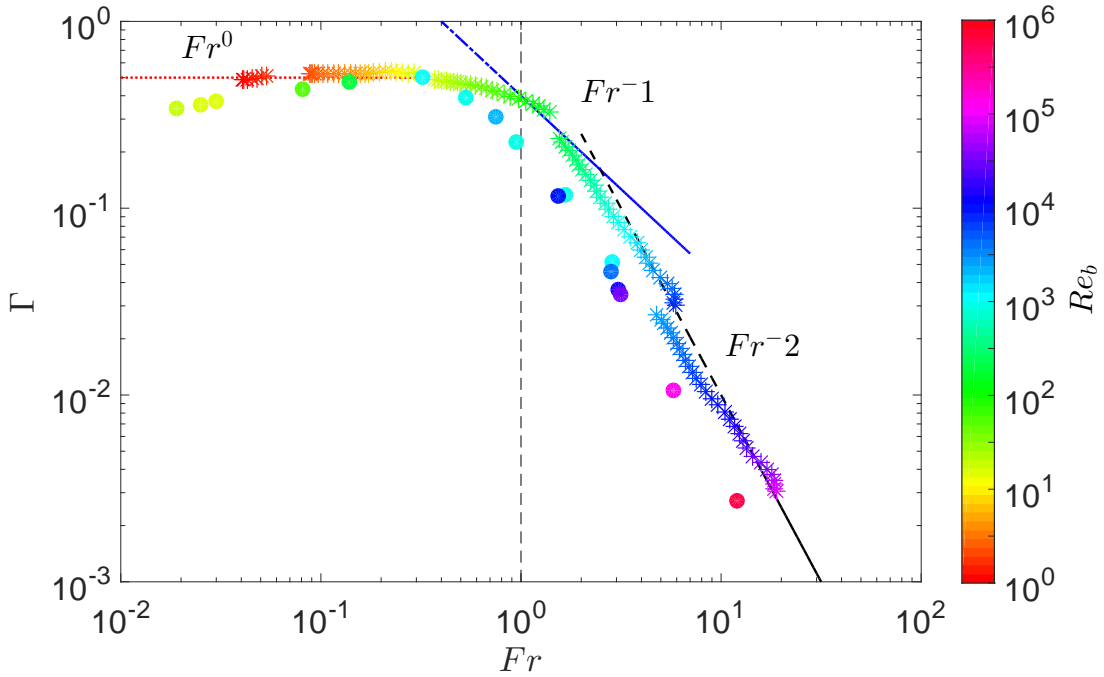


**Figure 6.1:** Mixing coefficient,  $\Gamma$  as a function of turbulent Froude number  $Fr$ . The color bar shows values of  $Re_b$ . star: decaying DNS; circle: forced DNS of Maffioli *et al.* (2016).

in estimating mixing efficiency. Similar arguments have been provided by Maffioli *et al.* (2016). If one considers any  $Fr$  value, and compare the corresponding  $Re_b$  and  $\Gamma$  values from both the datasets, it is clear that different  $Re_b$  values correspond to similar mixing efficiencies suggesting that  $Re_b$  is not a unique parameter to parameterize mixing in a stratified flow and thus it is a highly ambiguous parameter. That is, for a given  $Re_b$ , the mixing coefficient can be either high or low depending on the strength of the stratification as denoted by  $Fr$ .

The second key observation is that both decaying and forced DNS data remarkably agree with our scaling results for  $\Gamma$ . Maffioli *et al.* (2016) have shown the scaling of  $\Gamma \sim Fr^{-2}$  in the limit of high  $Fr$  from the governing equations by considering balance between advection and background stratification. Geophysical flows experience the effects of shear and stratification. Hence, we have also validated our scaling arguments using sheared DNS data of Shih *et al.* (2005) in figure 6.2. Even though the range of data does not cover a broader spectrum of Froude number as in the other two cases, still the three regimes of the flow are visible from the data with reasonable agreement with

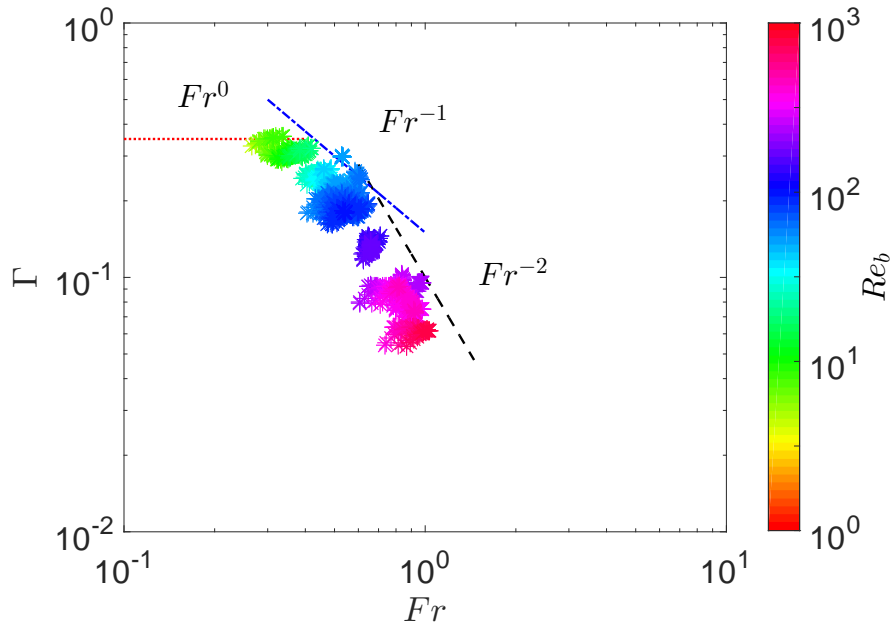


**Figure 6.2:** Mixing coefficient,  $\Gamma$  as a function of turbulent Froude number  $Fr$  for sheared DNS of Shih *et al.* (2005). The color bar shows values of  $Re_b$ .

our scaling results. The transition from strong stratification to weak stratification occurs around  $Fr = 0.3$  similar to Maffioli *et al.* (2016) which is of order one. Note, for this analysis all data in the diffusive regime (Shih *et al.*, 2005) are discarded. From these results, it can emphatically concluded that, the appropriate way to describe mixing efficiency (mixing coefficient) is through a  $Fr$  based parameterization.

In praxis, mixing efficiency is generally parameterized with  $Re_b$  since  $Re_b$  is readily computed from field observations. However, as has been shown,  $Re_b$  is a fundamentally flawed parameter to use for this purpose. Regardless, it should be noted that the turbulent Froude number is not easily measurable in the ocean with current instrumentations and methodologies. Hence, it is important to find practical approach to estimate  $Fr$  in the field.

### 6.4.2 Thorpe length scale, Ellison length scale and Ozmidov length scale

Figure 6.3 shows that the Thorpe scale and Ellison length scales agree remarkably well across a broad range of  $Fr$ . Similar results have been shown by Mater *et al.* (2013) and Itsweire *et al.*

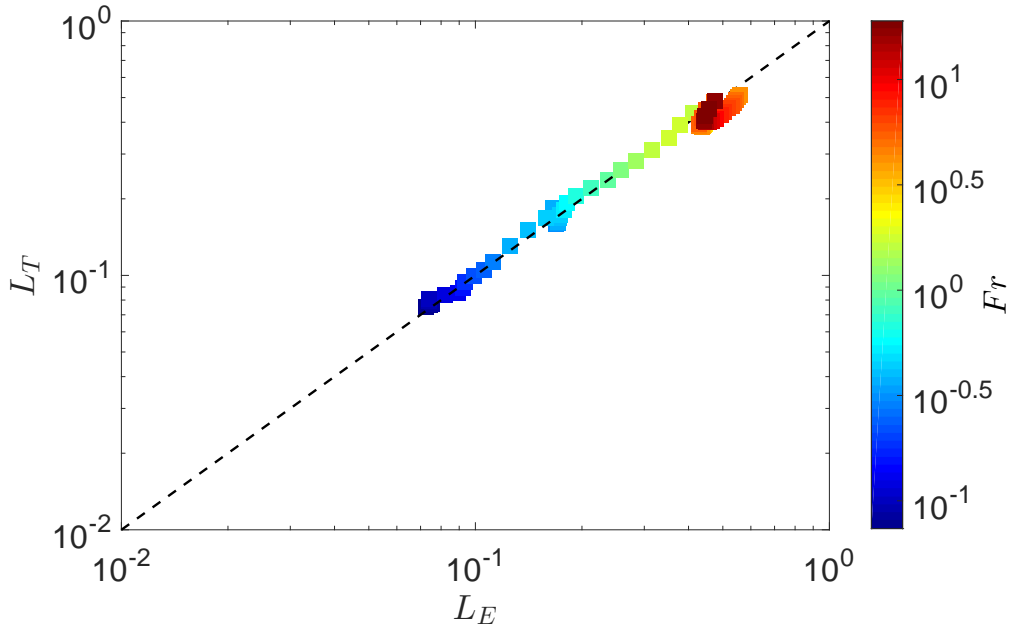


**Figure 6.3:** Relation between Thorpe length scale and Ellison length scale from high resolution DNS data of decaying stably stratified turbulence.

(1993) for lower resolution data. Using  $128^3$  DNS Itsweire *et al.* (1993) have shown that  $L_T$  and  $L_E$  have near one-to-one relation only for lower stratification and the relation is not quite prominent for strong stratification. Our simulation of high resolution DNS clearly shows that there is a one-to-one relation between  $L_T$  and  $L_E$ . This implies that  $L_T$  and  $L_E$  can be used interchangeably.

Figure 6.4 shows the relation between Thorpe length scale and Ozmidov length scale similar to Mater *et al.* (2013), but for higher resolution DNS data. This figure clears that  $L_T$  and  $L_O$  are equal only for turbulent Froude number of order one as indicated in the color bar. In the limit of strong stratification (low  $Fr$ ),  $L_T$  over predicts  $L_O$  and in the limit of weak stratification,  $L_O$  is significantly larger.

### 6.4.3 $Fr$ as a function of $L_E/L_O$ : Inferring the state of turbulence

The scaling arguments to find a relation between  $L_E/L_O$  and turbulent Froude number was discussed in section 6.2.2. The validation results for decaying and forced turbulence are presented in figure 6.5 and for sheared DNS data in figure 6.6. Both the figures validate the scaling results

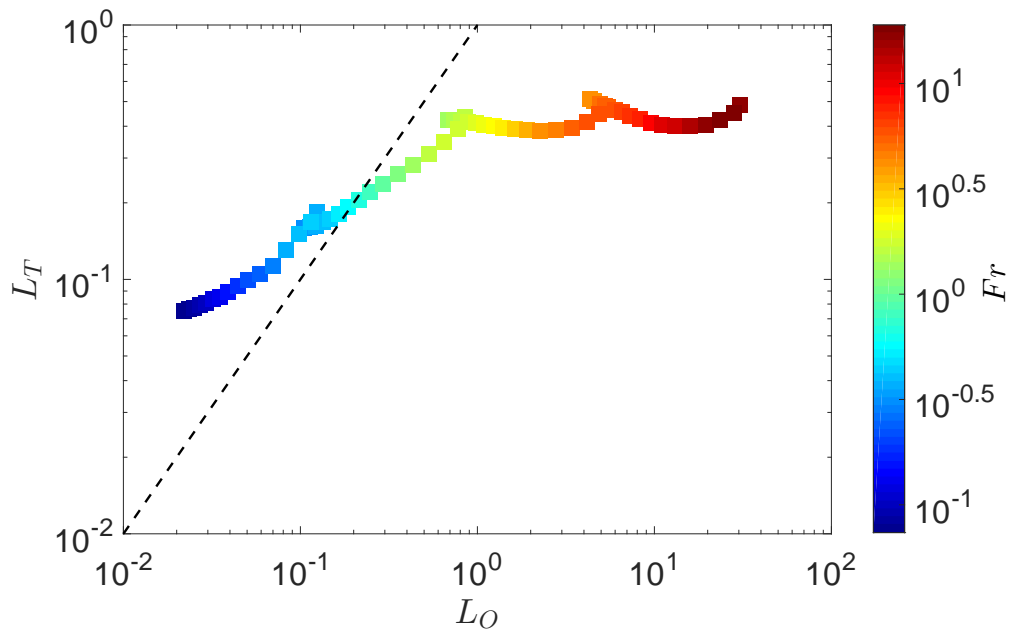


**Figure 6.4:** Relation between Thorpe length scale and Ozmidov length scale from high resolution DNS data of decaying stably stratified turbulence.

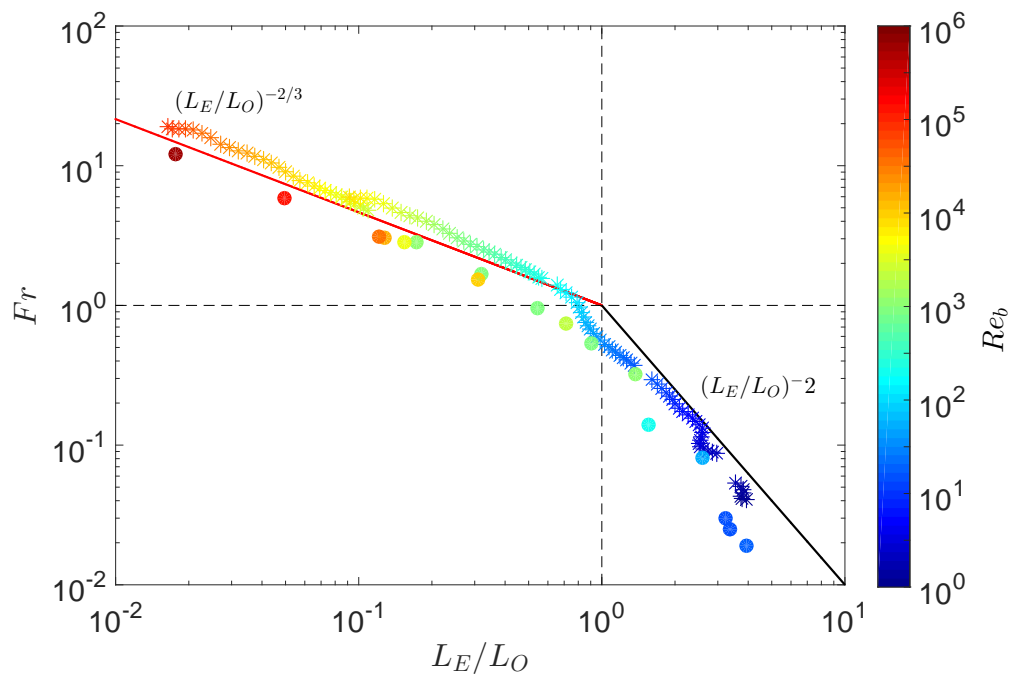


**Figure 6.5:** Froude number as a function of  $L_E/L_O$  for decaying and forced DNS data.

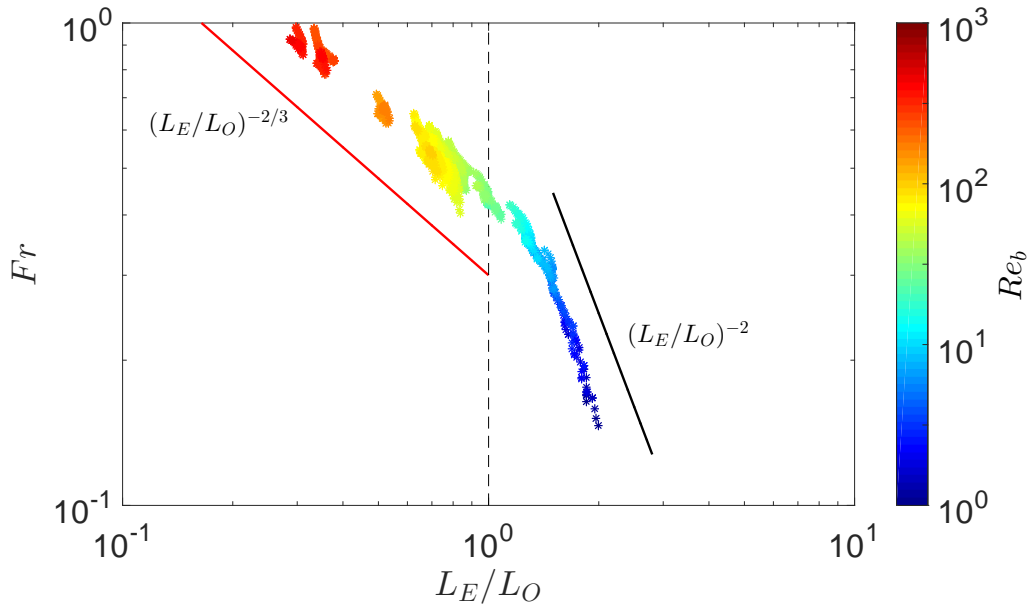


**Figure 6.6:** Froude number as a function of  $L_E/L_O$  for sheared DNS data.

shown in equations 6.10 and 6.13, respectively. The data indicate that  $Fr \sim (L_E/L_O)^{-2/3}$  for  $(L_E/L_O) < \mathcal{O}(1)$  and  $Fr \sim (L_E/L_O)^{-2}$  for  $(L_E/L_O) > \mathcal{O}(1)$ . As indicated earlier the transition for strong and weak regime of stratification is noticeable at  $Fr \sim \mathcal{O}(1)$  (0.3 for data in Shih *et al.*, 2005) These results are indeed powerful because they show that with  $L_T$  and  $L_O$  know, it is possible (for the first time) to estimate  $Fr$  in the field. This in turn permits the use of a more accurate parameterization to predict  $\Gamma$  which is crucial for obtaining robust estimates of diapycnal mixing.

## 6.5 Concluding remarks

In this chapter, we have first derived new scaling results for  $\Gamma$  as a function of  $Fr$  and then for  $Fr$  as a function of  $L_T/L_O$ . We have then used direct numerical simulation data from three independent researches to validate the scaling results. Three significant findings can be concluded from above discussions. First, high resolution decaying DNS data and forced DNS (Maffioli *et al.*, 2016) suggest that  $Re_b$  is an ambiguous parameter and hence parameterizations of  $\Gamma$  based on  $Re_b$  are not useful. Second, with scaling arguments and using high resolution DNS data we have

shown that the mixing coefficient scales with turbulent Froude number. The functions are different for three different distinct regions. The third key finding is that the ratio  $L_T/L_O$  is not only a representation of time of event (younger turbulence or older turbulence), but it represents the state of the flow i.e. whether the flow is in a strongly stratified regime, or in a weakly stratified regime. This finding will help oceanographers to infer the state of turbulence and thereby use appropriate parameterizations for  $\Gamma$  such as the new parameterizations that have been formulated in this study. To the knowledge of authors, this is the first time such analysis have been provided to identify both the state of turbulence and quantify the mixing efficiency in an unambiguous manner. The natural next step is to evaluate the utility of the proposed parameterizations in the field.

# Chapter 7

## Lagrangian analysis for diapycnal mixing and dispersion<sup>9</sup>

### 7.1 Introduction

Lagrangian statistics provide an in-depth understanding of particle dispersion in a fluid in motion (Sawford, 2001). A particle dispersion study therefore provides fundamental insights on turbulent diffusion and ultimately turbulent mixing in stably stratified turbulent flows. In this study we have used a Lagrangian framework to study diapycnal mixing by identifying the true diapycnal length scale and velocity scale.

Most geophysical flows are affected by vertical density stratification. Understanding diapycnal mixing and diapycnal dispersion in these flows will help to develop effective models of turbulent dispersion for air quality, nutrients distributions in the ocean, phytoplankton migration, tracers and climate variability (Gregg, 1987; Holford & Linden, 1999; Peltier & Caulfield, 2003). For an unstratified turbulent flow, fluid particles can move freely in vertical direction by advection over unlimited distance depending on the strength of turbulence. This is because the buoyancy force do not restrict the vertical motion in an unstratified flow. On the contrary, in a stably stratified fluid, the vertical motion of fluid particles are inhibited by buoyancy forces acting in vertical direction. Without molecular diffusion, the density of particle does not change and the particles oscillates about their equilibrium position (isopycnal surface). With molecular diffusion, there is an interchange of density between the particle and the background fluid. Hence if displaced, the fluid particle settles further away from its original equilibrium position by changing its density with background and thereby simultaneously altering the background density. Vertical turbulent

---

<sup>9</sup>The research presented in this chapter is under preparation to be submitted to the Journal of Fluid Mechanics under the title "Lagrangian analysis for diapycnal mixing and particle dispersion in stably stratified turbulence" by A. Garanaik and S. K. Venayagamoorthy. The chapter is written in a collective "we" voice to acknowledge collaboration with Dr. S. K. Venayagamoorthy.

dispersion in a stratified flow is a result of two processes, large scale vertical advection through isopycnal components and small scale molecular mixing through diapycnal components (Pearson *et al.*, 1983).

In a continuous turbulent motion, mean square particle displacement  $\langle(\delta r)^2\rangle$  or standard deviation of position of a single particle with uniform mean velocity is directly proportional to square of time for short time intervals and proportional to time at large times (Taylor, 1921). This is similar to Einstein's Brownian motion (1905) for molecular diffusion which shows an initial ballistic region ( $\sim t^2$ ) and later diffusive region ( $\sim t$ ). These concepts of turbulent diffusion have been extended to stably stratified flows by considering the vertically stabilizing buoyancy force (Csanady, 1964; Weinstock, 1992). Experimental studies are not amenable for collection of Lagrangian data and hence we rely on DNS simulations. Riley & Patterson (1974) extracted Lagrangian data from Eulerian fields in DNS for the first time in turbulent flows. Numerical analysis of vertical particle dispersion in stably stratified turbulent flows have been studied with a Langevin model (Csanady, 1964; Pearson *et al.*, 1983), rapid distortion theory (RTD) for decaying turbulence Kaneda & Ishida (2000), kinematic simulations for non decaying turbulence (Nicolleau & Vassilicos, 2000), DNS for decaying turbulence (Kimura & Herring, 1996; Venayagamoorthy & Stretch, 2006), DNS for stationary stratified turbulence (Aartrijk *et al.*, 2008), DNS for stationary turbulence with hyper viscosity (Brethouwer & Lindborg, 2009).

The diffusivity coefficient is a function a characteristic velocity scale and a characteristic length scale. In this work, we have extended the work of Venayagamoorthy & Stretch (2006) using higher resolution direct numerical simulation to identify appropriate characteristic length scale and velocity scale from Lagrangian mean square particle displacement analysis. In section 7.2 isopycnal and diapycnal decompositions of the total displacement and velocity are discussed. This is followed by a brief description of the particle tracking method that is used to obtain Lagrangian statistics from Eulerian statistics in section 7.3. Results are discussed in section 7.4. Concluding remarks are presents in section 7.5.

## 7.2 Isopycnal and diapycnal components of length and velocity scales from Lagrangian perspective

Lagrangian mixing is the measure of small scale diapycnal mixing obtained by following fluid particles. This is quantified by the local divergence of diapycnal density flux. Density perturbation following a fluid particle consists of two parts, isopycnal and diapycnal flux (Csanady, 1964; Pearson *et al.*, 1983; Venayagamoorthy & Stretch, 2006) and is defined as

$$\frac{d}{dt}\rho'\langle t \rangle = -\frac{\partial\langle\rho\rangle}{\partial z}w\langle t \rangle + \kappa\nabla^2\rho'\langle t \rangle, \quad (7.1)$$

where  $\langle t \rangle$  denotes coordinate following fluid particle,  $\kappa$  is molecular diffusivity,  $\rho'$  density perturbation from mean background density  $\langle\rho\rangle$ . The first term on the right hand side of equation 7.1 is the isopycnal component which is the vertical advection term that represents stirring or reversible mixing. The second term on the right hand side is the diapycnal flux, which is the direct measure of irreversible mixing rate due to density changes of particle with surrounding fluid by molecular diffusion processes (denoted as the Lagrangian mixing by Venayagamoorthy & Stretch, 2006). When a fluid particle is vertically displaced from its equilibrium position in a stably stratified fluid, two processes may occur. First, the particle will be advected due to inertial effects and will be restored back to its original equilibrium position due to buoyancy, a process known as isopycnal dispersion defined as

$$z_i\langle t \rangle = -\rho'\langle t \rangle/(\partial\langle\rho\rangle/\partial z). \quad (7.2)$$

Second, the particle will attain another level of equilibrium due to changes in its density, a measure of which is given by the diapycnal displacement defined as

$$z_d\langle t \rangle = \Delta\rho/(\partial\langle\rho\rangle/\partial z), \quad (7.3)$$

where  $\rho'\langle t \rangle$  is density perturbation of fluid particle and  $\Delta\rho$  is change of density of fluid particle. The change in density of fluid particle (irreversible mixing) is given as

$$\Delta\rho\langle t\rangle = \int_0^t \kappa \nabla^2 \rho' \langle t\rangle. \quad (7.4)$$

This shows that the total displacement of a single particle is a sum of its isopycnal and diapycnal components as

$$z\langle t\rangle = z_i\langle t\rangle + z_d\langle t\rangle \implies \partial z\langle t\rangle/\partial t = \partial z_i\langle t\rangle/\partial t + \partial z_d\langle t\rangle/\partial t \implies w\langle t\rangle = w_i\langle t\rangle + w_d\langle t\rangle. \quad (7.5)$$

Following the work of Venayagamoorthy & Stretch (2006), dispersion coefficients associated with total vertical displacement are defined as

$$k_z = \frac{1}{2} \frac{\partial \langle z^2 \rangle}{\partial t} = \langle zw \rangle. \quad (7.6)$$

(Here, we have removed the notation  $\langle t \rangle$  for simplicity. The correlation is taken for each particle and then the ensemble average is determined.)

The Isopycnal dispersion associated with isopycnal displacement is defined as

$$k_i = \frac{1}{2} \frac{\partial \langle z_i^2 \rangle}{\partial t} = \langle z_i w_i \rangle. \quad (7.7)$$

Similarly, the diapycnal dispersion coefficient associated with diapycnal displacement is defined as

$$k_d = \frac{1}{2} \frac{\partial \langle z_d^2 \rangle}{\partial t} = \langle z_d w_d \rangle. \quad (7.8)$$

The true diapycnal diffusivity is defined as

$$K_\rho = \frac{\epsilon_\rho}{(\partial \langle \rho \rangle / \partial z)^2}, \quad (7.9)$$

where  $\epsilon_\rho$  is the rate of dissipation of density variance and  $\partial \langle \rho \rangle / \partial z$  is the mean background density gradient. (For a detail derivation see: Venayagamoorthy & Stretch, 2010). The diapycnal disper-

sion coefficient is generally not equal to diapycnal diffusivity. The diapycnal dispersion coefficient is equivalent to diapycnal diffusivity only if the fluid particle densities are independent of velocity.

### 7.3 Methodology

Eulerian simulation: Direct Numerical simulation (DNS) provides full description of turbulent flow field ranging from energy containing large eddy scale ( $\mathcal{L}$ ) to small dissipative Kolmogorov scale ( $\eta$ ) without involving any parameterization of small-scale physics. The numerical simulations for our study were carried out using pseudo-spectral DNS code developed by Riley *et al.* (1981) for stably stratified homogeneous turbulent flows. A cubical periodic domain with dimension  $2\pi$  with  $256^3$  grid points was considered for all simulations. The turbulent flow was initialized with a Gaussian isotropic three dimensional solenoidal velocity field and allowed to evolve and decay under the influence of a constant background stratification. The mean shear was zero for all the simulations and the only large scale anisotropy considered was vertical stable stratification. Flow was characterized with an initial Reynolds number of 625 defined as  $Re_0 = u_0 L_0 / \nu$ , where  $u_0$  is the initial velocity scale and  $L_0$  is the initial length scale. Background stratification was characterized with an initial Richardson number, defined as  $Ri_0 = (NL_0/u_0)^2$ , where  $N$  is the buoyancy frequency. Six DNS simulations were performed for the present study with  $Ri_0 = 0, 0.01, 0.1, 1.0, 10$  and  $100$ , respectively, for a duration of  $5L_0/u_0$  in order to investigate the effects of weakly stratified to strongly stratified conditions on the small scales of turbulence. The molecular Prandtl number  $Pr = \nu/\kappa = 1$  for all the simulations.

Lagrangian simulation of particle tracking: A particle tracking algorithm was incorporated in the DNS as described by Venayagamoorthy & Stretch (2006). Knowing the Eulerian velocity field at each grid point for a  $256^3$  domain, the velocity at any intermediate point or any arbitrary location ( $u$ ) was found through a cubic spline interpolation scheme. For our study,  $24^3$  particles were used for obtaining Lagrangian statistics. Knowing the initial position of a particle  $x_0$  at  $t = 0$ , and interpolated velocity  $u$  from Eulerian field (Lagrangian velocity), the equation of motion for a

position  $x$  at time  $t$ , can be derived as  $dx/dt = u$ . Using a suitable numerical integration scheme, the particle position can then be determined.

## 7.4 Results

### 7.4.1 Validation of Lagrangian statistics with Eulerian statistics

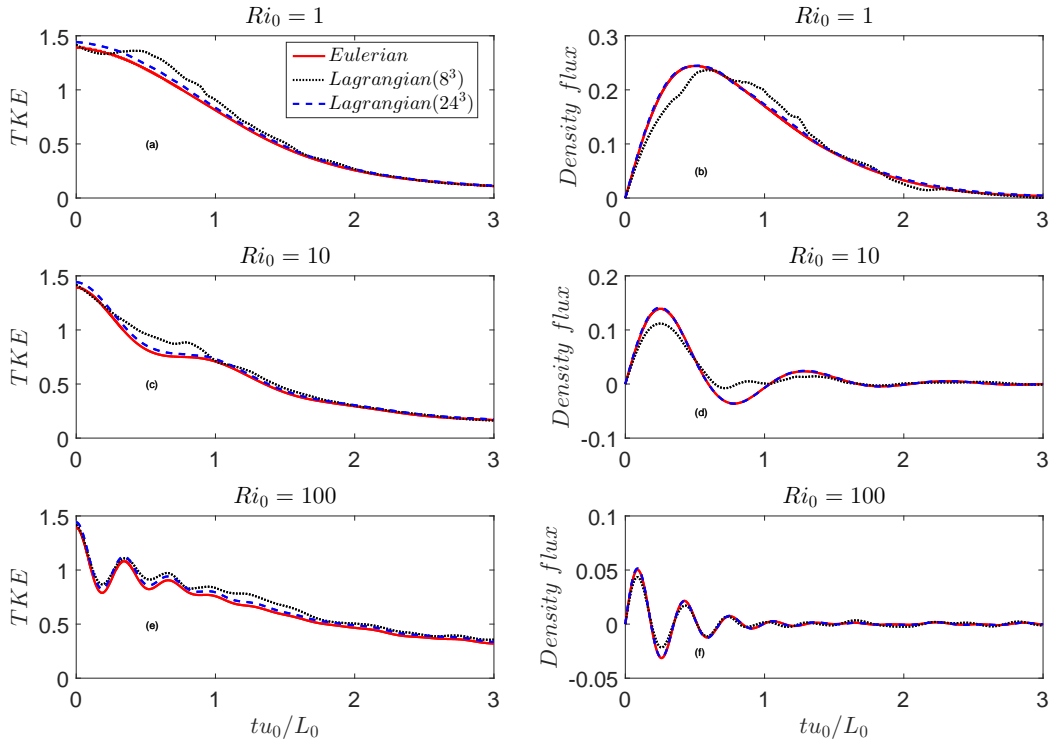


**Figure 7.1:** Validation of Lagrangian statistics and Eulerian statistics for turbulent kinetic energy (TKE,  $1/2u_i^2$ ) in (a, c and e) and for density flux ( $\langle \rho' w' \rangle$ ) in (b, d and f). with varying stratification

A comparisons of Lagrangian and Eulerian statistics for turbulent kinetic energy (TKE) and density flux  $\langle w' \rho' \rangle$  are provided in figure 7.1. The Eulerian statistics discussed here are volume averages and the Lagrangian statistics are the ensemble averages of all the particles selected in the box. The Eulerian statistics are obtained from  $256^3$  DNS simulations. For Lagrangian statistics, both  $8^3$  and  $24^3$  particles are considered as shown in the figure 7.1.  $24^3$  particles are shown to be sufficient to mimic the corresponding Eulerian statistics. The simulation of  $256^3$  DNS box with

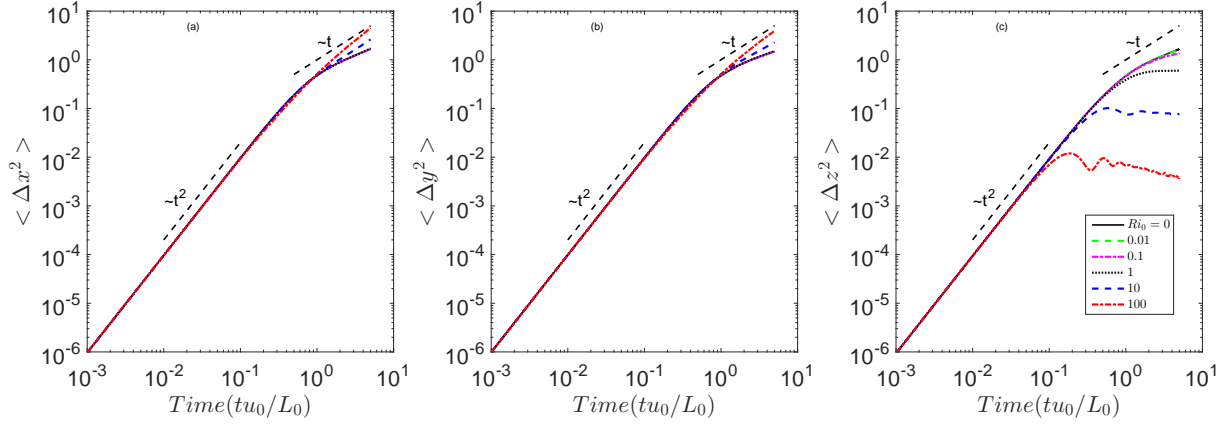


**Figure 7.2:** The mean square of the horizontal displacement (a)  $\langle \Delta x^2 \rangle$ , (b)  $\langle \Delta y^2 \rangle$  and (c) vertical displacement  $\langle \Delta z^2 \rangle$  showing ballistic and diffusive region for various  $Ri_0$  values.

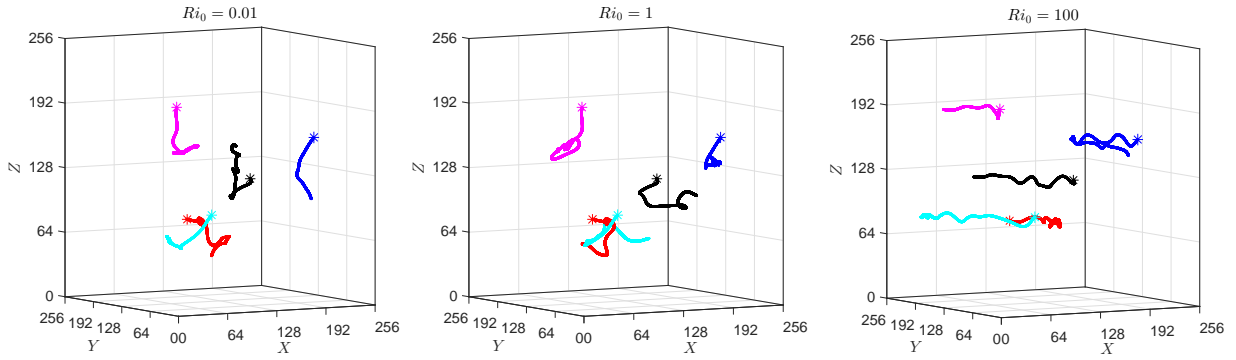


**Figure 7.3:** Sample particle tracks.

$8^3$  particle took 35s CPU time on a system with I7, 256 GB RAM with dual processors. On the same system,  $256^3 - 12^3$  took 70 s ,  $256^3 - 24^3$  took 430 s,  $256^3 - 32^3$  took 900 s,  $512^3 - 8^3$  took 400 s and  $512^3 - 32^3$  took 2 hr CPU time for a single time step. To obtain 5 turnover times, (when TKE is expected to decay 90%), we need 5000 time steps with  $dt = 0.001$ , which increases the computational cost for higher number of particles. Thus, the selection of  $24^3$  particles in  $256^3$  Eulerian box was finalized for this study by considering a trade off between accuracy and computational cost.

## 7.4.2 Lagrangian particle dispersion

The mean square Lagrangian particle displacements for both horizontal  $\langle \Delta x^2 \rangle$ ,  $\langle \Delta y^2 \rangle$  and vertical  $\langle \Delta z^2 \rangle$  as a function of eddy time ( $tu_0/L_0$ ) are shown in figure 7.2. For unstratified flow

$Ri_0 = 0$ , the mean square vertical displacement grows as  $\sim t^2$  for initial time and as  $\sim t$  for later time as discussed by Taylor (1921) for ballistic and diffusive regimes respectively (Xia *et al.*, 2013). For  $Ri_0 \gg 0$ , mean square vertical displacement levels off. Such a behavior is not evident in the statistics of the horizontal displacements  $\langle \Delta x^2 \rangle$  and  $\langle \Delta y^2 \rangle$ . This is because the imposed stratification is only in vertical direction which inhibits growth of  $\langle \Delta z^2 \rangle$ . The mean square horizontal displacements are seldom affected by vertical stratification. These statistics are consistent with earlier results (Kaneda & Ishida, 2000; Kimura & Herring, 1996; Venayagamoorthy & Stretch, 2006). Three dimensional particle tracks (for five arbitrarily selected particles) for  $Ri_0 = 0.01, 1$  and  $100$  are shown in figure 7.3. The tracks of low  $Ri_0$  flows show that the particles wander with freedom in all three directions. On the other hand, for the strongly stable case  $Ri_0 = 100$ , the particles are more or less restricted to the horizontal plane with small vertical oscillations.

### 7.4.3 Isopycnal and diapycnal displacement

The goal of Lagrangian study by tracking the particle position is to distinguish the isopycnal and diapycnal components of vertical displacement and vertical velocity, which is difficult in Eulerian simulation and in field measurements. In figure 7.4 the mean square vertical displacements of particles are shown as a function of time for various stratifications.

For an initial time,  $tu_0/L_O = 1.5$ , isopycnal component of displacement dominates. After the initial transient, diapycnal displacement increases and dominates the total particle displacement due to diapycnal mixing which becomes significant with increase of stratification. When stratification is very strong (e.g.  $Ri_0 = 100$ ), mixing is strongly suppressed and the vertical displacements strongly inhibited. For strong stratification, the isopycnal component grows initially and then gradually decays with time when the diapycnal component accounts for the total displacement of the particles. If there were no mixing, then the diapycnal component should be zero.

### 7.4.4 Isopycnal and diapycnal velocity

Root mean square vertical velocity and its isopycnal and diapycnal components are shown in figure 7.5 as a function of time for different stratifications. With increase of stratification, the

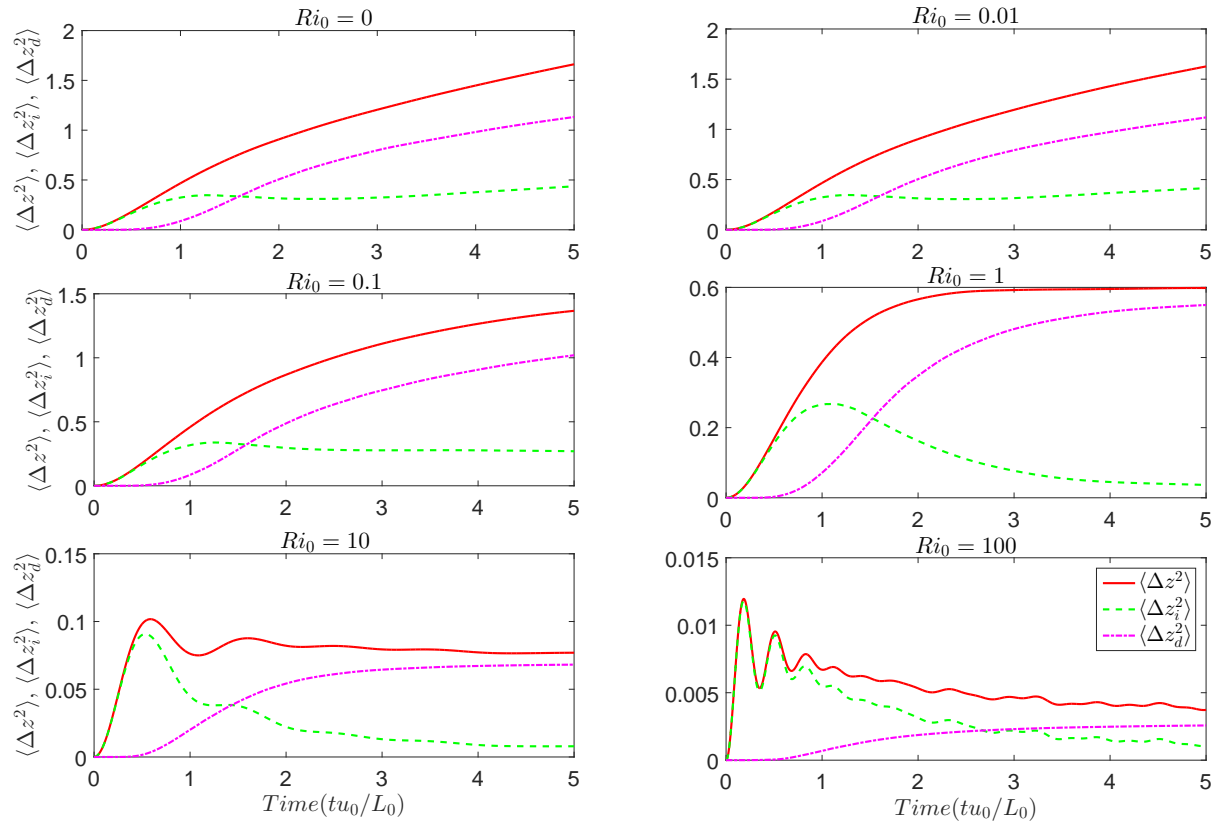


**Figure 7.4:** Mean square of total displacement (solid line), mean square of isopycnal displacement (dashed line) and mean square of diapycnal displacement (dotted line) for different initial Richardson numbers.

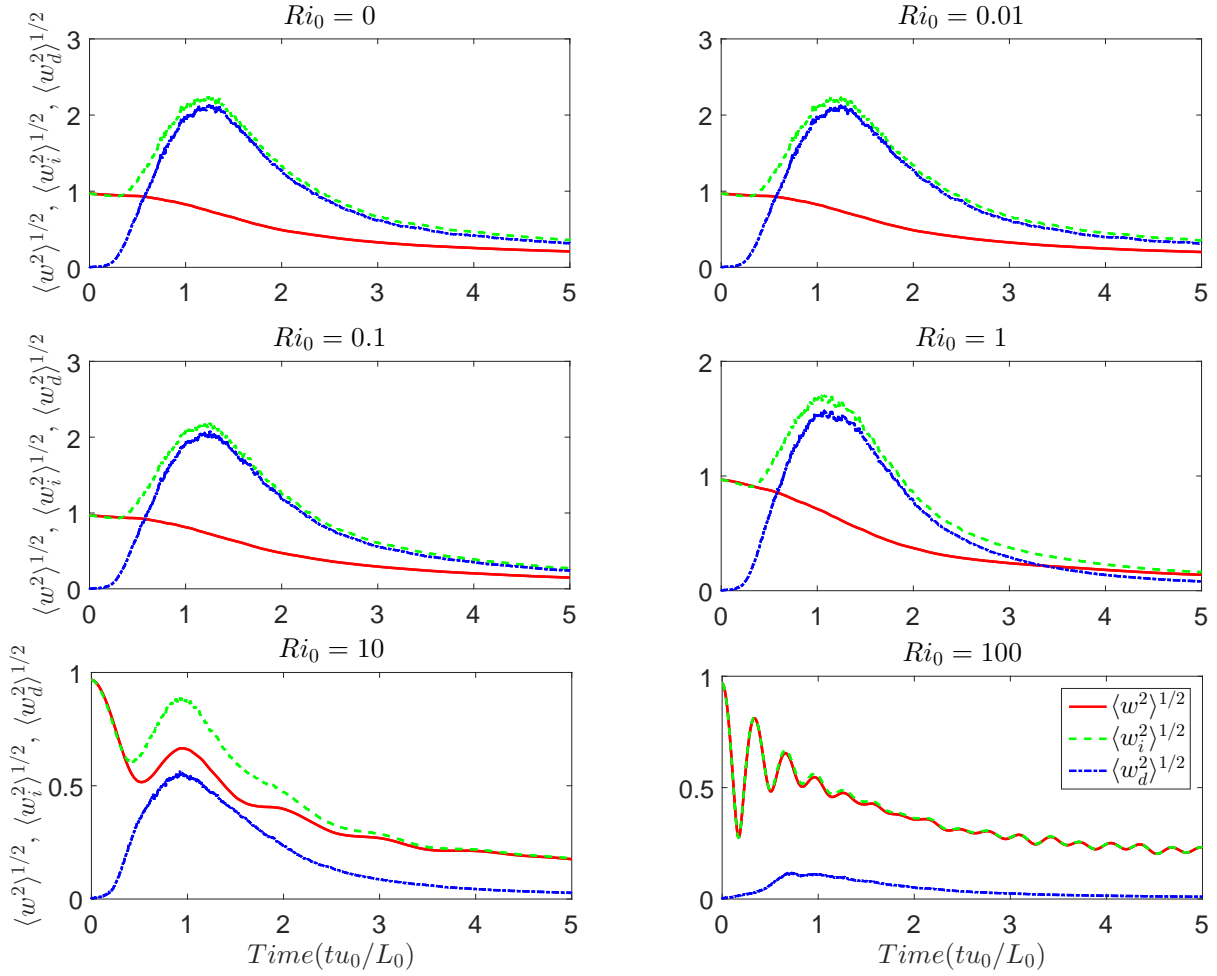


**Figure 7.5:** Root mean square of total velocity (solid line), root mean square of isopycnal velocity (dashed line) and root mean square of diapycnal velocity (dotted line) for different initial Richardson numbers.

vertical velocity  $\langle w^2 \rangle^{1/2}$  has a characteristic oscillatory behavior consistent with the presence of internal waves. For low stratification, the diapycnal velocity and isopycnal velocity are almost equal. With increase of stratification the maximum value of all the vertical velocities decrease as expected. The isopycnal and diapycnal velocity separate from each other for strong stratification as isopycnal component represents the reversible part and diapycnal component represents the irreversible part of total velocity.

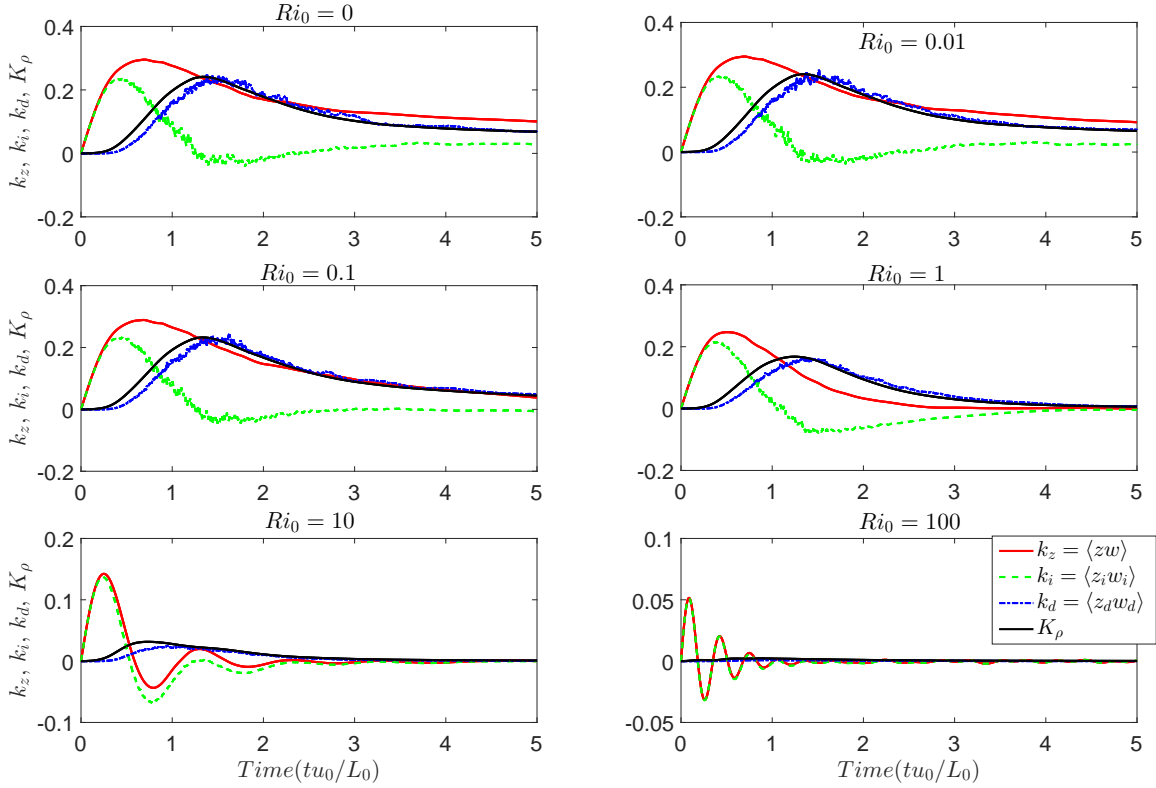


**Figure 7.6:** Dispersion coefficients for different initial Richardson number.

### 7.4.5 Diapycnal dispersion

The dispersion coefficients along with true diapycnal diffusivity (see: section 7.2) are shown in figure 7.6. The wave effects of isopycnal dispersion are noticeable for higher stratification. Isopycnal dispersion does not contribute to irreversible mixing. Diapycnal dispersion coefficient can represent the true diffusivity for weakly stratified flow after the flow is fully developed.

### 7.4.6 Diapycnal diffusivity from isopycnal length scale and diapycnal velocity scale

In the context of oceanography, the overturning length scales are represented by Ellison length scale  $L_E$  (Ellison, 1957). Here we have shown that this outer length scale is equivalent to isopycnal displacement. The relation between root mean square isopycnal component of vertical velocity and a overturning length scale  $L_E$  is shown in figure 7.7. This shows that the overturning length scale

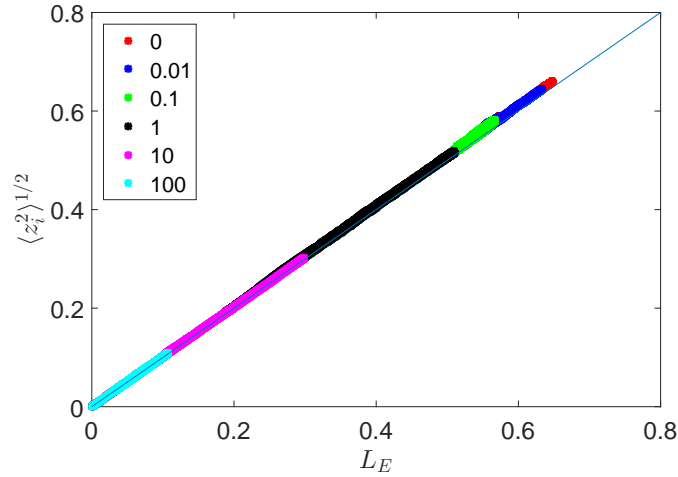


**Figure 7.7:** Relation between root mean square isopycnal displacement with Ellison length scale for different initial Richardson numbers  $Ri_0$  as shown in the legend.

(an Eulerian statistic) is actually equal to the isopycnal displacement obtained from Lagrangian statistics.

The ratio of root mean square diapycnal velocity and isopycnal velocity is shown in figure 7.8 as a function of turbulent Froude number  $Fr$ . This indicates that for a low stratification ( $Fr > \mathcal{O}(1)$ ), the root mean square isopycnal velocity and root mean square diapycnal velocity components are equivalent (also shown in figure 7.5) but for high stratification ( $Fr < \mathcal{O}(1)$ ), the diapycnal velocity is smaller than the isopycnal velocity due to presence of internal wave motions.

Figure 7.9(a) shows the relation between true diapycnal diffusivity  $K_\rho$  obtained from Eulerian statistics and diapycnal dispersion  $k_d$  from the Lagrangian statistics. Diapycnal diffusivity from Lagrangian statistics  $K_d$  and diapycnal diffusivity from Eulerian statistics  $K_\rho$  are presented in figure 7.9(b). The true diffusivity is represented by the isopycnal length scale and a diapycnal velocity scale.

## 7.5 Concluding remarks

In this chapter preliminary results from a Lagrangian analysis of stably stratified turbulence has been presented. This method helps to isolate the isopycnal components from diapycnal components to provide insight into the true length scales and velocity scales for irreversible diapycnal

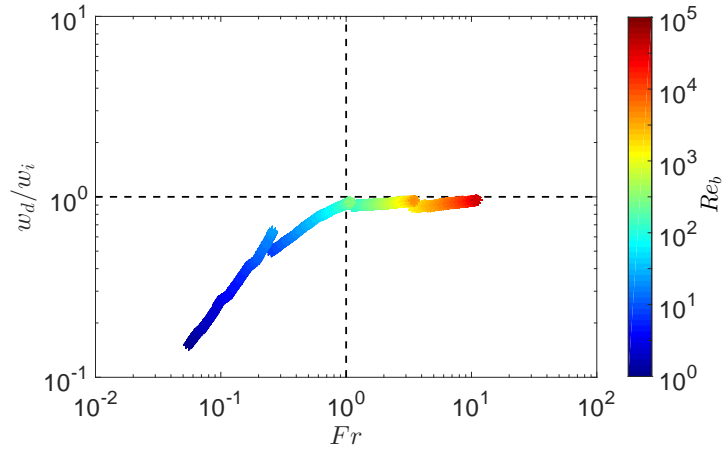


**Figure 7.8:** The ratio of rms diapycnal velocity to rms isopycnal velocity with turbulent Froude number with  $Re_b$  in the color bar.

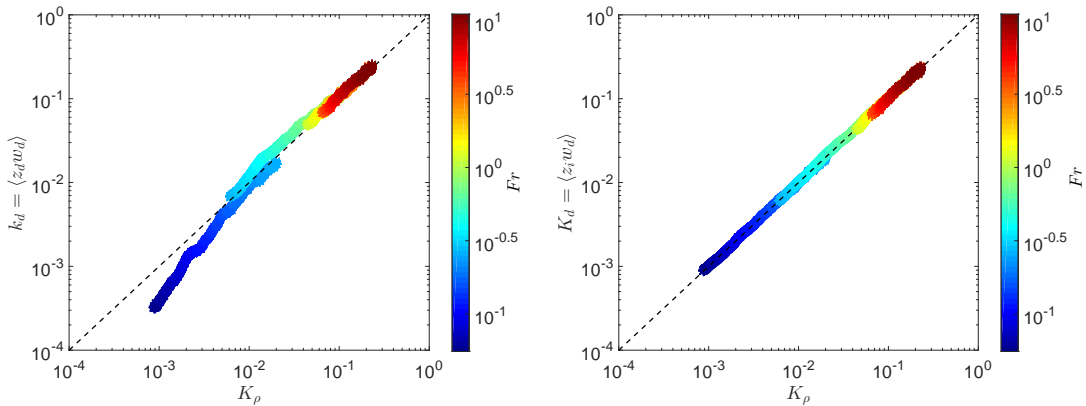


**Figure 7.9:** Left panel: Relation between true diapycnal diffusivity and diapycnal dispersion. Right panel: Relation between true diapycnal diffusivity with modeled diapycnal diffusivity. The Color bar is showing turbulent Froude number.

mixing. The overturning length scale in oceanography is actually an isopycnal displacement not diapycnal length scale which contributes towards mixing. The representative velocity scale for diapycnal mixing is the diapycnal component of velocity scale. Thus the true diapycnal diffusivity is obtained from ensemble average of the product of isopycnal length scale and diapycnal velocity scale. The diapycnal dispersion is the statistical average of the product of diapycnal displacement and diapycnal velocity which is equivalent to true diapycnal diffusivity in the limit of low stratification.

# Chapter 8

## Summary and Conclusions

### 8.1 Key findings

The following is a brief description of the main outcomes of this study:

1. Parameterization of diapycnal mixing from field data analysis suggests that a constant mixing coefficient,  $\Gamma$  can be used only in thermocline regime which is typically strongly stratified. The maximum constant value of  $\Gamma$  can be lower or higher than the canonical value depending on strength of stratification and available turbulent kinetic energy (as indicated by the rate of dissipation of turbulent kinetic energy  $\epsilon$ ). Constant mixing coefficient of 0.2, might result in overprediction of oceanic mixing when stratification is negligible (e.g. in the upper ocean). There is no unique relationship of  $\Gamma$  or  $R_f$  with buoyancy Reynolds number  $Re_b$ . Similar result was also found in chapter 6 that clearly shows that  $Re_b$  is without a doubt an ambiguous parameter for quantifying the mixing efficiency in stably stratified flows.
2. A new method to identify background shear  $S_{across}$  of a turbulent patch was proposed. Gradient Richardson number  $Ri_g$  estimated from  $S_{across}$  suggest that mixing efficiency increases in a shear dominated regime ( $Ri_g < 0.25$ ) similar to other results, and approaches a constant value at  $Ri_g \sim \mathcal{O}(1)$  and then decreases. The mechanism is unknown and this needs further investigations. It is highlighted that the methodology used for data analysis is critical and without knowledge of the underlying physics, any analysis can result in wrong estimates of oceanic mixing.
3. The state-of-the-art instruments to measure the turbulent quantities operate under certain assumptions. The microstructure profilers measure small scale quantities such as the rate of dissipation of turbulent kinetic energy and the rate of dissipation of thermal variance from single spatial gradients in lieu of all the gradients, by invoking the small scale isotropy

assumptions. It was found that the small scale isotropy assumption for a less energetic stratified ocean leads to overprediction of the measurements of turbulent quantities by 200%. We have provided a correction such that the true dissipation ( $\epsilon_{3D}$ ) can be obtained from measured isotropic dissipation ( $\epsilon_{1D}$ ).

4. Considering scaling analysis based on physical reasoning, it was shown that the true diapycnal diffusivity  $K_d$  can be obtained from the the root mean square vertical velocity  $w'$  and the famous Ellison length scale  $L_E$ , which denotes the outer length scale of turbulence. For strongly stratified flows, these scales are contaminated by internal wave motions and hence, corrections are needed. It was shown that the true diapycnal velocity can be obtained from the root mean square vertical velocity through a Froude number parameter as  $w'/w_d \sim Fr^{-1/2}$ . Similarly, the diapycnal length scale can be obtained from  $L_E$  as  $L_E/L_d \sim Fr^{-1/2}$ . In this manner, for a weakly stratified regime,  $K_d \sim w'L_E$  and for a strongly stratified fluid  $K_d \sim w'L_E \times Fr$ .
5. A new overturn Reynolds number  $Re_O = w'L_E/\nu$  is introduced to infer  $Fr$  from oceanic measurements as present state-of-the-art instruments do not measure turbulent kinetic energy to estimate  $Fr$ . It was found that  $Re_O$  increases in the stratified regime and tends asymptotically to a constant in the unstratified regime.
6. Scaling analysis and direct numerical simulation of decaying, sheared and forced turbulence data of stably stratified fluid reveal that the mixing coefficient  $\Gamma$  scales with the turbulent Froude number  $Fr$ . For weakly stratified flow,  $\Gamma \sim Fr^{-2}$ , for moderate stratification,  $\Gamma \sim Fr^{-1}$  and for strongly stratified flow  $\Gamma \sim Fr^0$ .
7. A novel relationship between  $Fr$  and measurable Thorpe length scale  $L_T$  and Ozmidov length scale  $L_O$  has been proposed such that  $L_T/L_O < \mathcal{O}(1)$  represents weakly stratified regime and  $L_T/L_O > \mathcal{O}(1)$  represents strongly stratified regime. This is an important finding for estimates and parameterization of diapycnal mixing from field measurements. From

oceanic measurements, if data are in strongly stratified regime as denoted by  $L_T/L_O$ , constant mixing efficiency should be used. Otherwise a parameterization is needed.

8. From Lagrangian analysis it was shown that the Ellison length scale is an isopycnal length scale. The diapycnal diffusivity and diapycnal dispersion are equivalent for moderate to weak stratification. The diapycnal diffusivity is a product of diapycnal velocity scale and an isopycnal length scale.

## 8.2 Suggestions for future works

Accurate parameterizations of mixing is an important issue for many applications in engineering and nature including climate prediction. In this dissertation, some new (promising) methods for improved inference and parameterization of mixing have been provided. Further research is needed to evaluate the utility and fidelity of these new methods in the field for a broad range of flow conditions. In chapter 5, we have proposed a new method to estimate diapycnal diffusivity from measurable velocity and length scales using DNS data. Further validation of this model is required using field data. Such a validation will bring light to the significance of this new model for small scale mixing that uses only fine scale measurements. In chapter 3 we have discussed different methods to obtain background stratification and shear. This work needs further investigations with different oceanic and atmospheric turbulence datasets in order to converge towards a robust methodology for data analysis. Development of instruments which can measure three dimensional turbulent quantities in the field would provide an avenue to test the proposed parameterizations using geophysical flow data. Lagrangian statistics needs further investigation to establish a relation of diapycnal diffusivity with measurable quantities. In sum, the proposed parameterizations and methods should be tested extensively in the field and in large scale models to assess their usefulness for real world applications.

# Bibliography

- AARTRIJK, M., CLERCX, H. J. H. & WINTERS, K. B. 2008 Single-particle, particle-pair and multiparticle dispersion of fluid particles in forced stably stratified turbulence. *Phys. Fluids* **20**, 025104.
- BARRY, M. E., IVEY, G. N., WINTERS, K. B. & IMBERGER, J. 2001 On the flux richardson number in stably stratified turbulence. *J. Fluid Mech.* **725**, 1–22.
- BELCHER, S. E., GRANT, A. L. M., HANLEY, K. E., KEMPER, B. F., ROEKEL, L. V., SULLIVAN, P. P., LARGE, W. G., BROWN, A., HINES, A., CALVERT, D., RUTGERSSON, A., PATTERSSON, H., BIDLOT, J. R., JANSSEN, P. A. E. M. & POLTON, J. F. 2012 A global perspective on langmuir turbulence in the ocean surface boundary layer. *Geophys. Res. Lett.* **174**, L18605.
- BOOS, W. R., SCOTT, J. R. & EMANUEL, K. A. 2003 Transient diapycnal mixing and the meridional overturning circulation. *J. Phys. Oceanogr.* **34**, 334–341.
- BOUFFARD, D. & BOEGMAN, L. 2013 A diapycnal diffusivity model for stratified environmental flows. *Dynamics of Atmospheres and Oceans* **61-62**, 14–34.
- BRANNIGAN, L. 2013 Shear at the base of the oceanic mixed layer generated by wind shear alignment. *J. Phys. Oceanogr.* **43**, 1798–1810.
- BRETHOUWER, G., BILLANT, P., LINDBORG, E. & CHOMAZ, J. M. 2007 Scaling analysis and simulation of strongly stratified turbulent flows. *J. Fluid Mech.* **585**, 343–368.
- BRETHOUWER, G. & LINDBORG, E. 2009 Numerical study of vertical dispersion by stratified turbulence. *J. Fluid mech.* **631**, 149–163.
- BRITTER, R. E., HUNT, J. C. R., MASH, G. L. & SYNDER, W. H. 1983 The effects of stratification on turbulent diffusion and the decay of grid turbulence. *J. Fluid Mech.* **127**, 27–44.

- CANUTO, V. M., HOWARD, A., CHENG, Y. & DUBOVIKOV, M. S. 2001 Ocean turbulence. part i: one-point closure model-momentum and heat vertical diffusivities. *J. Phys, Ocean.* p. 31.
- CIMATORIBUS, A. A., VAN HAREN, H. & GOSTIAUX, L. 2014 Comparison of ellison and thorpe scales from eulerian ocean temperature observations. *J. Geophys. Res. Oceans* **119**, 7047–7065.
- CSANADY, G. T. 1964 Turbulent diffusion in a stratified fluid. *J. Atmosph. Science* **21**, 439–447.
- DILLON, T. 1982 Vertical overturns: A comparison of thorpe and ozmidov scale. *J. Geophys. Res.* **87**, 9601–9613.
- DOSIO, A., DE ARELLANO, J. V. G. & HOLTSLAG, A. A. M. 2005 Relating eulerian and lagrangian statistics for the turbulent dispersion in the atmospheric convective boundary layer. *J. Atm. Sci.* **62**, 1175–1191.
- DUNCKLEY, J. F., KOSEFF, J. R., STEINBUCK, J. V., MONISMITH, S. G. & GENIN, A. 2012 Comparison of mixing efficiency and vertical diffusivity models from temperature microstructure. *J Geophysical Research* **17**, C10008.
- DURBIN, P. A. & PETERSON-REIF, B. A. 2011 *Statistical theory and modelling for turbulent flows.*
- EDGAR, MICHAEL 2011 Primary productivity nutrient cycle. *Slideshare* .
- ELLISON, T. H. 1957 Turbulent transport of heat and momentum from an infinite rough plane. *J. Fluid Mech.* **2**, 456–466.
- FERNANDO, H. J. S. 1991 Turbulent mixing in stratified fluids. *Annu. Rev. Fluid Mech.* **23**, 455–493.
- FERRON, B., MERCIER, H., SPEER, K., GARGETT, A. & POLZIN, K. 1998 Mixing in the romanche fracture zone. *J. Phys. Oceanogr* **28**, 1929–1945.

- FINCHAM, A. M., MAXWORTHY, T. & SPEDDING, G. R. 1996 Energy dissipation and vortex structure in freely decaying stratified grid turbulence. *Dyn. Atmos. Oceans* **23**, 155–169.
- FRIEDERICH, G.E. & CODISPOTI, L.A. 1981 The effects of mixing and regeneration on the nutrient content of upwelling waters off Peru. *American Geophysical Union, Washington, D. C.*. doi: 10.1029/CO001p0221 .
- GARGETT, A. & GARNER, T. 2008 Determining Thorpe scales from ship-lowered CTD density profiles. *J. Atmos. Oceanic Technol.* **25**, 1657–1670.
- GARGETT, A. E. 1988 The scaling of turbulence in the presence of stable stratification. *J. Geophys. Res.* **93(C5)**, 5021–5036.
- GARGETT, A. E., OSBORN, T. R. & NASMYTH, P. W. 1984 Local isotropy and the decay of turbulence in a stratified fluid. *J. Fluid Mech.* **144**, 231–280.
- GODEFERD, F. S. & STAQUET, C. 2003 Statistical modelling and direct numerical simulations of decaying stably stratified turbulence. part 2. large-scale and small-scale anisotropy. *J. Fluid Mech.* **486**, 115–159.
- GREGG, M.C., D'ASARO, E.A., RILEY, J.J. & KUNZE, E. 2018 Mixing efficiency in the ocean. *Annual Review of Marine Science* **10** (1), 443–473.
- GREGG, M. C. 1987 Diapycnal mixing in the thermocline. *J. Fluid Mech.* **92**, 5249–5286.
- GREGG, M. C. 1989 Scaling turbulent dissipation in the thermocline. *J. Geophys. Res.* **94**, 9686–9698.
- HOLFORD, J. M. & LINDEN, P. F. 1999 Turbulent mixing in a stratified fluid. *Dynamics of Atmosphere and Oceans* **30**, 173–198.
- ITSWEIRE, E. C., HELLAND, K. N. & VAN ATTA, C. W. 1986 The evolution of grid-generated turbulence in a stably stratified fluid. *J. Fluid Mech.* **162**, 299–338.

- ITSWEIRE, E. C., KOSEFF, J. R., BRIGGS, D. A. & FERZIGER, J. H. 1993 Turbulence in stratified shear flows: Implications for interpreting shear-induced mixing in the ocean. *J. Phys. Oceanogr.* **23**, 1508–1522.
- IVEY, G. N. & IMBERGER, J. 1991 On the nature of turbulence in a stratified fluid. part i: The energetics of mixing. *J. Phys. Oceanogr.* **21**, 650–659.
- IVEY, G. N., WINTERS, K. B. & KOSEFF, J. R. 2008 Density stratification, turbulence, but how much mixing? *Ann. Rev. Fluid Mech.* **40**, 169–184.
- JONES, W. P. & LAUNDER, B. E. 1972 The prediction of laminarization with a two equation model of turbulence. *Int. J. Heat Mass Transfer* **15**, 301–314.
- KANEDA, Y. & ISHIDA, T. 2000 Suppression of vertical diffusion in strongly stratified turbulence. *J. Fluid Mech.* **402**, 311–327.
- KARIMPOUR, F. & VENAYAGAMOORTHY, S. K. 2014 A simple turbulence model for stably stratified wall bounded flows. *J. Geophys. Res.* **119**, 870–880.
- KIM, J., MOIN, P. & MOSER, R. 1987 Turbulence statistics in fully developed channel flow at low Reynolds number. *J. Fluid Mech.* **177**(3), 133–166.
- KIMURA, Y. & HERRING, J. R. 1996 Diffusion in stably stratified turbulence. *J. Fluid Mech.* **328**, 256–269.
- KOLMOGOROV, A. N. 1941 The local structure of turbulence in an incompressible viscous fluid for very large Reynolds number. *C. R. Acad. Sci. USSR* **30**, 301–305.
- KUHLBRODT, T., GRIESEL, A., MONTAYA, M., LEVERMANN, A., HOFMANN, M. & RAHMSTORF, S. 2007 On the driving processes of the Atlantic meridional overturning circulation. *Rev. Geophysys.* **45**, RG2001.
- KUNDU, P. K., COHEN, I. R. & DOWLING, D. R. 2016 Fluid mechanics. *Elsevier Inc.*

- KUNZE, E., FIRING, E., HUMMON, J. M., CHERESKIN, T. K. & THURNHERR, A. M. 2006 Global abyssal mixing inferred from lowered adcp shear and ctd strain profiles. *J. Phys. Oceanogr.* **36**, 1553–1576.
- LAURENT, L. C. ST., SIMMONS, H. L., TAMG, T. Y. & WANG, Y. 2011 Turbulent properties of internal waves in the south china sea. *Oceanography* **24**, 78–87.
- LAURENT, L.C. ST. & SMITT, R. W. 1999 The contribution of salt fingers to vertical mixing in the north atlantic traces release experiments. *J. Phys. Oceanogr.* **29**, 1404–1424.
- LINDBORG, E. & BRETHOUWER, G. 2008 Vertical dispersion by stratified turbulence. *J. Fluid Mech.* **614**, 303–314.
- LINDEN, P. F. 1980 Mixing across a density interface produced by grid turbulence. *Geophys. Astrophys. Fluid Dyn* **13**, 3–23.
- LINDEN, P. F. 1984 Mixing in stratified fluids. *J. Fluid Mech.* **144**, 231–280.
- LOZOVATSKY, I. D. & FERNANDO, H. J. S. 2012 Mixing efficiency in natural flows. *Philos. Trans. R. Soc. A* **371**, 4662–4672.
- LUCAS, D. & CAULFIELD, C. P. 2017 Irreversible mixing by unstable periodic orbits in buoyancy dominated stratified turbulence. *J. Fluid Mech.* **832(R1)**.
- LUECK, R. G., WOLK, F. & YAMAZAKI, H. 2002 Oceanic velocity microstructure measurements in the 20<sup>th</sup> century. *J. Oceanography* **58**, 153–174.
- LUKETINA, D. & IMBERGER, J. 1989 Turbulence and entrainment in a buoyant surface plume. *J. Geophys. Res.* **94(C9)**, 12619–12636.
- MAFFIOLI, A., BRETHOUWER, G. & E.LINDBORG 2016 Mixing efficiency in stratified turbulence. *J. Fluid Mech.* **794**, R3.

- MAFFIOLI, A. & DAVIDSON, P. A. 2016 Dynamics of stratified turbulence decaying from a high buoyancy Reynolds number. *J. Fluid Mech.* **786**, 210–233.
- MARSHALL, J. & SPEER, K. 2012 Closure of the meridional overturning circulation through southern ocean upwelling. *Nat. Geosci.* **5**, 171–180.
- MATER, B. D., SCHAAD, S. M. & VENAYAGAMOORTHY, S. K. 2013 Relevance of the Thorpe scale in stably stratified turbulence. *Phys. Fluids* **25**, 076604.
- MATER, B. D. & VENAYAGAMOORTHY, S. K. 2014 The quest for an unambiguous parameterization of mixing efficiency in stably stratified geophysical flows. *Geophys. Res. Lett.* **41(13)**, 4646–4653.
- MATER, B. D., VENAYAGAMOORTHY, S. K., LAURENT, L. ST. & MOUM, J. N. 2015 Biases in thorpe-scale estimates of turbulence dissipation. part i: Assessments from large-scale overturns in oceanographic data. *J. Phys. Ocean.* **45**, 2497–2521.
- MCDUGALL, T. J. & BARKER, P. M. 2011 Getting started with teos–10 and the gibbs seawater (gsw) oceanographic toolbox. *SCOR/IAPSO WG127 ISBN 978 – 0 – 646 – 55621 – 5* p. 22.
- MELLOR, G. L. & YAMADA, T. 1982 Development of a turbulence closure model for geophysical fluid problems. *Rev. Geophys. Space Phys.* **20**, 851–875.
- MERRIFIELD, S. T., LAURENT, L. S., OWENS, B., THURNHERR, A. M. & TOOLE, J. M. 2016 Enhanced diapycnal diffusivity in intrusive regions of the drake passage. *Journal of Physical Oceanography* **46**, 1309–1321.
- MONIN, A. S., YAGLOM, A. M. & LUMLEY, J. L. 1971 Statistical uid mechanics- voll1: Mechanics of turbulence .
- MOUM, J., CALDWELL, D. R. & PAULSON, C. A. 1989 Mixing in the equatorial surface layer and thermocline. *J. Geophys. Res.* **94 (C2)**, 2005–2022.

- MOUM, J. N. 1990 Profiler measurements of vertical velocity fluctuations in the ocean. *J. Atmospheric and oceanic technology* **7**, 323–333.
- MOUM, J. N. 1996 Energy containing scales of turbulence in the ocean thermocline. *J. Geophys. Res.* **101 (C6)**, 14095–14109.
- MUNK, W. 1966 Abyssal recipes. *Deep sea Res* **13**, 707–730.
- MUNK, W. & WUNSCH, C. 1998 Abyssal recipes II: Energetics of tidal and wind mixing. *Deep-sea Res.* **45**, 1977–2010.
- NICOLLEAU, F. & VASSILICOS, J. C. 2000 Turbulent diffusion in stably stratified non decaying turbulence. *J. Fluid Mech.* **410**, 123.
- OAKEY, N. S. 1982 Determination of the rate of dissipation of turbulent energy from simultaneous temperature and velocity shear microstructure measurements. *Journal of Physical Oceanography* **12(3)**, 256–271.
- OLBERS, D. & EDEN, C. 2013 A global model for the diapycnal diffusivity induced by internal gravity waves. *J. Phys. Oceanogr.* **43**, 1759–1779.
- ORLANSKI, I. 1975 A rational subdivision of scales for atmospheric processes. *Bulletin of the American Meteorological Society* **56(5)**, 527–530.
- ORSZAG, S. A. & PATTERSON, G. S. 1972 Numerical simulation of three dimensional homogeneous isotropic turbulence. *Phys. Rev. Lett.* **28**, 76–79.
- OSBORN, T. R. 1980 Estimates of the local rate of vertical diffusion from dissipation measurements. *J. Phys. Oceanogr.* **10**, 83–89.
- OSBORN, T. R. & COX, C. S. 1972 Oceanic fine structure. *Geophys. Fluid Dyn.* **3**, 321–345.
- OSBORN, T. R. & LUECK, R. G. 1985 Turbulence measurements with a submarine. *J. Phys. Oceanogr.* **15**, 1502–1520.

- OZMIDOV, R. V. 1965 On the turbulent exchange in a stably stratified ocean. *Izv., Acad. Sci., USSR, Atmos. Oceanic Phys.* **1**, 853–860.
- PEARSON, H. J., PUTTOCK, J. S. & HUNT, J. C. 1983 A statistical model of fluid element motions and vertical diffusion in a homogeneous stratified turbulent flow. *J. Fluid mech.* **129**, 219–249.
- PELTIER, W. R. & CAULFIELD, C. P. 2003 Mixing efficiency in stratified shear flows. *Annu. Rev. Fluid Mech.* **35**, 135–167.
- POLZIN, K. J., TOOLE, J., LEDWELL, J. & SCHMITT, R. 1997 Spatial variability of turbulent mixing in the abyssal ocean. *Science* **276**, 93–96.
- POLZIN, K. L. 2009 An abyssal recipe. *Ocean Model* **30**, 298–309.
- POPE, S. B. 2000 Turbulent flows. *Cambridge University Press* .
- PRIESTLEY, C. H. B. 1959 Turbulent transfer in the lower atmosphere. *University of Chicago Press* **130**.
- REHMANN, C. R. & HWANG, J. H. 2005 Small-scale structure of strongly stratified turbulence. *J. Phys. Oceanogr.* **35**, 151–164.
- REYNOLDS, O. 1895 On the dynamical theory of incompressible viscous flows and the determination of criterion. *Geophys. Res. Lett.* **39**, 123–161.
- RICHARDS, K. J., XIE, S. P. & MIYAMA, T. 2009 Vertical mixing in the ocean and its impact on the coupled ocean-atmosphere system in the eastern tropical pacific. *J. Climate* **22**, 3703–3719.
- RICHARDSON, L. F. 1922 Weather prediction by numerical process. *Cambridge University Press* .
- RILEY, J. J., METCALFE, R. W. & WEISSMAN, M. A. 1981 Direct numerical simulations of homogeneous turbulence in density stratified fluids. *Nonlinear properties of internal waves AIP Conf. Prpc. 76* (ed. B. J. West) pp. 79–112.

- RILEY, J. J. & PATTERSON, G. S. 1974 Diffusion experiments with numerically integrated isotropic turbulence. *Phys. Fluids* **17**, 292–307.
- ROGALLO, R. S. 1981 Numerical experiments in homogeneous turbulence. *Report TM81315*, NASA. .
- RUDNICK, D. L. & KLINKE, J. 2007 The underway conductivity-temperature-depth instrument. *J. Atmos. Oceanic Technol*<https://doi.org/10.1175/JTECH2100.1> **24**, 1910–1923.
- SALEHIPOUR, H. & PELTIER, W. R. 2015 Diapycnal diffusivity, turbulent prandtl number and mixing efficiency in boussinesq stratified turbulence. *J. Fluid Mech.* **775**, 464–500.
- SALEHIPOUR, H., PELTIER, W. R., WHALEN, C. B. & MACKINNON, J. A. 2016 A new characterization of turbulent diapycnal diffusivities of mass and momentum in the ocean. *Geophys. Res. Lett.* **43**.
- SARKAR, S. 2003 The effect of stable stratification on turbulence anisotropy in uniformly sheared flow. *Computers and Mathematics with Applications* **46**, 639–646.
- SAWFORD, B. 2001 Turbulent relative dispersion. *Annu. Rev. Fluid Mech.* **33**, 289–317.
- SCHUMANN, U. & GERZ, T. 1995 Turbulent mixing in stably stratified turbulence. *J. Appl. Mete.* **34**, 33–48.
- SHANG, X., QI, Y., CHEN, G., LIANG, C., LUECK, R. G., PRAIRIE, B. & LI, H. 2017 An expendable microstructure profiler for deep ocean measurements. *Journal of Atmospheric and Oceanic Technology* **34** (1), 153–165.
- SHIH, L. H., KOSEFF, J. R., IVEY, G. N. & FERZIGER, J. H. 2005 Parameterization of turbulent fluxes and scales using homogeneous sheared stably stratified turbulence simulations. *J. Fluid Mech.* **525**, 193–214.

- SHROYER, E. L., RUDNICK, D. L., FARRAR, J. T., LIM, B., VENAYAGAMOORTHY, S. K., LAURENT, L. C. ST., GARANAİK, A. & MOUM, J. N. 2016 Modification of upper-ocean temperature structure by subsurface mixing in the presence of strong salinity stratification. *Oceanography* **29(2)**, 62–71.
- SMYTH, W. D. & MOUM, J. N. 2000 Anisotropy of turbulence in stably stratified mixing layers. *Phys. Fluids* **12(6)**, 1343–1362.
- SMYTH, W. D. & MOUM, J. N. 2013 Marginal instability and deep cycle turbulence in the eastern equatorial pacific ocean. *Geophys. Res. Letter* **40**, 6181–6185.
- SMYTH, W. D., MOUM, J. N. & CALDWELL, D. R. 2001 The efficiency of mixing in turbulent patches: Inferences from direct simulations and microstructure observations. *J. Phys. Oceanogr.* **31**, 1969–1992.
- SREENIVASAN, K. R. 1991 On local isotropy of passive scalars in turbulent shear flows. *Proc. R. Soc. Lond. A* **434**, 165–182.
- SREENIVASAN, K. R. 1995 On the universality of the kolmogorov constant. *Phys. Fluids* **7**, 2778–2784.
- STRANGE, E. J. & FERNANDO, H. J. S. 2001 Entrainment and mixing in stratified shear flows. *J. Fluid Mech.* **428**, 349–386.
- STRETCH, D. D. & VENAYAGAMOORTHY, S. K. 2010 Diapycnal diffusivities in homogeneous stratified turbulence. *Geophys. Res. Lett.* **37**, L02602.
- TAYLOR, G. I. 1921 Diffusion by continuous movements. *London Math Soc.* **20**, 125–181.
- TAYLOR, G. I. 1935 Statistical theory of turbulence. *Proceedings of the Royal society of London, Ser. A* **151**, 423–444.

- THOMPSON, D. J., LATORRE, E., LIU, X., ZHU, J. & HU, Z. 2015 Recent developments in the prediction and control of aerodynamic noise from high speed trains. *International Journal of Rail Transportation* **3:3**, 119–150.
- THORODDSEN, S. T. & ATTA, C. W. VAN 1992 The influence of stable stratification on small-scale anisotropy and dissipation in turbulence. *J. Geophys. Res.* **97 (C3)**, 3647–3658.
- THORPE, S. A. 1977 Turbulence and mixing in a Scottish loch. *Philos. Soc. London, Ser. A* **286**, 125–181.
- THORPE, S. A. 2005 The turbulent ocean. *Cambridge university press* .
- THURNHERR, A. M. 2011 Vertical velocity from ladcp data. *Preceeding, CWTMC'11(IEEE), Monterey, Calif* .
- THURNHERR, A. M., KUNZE, E., TOOLE, J. M., LAURENT, L. ST., RICHARDS, K. J. & RUIZ-ANGULO, A. 2015 Vertical kinetic energy and turbulent dissipation in the ocean. *Geophys. Res. Lett.* **42**, 7639–7647.
- VENAYAGAMOORTHY, S. K. & KOSEFF, J. 2016 On the flux richardson number in stably stratified turbulence. *J. Fluid Mech.* **798(R1)**.
- VENAYAGAMOORTHY, S. K. & STRETCH, D. D. 2006 Lagrangian mixing in decaying stably stratified turbulence. *J. Fluid Mech.* **564**, 197–226.
- VENAYAGAMOORTHY, S. K. & STRETCH, D. D. 2010 On the turbulent Prandtl number in homogeneous stably stratified turbulence. *J. Fluid Mech.* **644**, 359–369.
- WARD, B., FRISTEDT, T., CALLAGHAN, A. H., SUTHERLAND, G., SANCHEZ, X., VIALARD, J. & DOESCHATE, A. T. 2014 The air-sea interaction profiler (ASIP): An autonomous upwardly rising profiler for microstructure measurements in the upper ocean. *J. Atmospheric and oceanic technology* **31**, 2246–2266.

- WATERHOUSE, A. F., MACKINNON, J. A., NASH, J. D., ALFORD, M. H., KUNZE, E., SIMMONS, H. L., POLZIN, K. L., LAURENT, L. C. ST., SUN, O. M., PINKEL, R., TALLEY, L. D., WHALEN, C. B., HUUSSEN, T.N., CARTER, G. S., FER, I., WATERMAN, S., GARABATO, A. C. N., SANFORD, T. B. & LEE, C. M. 2014 Global patterns of diapycnal mixing from measurements of the turbulent dissipation rate. *Journal of Physical Oceanography* **44** (7), 1854–1872.
- WEINSTOCK, J. 1992 Vertical diffusivity and overturning length in stably stratified turbulence. *J. Geophysical Res.* **97**, 12653–12658.
- WELLS, M., CENEDESE, C. & CAULFIELD, C. P. 2010 The relationship between flux coefficient and entrainment ratio in density currents. *J. Phys. Oceanogr.* **40**, 2713–2727.
- WIJESSEKERA, HEMANTHA W., SHROYER, EMILY, TANDON, AMIT, RAVICHANDRAN, M., SENGUPTA, DEBASIS, JINADASA, S. U. P., FERNANDO, HARINDRA J. S., AGRAWAL, NEERAJ, ARULANANTHAN, K., BHAT, G. S., BAUMGARTNER, MARK, BUCKLEY, JARED, CENTURIONI, LUCA, CONRY, PATRICK, FARRAR, J. THOMAS, GORDON, ARNOLD L., HORMANN, VERENA, JAROSZ, EWA, JENSEN, TOMMY G., JOHNSTON, SHAUN, LANKHORST, MATTHIAS, LEE, CRAIG M., LEO, LAURA S., LOZOVATSKY, IOSSIF, LUCAS, ANDREW J., MACKINNON, JENNIFER, MAHADEVAN, AMALA, NASH, JONATHAN, OMAND, MELISSA M., PHAM, HIEU, PINKEL, ROBERT, RAINVILLE, LUC, RAMACHANDRAN, SANJIV, RUDNICK, DANIEL L., SARKAR, SUTANU, SEND, UWE, SHARMA, RASHMI, SIMMONS, HARPER, STAFFORD, KATHLEEN M., LAURENT, LOUIS ST., VENAYAGAMOORTHY, KARAN, VENKATESAN, RAMASAMY, TEAGUE, WILLIAM J., WANG, DAVID W., WATERHOUSE, AMY F., WELLER, ROBERT & WHALEN, CAITLIN B. 2016 Asiri: An oceanatmosphere initiative for bay of bengal. *Bulletin of the American Meteorological Society* **97** (10), 1859–1884.
- WINGSTEDT, E. M. M., FOSSUM, H. E., REIF, B. A. PETTERSSON & WERNE, J. 2015 Anisotropy and shear-layer edge dynamics of statistically unsteady, stratified turbulence. *Phys.*

*Fluids* **27**, 065106.

WINTERS, K. B. & D'ASARO, E. A. 1996 Diascalar flux and the rate of fluid mixing. *J. Fluid Mech.* **317**, 179–193.

WINTERS, K. B., LOMBARD, P. N., RILEY, J. J. & D'ASARO, E. A. 1995 Available potential energy and mixing in density-stratified fluids. *J. Fluid Mech.* **289**, 115–128.

WUNSCH, C. & FERRARI, R. 2004 Vertical mixing, energy, and the general circulation of the oceans. *Annu. Rev. Fluid Mech.* **36**, 281–314.

XIA, H., FRANCOIS, N., PUNZMANN, H. & SHATS, M. 2013 Lagrangian scale of particle dispersion in turbulence. *Nat. Commun.* **4**.

YAMAZAKI, H. & OSBORN, T. R. 1990 Dissipation estimates for stratified turbulence. *J. Geophys. Res.* **95(C6)**, 9739–9744.

YEUNG, P. K., BRASSEUR, J. G. & WANG, Q. 1995 Dynamics of direct large-small scale couplings in coherently forced turbulence: concurrent physical and Fourier-space views. *J. Fluid Mech.* **283**, 43–95.

YEUNG, P. K. & POPE, S. B. 1989 Lagrangian statistics from direct numerical simulations of isotropic turbulence. *J. Fluid Mech.* **207**, 531–586.